UNIVERSIDADE FEDERAL DO PARANÁ

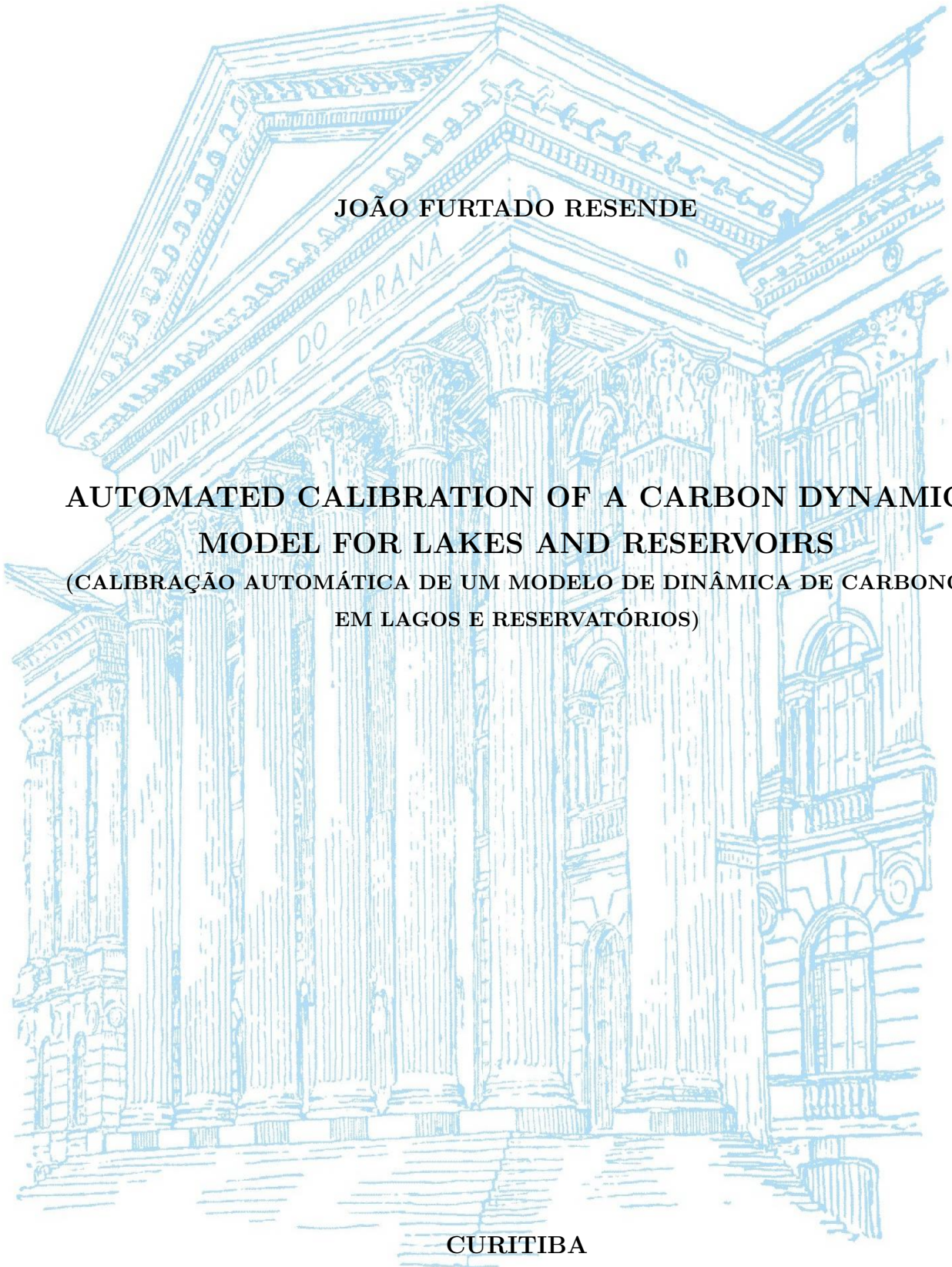

JOÃO FURTADO RESENDE

AUTOMATED CALIBRATION OF A CARBON DYNAMIC MODEL FOR LAKES AND RESERVOIRS

(CALIBRAÇÃO AUTOMÁTICA DE UM MODELO DE DINÂMICA DE CARBONO EM LAGOS E RESERVATÓRIOS)

CURITIBA

2017

JOÃO FURTADO RESENDE

AUTOMATED CALIBRATION OF A CARBON DYNAMIC MODEL FOR LAKES AND RESERVOIRS

(CALIBRAÇÃO AUTOMÁTICA DE UM MODELO DE DINÂMICA DE CARBONO EM LAGOS E RESERVATÓRIOS)

Dissertação apresentada ao Programa de Pós-Graduação em Engenharia de Recursos Hídricos e Ambiental, Departamento de Hidráulica e Saneamento, Setor de Tecnologia, Universidade Federal do Paraná, como parte das exigências para a obtenção do título de Mestre em Engenharia de Recursos Hídricos e Ambiental

Orientador: Michael Mannich
Co-orientador: Cristóvão Vicente Scapulatempo Fernandes

CURITIBA

2017

R433 Resende, João Furtado

Automated calibration of a carbon dynamic model for lakes and reservoirs (Calibração Automática de um Modelo de Dinâmica de Carbono em Lagos e Reservatórios). / João Furtado Resende. – Curitiba, 2017.
131 f.: il.; tabs. : color. : 30 cm.

Dissertação (mestrado) - Universidade Federal do Paraná, Programa de Pós Graduação em Engenharia de Recursos Hídricos e Ambiental, Departamento de Hidráulica e Saneamento, Setor de Tecnologia.

Orientador: Prof. Dr. Michael Mannich
Co-orientador: Prof Dr. Cristóvão Vicente Scapulatempo Fernandes
Bibliografia: p.105-111

1. Recursos hídricos. 2. Carbono. 3. Efeito estufa - atmosfera. I. Universidade Federal do Paraná. II. Mannich, Michael. III. Título.
CDD 628.132

MINISTÉRIO DA EDUCAÇÃO
UNIVERSIDADE FEDERAL DO PARANÁ
PRÓ-REITORIA DE PESQUISA E PÓS-GRADUAÇÃO
Setor TECNOLOGIA
Programa de Pós-Graduação ENGENHARIA DE RECURSOS HÍDRICOS E AMBIENTAL

TERMO DE APROVAÇÃO

Os membros da Banca Examinadora designada pelo Colegiado do Programa de Pós-Graduação em ENGENHARIA DE RECURSOS HÍDRICOS E AMBIENTAL da Universidade Federal do Paraná foram convocados para realizar a arguição da Dissertação de Mestrado de **JOÃO FURTADO RESENDE** intitulada: **Automated calibration of a carbon dynamic model for lakes and reservoir**, após terem inquirido o aluno e realizado a avaliação do trabalho, são de parecer pela sua APROVAÇÃO.

Curitiba, 16 de Março de 2017.

MICHAEL MANNICH
Presidente da Banca Examinadora (UFPR)

MARCELO RODRIGUES BESSA
Avaliador Interno (UFPR)

CRISTOVÃO VICENTE SCAPULATEMPO FERNANDES
Avaliador Interno (UFPR)

MAURÍCIO FELGA GOBBI
Avaliador Externo (UFPR)

DANIEL WEINGAERTNER
Avaliador Externo ()

To Benn, Lupe and Newton, to which I owe all

ACKNOWLEDGEMENTS

Ao meu orientador e amigo professor Michael Mannich que, além da tradicional instrução acadêmica, proporcionou-me conversas lúdicas e filosóficas sobre os mais diversos tópicos. Pelas diversas horas consumidas discutindo abordagens teóricas e de implementação do nosso modelo e ajustes manuais de seus parâmetros, desde a época da minha iniciação científica.

Ao meu coorientador e mentor professor Cristóvão Fernandes pela presença e suporte no decorrer de toda a minha formação acadêmica na universidade nos últimos 6 anos. Você foi a faísca do meu interesse pelas engenharias e uma das principais razões por ter ingressado nesse mestrado e por estar aonde hoje estou.

Aos meus pais Benn e Lupe e ao meu irmãozinho Newton, por me apoiar nos momentos de dúvida e pelas carnes com batata frita de sexta-feira.

Aos meus colegas e amigos: Jhonatas, Tábata, Cíntha, Mizu, Cesar, Gabi, Jú, Leandro, Steffany, Bruna, Jean, Anderson e Ricardo pelas diversas tardes e noites divertidas, algumas das quais a minha memória não me permite elucidar. Ao Júlio pelas incontáveis horas de discussão sobre computadores, modelos, matemática e seriados e ao Marcelo por me ceder a Fender e me apresentar a banda Them Crooked Vultures.

À AMD, por fazer meu processador que passou dias e noites na labuta e ao Dropbox por armazenar meus arquivos. Ao PoP-PR da RNP por transmitir meus dados e ao Google Scholar, ScienceDirect e ResearchGate por me ajudar a procurar estudos relevantes e ao *tex.stackexchange* por resolver minhas inúmeras dúvidas de comandos no LaTeX.

RESUMO

A carência de medidas de fluxos de gases de efeito estufa (GEE), junto com as incertezas referentes às extrapolações de emissões pontuais para emissões totais, resultam em conclusões imprecisas referente a participação de reservatórios no clima global. O modelo matemático CICLAR é usado para simular fluxos de CO_2 e CH_4 por 45 anos no reservatório de Capivari, Paraná, Brasil. O modelo é estruturado em compartimentos de diferentes formas de carbono, como o carbono inorgânico dissolvido (CID) e o carbono orgânico particulado vivo (COP_L). Processos químicos de transferência de massa entre compartimentos são modelados como reações de primeira ordem e de saturação que são controladas por parâmetros numéricos. O valor destes parâmetros são calibrados através da minimização de diferenças entre dados observados e modelados através de algoritmos de calibração. O algoritmo metaheuristico de Otimização Multi-objetivo por Enxame de Particulas Combinada de Pareto (CPMOPSO), que combina técnicas de seleção de líderes, mutações e subenxames, foi desenvolvido e aplicado como método de otimização. O algoritmo de calibração automática utiliza dados provenientes da calibração manual. Quatro cenários foram analisados: o avaliativo, que usa os primeiros 30 e os últimos 15 anos de dados do reservatório para calibrar e validar o modelo; e o retrospective, o prospectivo e o ideal, que usam 9 anos de dados, distribuídos de maneiras diferentes, para calibrar o modelo. A qualidade dos resultados da calibração foi positivamente considerada através do uso do cenário avaliativo. Os resultados da calibração sob os cenários retrospectivo e prospectivo mostraram que o algoritmo tende a superestimar emissões de metano se dados mal distribuídos são utilizados. A otimização sob o cenário ideal obteve melhores resultados e mostrou que a disposição dos dados tem maior impacto do que a quantidade sobre a calibração. Todas as soluções sob todos os cenários obtiveram soluções com coeficientes de Nash-Sutcliffe superiores a 0.95 para o período de calibração. As distribuições acumuladas das médias dos Potenciais de Aquecimento Global (GWP) mostraram que a maioria das soluções calibradas classificam o reservatório como um sumidouro de dióxido de carbono equivalente, absorvendo até 90 Gg de CO_2 eq. Estimativas alternativas de estoque de carbono foram utilizadas para calibrar o modelo em um escopo em que nenhuma solução prévia é conhecida. São feitas considerações adicionas referentes a aplicação de métodos de análise de incertezas e agregação Bayesiana para melhor aferir múltiplos conjuntos de parâmetros.

Palavras-chaves: Modelagem matemática. Dinâmica do carbono. Gases de efeito estufa. Potencial de aquecimento global. Enxame de partículas. Dominância de Pareto.

ABSTRACT

The low availability of measured greenhouse gas (GHG) fluxes for lakes and reservoirs, coupled with uncertainties regarding extrapolating total reservoir emissions from point measurements, result in inaccurate conclusions regarding the role of reservoirs in the global climate. The Carbon Cycle in Lakes and Reservoirs (CICLAR) model is used to study potential contributions, through carbon dioxide (CO_2) and methane (CH4) emissions, of the Capivari reservoir, Brazil, since its construction in 1970. The model is structured in compartments for different carbon forms, such as dissolved inorganic carbon (DIC) and live particulate organic carbon (POC_L), and model chemical processes as first order reactions controlled by numerical parameters. The values of these parameters are calibrated by minimizing differences between original and modeled data through an optimization algorithm. The Combined Pareto Multi-objective Particle Swarm Optimization (CPMOPSO) metaheuristic algorithm, which combines leader selection, mutation and subswarm techniques, is developed and successfully used as the optimization technique. The automated calibration algorithm uses data originated from the manual calibration. Four calibration scenarios are used to analyze the impact of data disposition in the calibration results: the evaluative scenario that has the initial 30 years to calibrate and the final 15 to validate the model; and the retrospective, prospective and ideal scenarios, that uses 9 years of data differently distributed. The evaluative data scenario is used to assess the quality of the calibration results, which successfully fit the validation data. The retrospective and prospective scenario are used to analyze the performance of the calibration under unevenly spread data, and the results show that the model had a bias to overestimate methane emissions. The calibration under the ideal scenario is used to show that having evenly spread data has a bigger impact on calibration results than having larger amounts of data. All calibrated solutions for all scenarios present Nash-Sutcliffe coefficient values higher than 0.95 for the calibration period. The cumulative distribution of average Global Warming Potential (GWP) indexes shows that most calibrated solutions estimated that the Capivari reservoir is a sinkhole for equivalent carbon dioxide and that it can absorb up to 90 Gg of equivalent CO_2. Alternative carbon stock estimations are used to calibrate the model under a framework in which the results cannot be validated due to no previous solutions being known. Further consideration are drawn regarding the application of uncertainty analysis and Bayesian aggregation methods to better assess the combination of multiple set of parameters.

Keywords: Mathematical modeling. Carbon dynamics. Greenhouse gases. Global warming potential. Particle swarm optimization. Pareto dominance.

LIST OF FIGURES

LIST OF TABLES

LIST OF ABBREVIATIONS AND ACRONYMS

GHG	Greenhouse Gases
CICLAR	Carbon Cycle on Lakes and Reservoir
DIC	Dissolved Inorganic Carbon
DOC	Dissolved Organic Carbon
POC	Particulated Organic Carbon
OM	Organic Matter
DO	Dissolved Oxygen
GWP	Global Warming Potential
TP	Total Phosphorus
MO	Multi-objective
MOP	Multi-objective Problem
NFL	No Free Lunch
GA	Genetic Algorithm
PSO	Particle Swarm Optimization
MOPSO	Multi-objective Particle Swarm Optimization
GD	Generational distance
SP	Spacing
IPSO	Improved Particle Swarm Optimization
MSSEPSO	Master Slave Swarm Shuffling Evolution Particle Swarm Optimization
ASD	Adaptive Search Diversification
AMOPSO	Aggregated Multi-objective Particle Swarm Optimization
CPMOPSO	Combined Pareto Multi-objective Particle Swarm Optimization

LIST OF SYMBOLS

CO_2	Carbon Dioxide
CH_4	Methane
NO_2	Nitrogen Dioxide
HCO_3^-	Bicarbonate
CO_3^{2-}	Carbon Trioxide
POC_L	Live Particulated Organic Carbon
POC_D	Dead Particulated Organic Carbon
SC_R	Refractory Sedimented Carbon
SC_L	Labile Sedimented Carbon
p_{LR}	Percentage of the sedimentation to labile sedimented compartment
K_{AB}	DOC Breathing
K_{CA}	POC_L Excretion
K_{CB}	POC_L Breathing
K_{CD}	POC_L Death
K_{DB}	POC_D Breathing
K_{CE}	POC_L Sedimentation
K_{DE}	POC_D Sedimentation
K_{ED}	SC_L Resuspension
K_{EB}	SC_L Breathing
K_{EEB}	SC_L Ebullition
K_{EF}	SC_R Decay
K_{FEB}	SC_R Ebullition
K_{PP}	Primary Production
K_{DIC}	DIC Half-Saturation
Q_{in}	Inflow
T_{Win}	Inflow Temperature
Q_{out}	Outflow
pH_{in}	Inflow pH
T_{air}	Air Temperature
DOC_{in}	Inflow DOC
U	Relative air Humidity

DIC_{in}	Inflow DIC
V_w	Wind Velocity
POC_{Lin}	Inflow POC_L
POC_{Din}	Inflow POC_D
K_1	Carbonic acid dissociation constant
K_2	Bicarbonate dissociation constant
K_w	Water dissociation constant
V	Reservoir volume
V_s	Sediment volume
A	Surface area
PP	Primary production
F_{CO_2}	Carbon dioxide flux to the atmosphere
T	Temperature
K_{20}	Parameter value at 20^oC
K^*	Temperature adjusted parameter value
I	Solar radiation
I_S	Peak primary production solar radiation
k	Gas transfer velocity
Sc	Adimensional Schmidt number
u_{10}	Wind velocity at 10 meters height
K_H	Henry's coefficient
pCO_2	Atmospheric carbon dioxide partial pressure
TA	Total alkalinity
H^+	Hidron
p	Particle
x_p	Particle position
v_p	Particle velocity
r_1	Pseudorandom uniform number
r_2	Pseudorandom uniform number
ω	Particle inertia
c_1	Particle acceleration towards personal optima
c_2	Particle acceleration towards global optima
$P_{b,p}$	Personal best of the particle
G_b	Global best or leader

X	Swarm
NP	Number of particles
NI	Number of iterations
ND	Number of dimensions
NO	Number of objectives
f	Optimization function or particle evaluation
v_{max}	Maximum modular velocity
LB	Particle lower boundary
UB	Particle upper boundary
AD	Absolute difference
$RMSE$	Root Mean Square Error
NS	Nash-Sutcliffe coefficient
w_C	Carbon stock aggregation weight
w_{CO_2}	Carbon dioxide aggregation weight
w_{CH_4}	Methane aggregation weight
A	External archive
e_k	Velocity mutation
p_m^{vel}	Velocity mutation probability
μ	Mean
σ	Standard deviation
S_{x_p}	Subset of the external archive formed by solutions that dominate x_p
age_a	Age criteria of archive solution a
k_a	Number of iterations a persisted in the archive
dom_a	Domination criteria of solution a
p_{x_p}	Discrete leader selection probability distribution of particle x_p
$c_{1_{max}}$	Upper boundary for adaptive c_1 coefficient
$c_{2_{min}}$	Lower boundary for adaptive c_2 coefficient
$c_{2_{max}}$	Upper boundary for adaptive c_2 coefficient
ω_{min}	Lower boundary for adaptive ω coefficient
ω_{max}	Upper boundary for adaptive ω coefficient
d_p	Distance of particle p to Pareto-front
d_{max}	Maximum distance from particles to Pareto-front
A_{master}	Master archive
NSS_{set}	Number of settler subswarms

NSS_{exp}	Number of explorer subswarms
NSS	Number of subswarms
$SS_{settler}$	Set of settler subswarms
$SS_{explorer}$	Set of explorer subswarms

CONTENTS

1 INTRODUCTION

The role of lakes and reservoirs on the global warming effect is an ongoing and controversial research topic. The magnitude of greenhouse gases (GHG) emission on inland aquatic systems is still uncertain. Due to the highly complex physical, chemical and biological processes involved in gas emission on lakes and reservoirs, a full understanding of the theme has not been achieved yet.

Rudd et al. (1993) estimated that the global impact of the carbon dioxide (CO_2) and methane (CH_4) emissions in a Canadian hydroelectric dam is equivalent to thermoelectric powerplants. This is a result of the high organic matter concentration in the reservoir area prior to its construction, e. g. forests and swamps, and its subsequent decomposition by aquatic based bacteria. These results question the characterization of hydroelectric power plants as clean energy sources. Albeit, these results were based on the extrapolation of sample point measures, and, therefore, have a high degree of uncertainty. Also, the methane global warming potential used was approximately twice the current revised value (IPCC, 2013), which implies on a overestimation of the emission per unit energy attributed to the reservoir.

Reservoirs are constructed and widely used to maintain several demands of society, including water storage for human consumption, irrigation, flow regularization and hydroelectric power generation. In Brazil, the main energy production matrix component is hydroelectric, which, in most cases, rely on reservoirs (ALBUQUERQUE FILHO; SAAD; ALVARENGA, 2010).

Despite being the main electric power source in Brazil, the hydroelectric energy, which made up 84.5% of the energy matrix in 2012, had its contribution decreased to 65.2% in 2015. Such decrease occurred despite an increase in total installed potential and may be due to unfavorable hydrological conditions (EPE, 2015).

Lakes and reservoirs have a significant role on both the local climate through local air-water heat exchange, and the global scale through its participation in the global carbon cycle. Despite amounting to only 2% of Earth's surface, inland aquatic systems sink a total of approximately 300 Tg of carbon per year, about the triple of the organic carbon stocked in oceans (TRANVIK et al., 2009) (DEAN; GORHAM, 1998).

Despite acting as carbon sinkholes, according to Cole et al. (2007) inland aquatic systems emit around 0.8 Pg of carbon to the atmosphere every year. Such emissions are mainly through CO_2 and CH_4 and their magnitudes vary according to carbon availability on soil and local vegetation, depending on the ecosystem in which the system is located (LOUIS et al., 2000)(DUCHEMIN et al., 1995).

However, such carbon flux estimates for aquatic systems, both inland and oceanic, must be analyzed with caution, since their values are based on extrapolation, both spatial, due to fluxes only being measured in specific points, and temporal, due to fluxes only being measured for relatively short time periods. There are also uncertainties regarding the point measurements themselves, since the measuring method may have significant impacts on several of the system variables, and possible impacts in the measured fluxes fluxes (MANNICH, 2013).

Many mathematical models have been developed to investigate reservoir biochemical processes and possibly assess uncertainties regarding estimations of GHG emissions. If the model is properly validated it can be used to offer prognostics to assist in various decision making processes. There are, however, a wide range of theoretical and numerical approaches for modeling water quality of inland systems that are based on different biochemical and physical concepts and result in potentially different conclusions.

Many researchers, e. g., Mukherjee, Pandey e Singh (2002), Barrette e Laprise (2002), Hanson et al. (2004), Weiping et al. (2011), Sbrissia et al. (2011), Lu, Gan e Dai (2012), Mannich (2013), and Mannich et al. (2015), turned their attention to the problem of mathematically assessing the processes involved in carbon cycle on aquatic systems. However, the use of such models is limited by the quantity and quality of available measured data.

As a result of the theoretical simplifications that are innate to any physical based mathematical model, many uncertainties, physical and numerical, are reflected on the parameters. In some cases, such parameters are not measurable but can only be estimated based on physical variables, such as temperature and density, while in other cases, they can only be numerically set in such a way to adjust modeled to observed data. Such adjustment process is referred to as calibration, and its success is heavily tied to both the complexity of the physical system/mathematical model and the data quality and availability.

The lack of measured GHG data on Brazilian reservoirs compromise the overall model results and the elucidation of chemical, physical and biological characteristics that need to be incorporated in such models so that they can produce the desired prognostics.

However, the use of automated calibration techniques enables, by relying on the vastly available computational power, the assessment of multiple scenarios and uncertainties regarding available data. Although the calibration of heat and mass budget models are typically computationally expensive, it offers a tool for producing probabilistic prognostics that can be used in reservoir management.

1.1 OBJECTIVES

The main objective of this dissertation is the development of a calibration routine and evaluation of the performance of a simplified carbon dynamic model for lakes and reservoirs under different calibration scenarios.

The CICLAR model proposed by by Mannich et al. (2015), is used to assess carbon dynamics on lakes and reservoirs. Multi-objective particle swarm optimization algorithms are developed to automatically calibrate the model.

Four calibration scenarios were designed to assess the impact of both the amount and spread of data on the outcome of the model calibration. All scenarios are based on data generated by the model itself and total carbon stock estimations from point measures. The CICLAR model was previously manually calibrated to fit observed data on the Capivari reservoir, Parana, Brazil.

Specifically, this dissertation aims to:

- Optimize the code of the CICLAR carbon dynamic model to lower computational costs
- Simulate CICLAR with available data and previously calibrated parameters for the Capivari reservoir
- Develop and implement efficient calibration algorithms
- Develop comprehensive calibration scenarios
- Evaluate the calibration routine through predetermined statistical metrics
- Evaluate the calibration under different greenhouse gases scenarios and total carbon stock estimations

The outcome of this dissertation can also be used as a tool that, based on meteorological, hydrological, water quality and geomorphological data, can offer approximate greenhouse gas flux prognostics. A combined swarm intelligence optimization method is also developed.

1.2 OUTLINE

The dissertation is organized to present the concepts regarding the two different parts: carbon dynamic model and the calibration technique. Literature review is in Chapter 2 and shows the state-of-the art research that aid the understanding of the motivations, decisions and contents that are presented in further chapters.

Chapter 3 presents the CICLAR carbon dynamic model and all mathematical equations and the processes they describe. Some of the equations can be found in Appendix A for the sake of brevity. Characteristics about the Capivari reservoir study area, are also briefly described in this chapter and meteorological, water quality and hydrological data are shown in Appendix B.

In Chapter 4 both the Aggregated Multi-objective Particle Swarm Optimization and Combined Pareto Multi-Objective Particle Swarm Optimization methods are presented and their application as calibration techniques is outlined. Different calibration scenarios that were developed to analyze different characteristics, such as retrospective and prospective capabilities, and the manual calibration guidelines are also presented. The performance of the optimization algorithm on mathematical benchmark functions is discussed in Appendix C.

The results of the calibration for all scenarios are presented and discussed in Chapter 5. The impact of the temporal distribution of calibration data on the quality of solutions is assessed and cumulative probabilities distributions for statistic metrics are calculated. An alternative total carbon stock estimate is used to calibrate the model providing a framework in which no previous solution is known.

Conclusions regarding the results of the calibrations and the modeled GHG fluxes and recommendations for future work are presented in the last chapter.

2 LITERATURE REVIEW

> The true sign of intelligence is not knowledge but imagination
>
> Albert Einstein

A literature review regarding carbon cycle and carbon dynamics in lakes and reservoirs, as well as studies regarding greenhouse gas flux measurement and global warming potential indexes are presented in this chapter. Several mathematical models of GHG related processes in both inland water and oceans are also reviewed. A review of existing works on calibration of numerical parameters of mathematical model in several water resources and water quality models is presented. Previous mathematical and computational techniques regarding the use of artificial intelligence, mainly evolutionary computation and swarm intelligence algorithms, to optimize both single and multi objective problems are shown.

2.1 CARBON CYCLE ON INLAND WATERS

Carbon dioxide (CO_2), methane (CH_4) and nitrous oxide (NO_2) related processes in lakes and reservoirs are directly tied to their concentrations in the atmosphere. These gases have a role in the planetary heat budget by acting on the greenhouse effect. Despite covering a relatively small portion of the surface of the planet, inland aquatic systems have a vital role in the carbon cycle, and therefore, must not be neglected (TRANVIK et al., 2009).

To understand the roles of lakes and reservoirs on a global scale, it is necessary to determine the processes that compose the internal carbon dynamics in the system. The main carbon inputs to the system are: dissolved inorganic carbon (DIC) and dissolved organic carbon (DOC), with a minor portion as particulate organic carbon (POC). Since the majority of the carbon comes from the corresponding hydrological basin, the magnitude of each of these inputs may vary according to: latitude, land use, local climate, and geochemical characteristics (TRANVIK et al., 2009).

The photosynthetic primary production transforms inorganic carbon into organic carbon and oxygen. The importance of such process depends on the presence of the living organisms, such as algae, and the availability of solar energy and nutrients. According to Downing et al. (2006), shallow systems, composing around 90% of the inland waters, have the most abundance of these components and may be classified as one of the main productive systems of the Earth.

Carbon dioxide flux at the air-water interface may present significant diurnal variations due to photosynthetic processes and solar radiation availability. Typically CO_2 is absorbed during the day and emitted at night. Analogously the dissolved oxygen concentration in the system is higher during the day and lower at night (WEIPING et al., 2011).

Organic substances, referred to as organic matter (OM), and the process by which they are originated, such as photoreduction and photooxidation, are extremely complex. The biogenic generated OM is highly heterogenic and named humic, while substances like carbohydrates and amino acids are non-humic (TUNDISI; MATSUMURA-TUNDISI, 2011).

Most GHG emissions from lakes and reservoirs are originated from the OM decomposition inside the aquatic system, in both water and bottom. Organic matter in the reservoir is commonly divided in three different classes: the OM in biomass and soil present in the area prior to the impoundment of the dam; the *autochtonous*, produced through processes such as photosynthesis, inside the reservoir itself; and the *allochtonous*, originated in the drainage area of the hydrological basin and which enters the system via processes such as surface runoff. As a consequence of these different origins, different classes of organic matter are also different regarding their compositions and characteristics such as rate of light absorption (LOZOVIK et al., 2007).

The *aerobic* organic matter decomposition occurs with the presence of oxygen and produces CO_2 that is for the most part dissolved in the water. When the dissolved carbon dioxide concentration is higher than the atmospheric concentration, the CO_2 is emitted from the aquatic system to the atmosphere according to Henry's law until an equilibrium is reached.

Carbon dioxide in aquatic systems may also be produced by the respiration process of aquatic organisms. In most cases, the magnitude of the two CO_2 producing processes is superior to the internal photosynthetic primary production. The system then becomes supersaturated and emits carbonic gas to the atmosphere. According to Downing et al. (2006) total carbonic gas emission in lakes can be as high as 0.53 Pg C per year.

Dissolved oxygen (DO) concentration in lakes and reservoirs is not vertically uniform, its solubility is temperature dependent, and its concentration depends on processes such as thermal stratification and vertical circulation. While DO has a concentration close to saturation near the surface, it is in some cases, absent in lower levels that are close to the bottom interface, characterizing *anoxic* layers. Such oxygenic surface saturation and depletion in deeper layers determine a concentration-depth curve that is referred to as *clinograde* (TUNDISI; MATSUMURA-TUNDISI, 2011).

On anaerobic layers and in some portions of the sediment, *anaerobic* decomposition

produces methane. CH_4 produced in the anoxic layer can be diffusively transported to the oxic upper layers and oxidized by methanotrophic organisms, producing CO_2, or accumulated in bubbles within the sediment. Upon reaching a certain inner partial pressure and a proper size, these bubbles rise to the upper layers, and eventually to the atmosphere, characterizing the *ebullition* process.

Most of methane production in aquatic systems occur in the bottom layer, and its emission to the atmosphere is considerably higher in shallow waters. This occurs due to the path from the anoxic regions to the water-air interface being shorter, giving less time for the oxidation process to occur. Bastviken et al. (2008) estimated that the CH_4 emitted through ebullition is at least twice as large as the diffusive emission.

The total sediment of continental aquatic system can be considered the largest compartment in the global carbon cycle (TRANVIK et al., 2009). The process by which substances are incorporated in the sediment is called sedimentation, and is the main responsible for the carbon sinkhole characteristic of lakes and reservoirs. According to Downing et al. (2006) the sedimentation process occurs faster, implying higher sedimentation rates, in small shallow lakes rather than deep ones. In order to be incorporated into the sediment, the dissolved organic carbon undergoes a flocculation process in which it is transformed in particulate organic carbon, that is in turn directly subject to sedimentation (TRANVIK et al., 2009).

Since a large amount of biomass and organic soil is flooded during the impoundment of the dam, the organic carbon availability is typically higher in reservoirs than in lakes. According to Rudd et al. (1993), such abundance can result in high CH_4 and CO_2 emissions during the early ages of the reservoir. However, according to Tremblay, Lambert e Gagnon (2004), these emissions decay significantly 10 years after the dam's impoundment, approaching the fluxes encountered in natural lakes.

Lakes and reservoirs are also different regarding the depth of the water outlet, which is closer to the surface in natural lakes, and typically deeper in artificial reservoirs. Since the dissolved methane concentration is higher at deeper levels, a large quantity of the dissolved CH_4 exits the system through outflow, bypassing the methanotrophic process that would occur in upper layers. Along with the high methane concentration, the abrupt pressure drop that occur when water flows through the turbines, contribute to a high ebullitive methane emission downstream of the dam (TRANVIK et al., 2009).

2.2 GHG EMISSION ON RESERVOIRS AND GLOBAL WARMING POTENTIALS

The assessment of GHG emission on lakes and reservoirs has been an ongoing topic of research since the early nineties. The pioneer study by (RUDD et al., 1993) sprouted related research such as (ROSA; SCHAEFFER, 1995) and (FEARNSIDE, 1995) with

significant divergence regarding its conclusions, which then became an open scientific debate among the two research groups.

Such debate is mainly focused on the comparison among hydroelectric and thermoelectric power plants based on a GHG emission per produced unit energy rate. The estimation of whether hydroelectric or thermoelectric energy generation contribute more to the global warming effect is based on indexes, such as the Global Warming Potential (GWP), which transforms various gas emissions into CO_2 equivalent values.

The GWP index measures the relative radiative effect of equal emissions of each gas according to the different times that they may remain in the atmosphere. It is defined as the time-integrated warming effect due to an instantaneous release of unit mass of a given greenhouse gas to the atmosphere, relative to that of a carbon dioxide. Being a time-integrated value it varies according to the chosen time-horizon, which is commonly 20, 50 or 100 years (IPCC, 1990).

Besides the direct effect of the GHG as radiative forcings, indirect effects such as chemical reaction with other substances on the atmosphere that produces other gases with different radiative effects, must also be accounted for. This effect is typically addressed through the use of *direct* or *indirect* GWP values. However, since GWP summarizes the complex interaction between different gases in the atmosphere and the infrared radiation emitted by the earth's surface, high degrees of uncertainties, e. g. $\pm 35\%$, are attached to it. Most of the GWP values used throughout research are extracted from the International Panel on Climate Change Panel (IPCC) periodical scientific report assessments (MYHRE et al., 2013).

Although there are different methods to assess the global warming potential of different gases, e. g., (ROSA; SCHAEFFER, 1995), the IPCC published values for a 100-years time horizon are commonly used. The main GHGs emitted by reservoirs are CO_2, whose GWP value is by definition 1, and CH_4, whose value vary according to different hypothesis. Given that the main methane sink in the atmosphere is its reaction with OH, which forms ozone, and that increasing its concentration will decrease the OH concentration, it also has a positive indirect effect on the global warming that needs to be accounted for IPCC (1994). Figure 1 presents the evolution of the indirect GWP values for methane over time, as well as some significant works related to GHG emissions on lakes and reservoirs over the 1990-2000 decades.

In IPCC (1990) the global warming potential concept was introduced and estimated as 21 for the 100-year time horizon indirect methane GWP. In a subsequent report (IPCC, 1992) it was stated that "most of the indirect GWPs reported in IPCC (1990) are likely to be in substantial error, and none of them can be recommended" due to uncertainties regarding chemical processes related to indirect effects of GHG. IPCC (1994) attributed a 24.5 value for the indirect methane GWP, while I (1995) returned to the previous estimate

Figure 1 – Timeline of research related to GHG emission on reservoirs. Based on Mendonça et al. (2012)

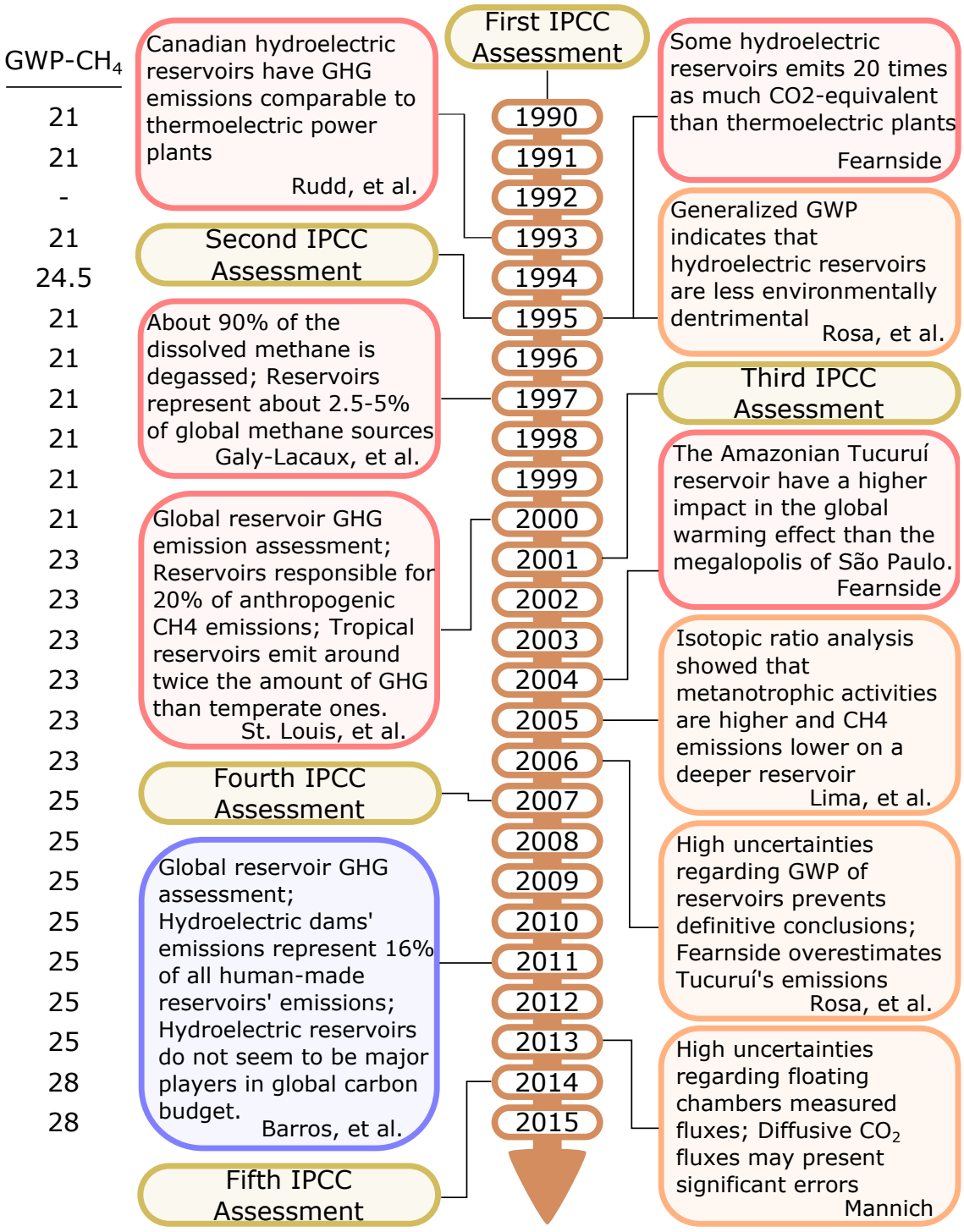

of 21. The estimate was then updated to 23 by IPCC (2001), and subsequently to 25 by IPCC (2007) and to the current value of 28 by Myhre et al. (2013).

Rudd et al. (1993) argued that the global warming impact of two different hydroelectric energy generation systems in Canada are similar to thermoelectric power plants. However, to achieve such result, the authors used the value of 60 to the GWP of

methane without indicating the desired time horizon, which can subsequently represent a significant overestimation of such global warming impact when compared to the current GWP estimate for a 100-year horizon.

Using 11 as the GWP index for methane, Fearnside (1995) estimated that the Amazonian hydroelectric reservoirs in 1990 emitted approximately 11 million tons of CO_2-equivalent carbon. The author argues that, based on generated energy, some reservoirs contribute at least 20 times more to the greenhouse effect than thermoelectric power plants. This is mainly due to the energy generation/flooded area ratio of the reservoirs, with lower rates contributing more to global warming than higher ones. Fearnside (1995) raises awareness regarding the expansion of the complex of hydroelectric reservoirs that was supposed to take place in the late nineties, which could potentially increase by a factor of 20 the GHG emissions from the region.

Rosa e Schaeffer (1995) presented a generalized global warming potential index to assist on the hydro/thermoelectric environmental impact comparison. This generalization was developed to account for the fact that emissions are concentrated in the early ages of the reservoir, while the emissions from thermoelectric power plants remain constant over time. Instead of being an index that represents the ratio of integrated radiative forcing due to a single pulse emissions, this generalized version is the ratio of radiative heatings at the end of a given time horizon, under distinct and possibly continuous emission throughout the time interval. This yielded considerably lower values ranging from 1.8 to 6.7 according to different integration times and time dependency models of radiative forcings. The authors also analyzed the evolution of the reservoir emitted methane/thermoelectric generated carbonic gas ratio over time, beginning on the dam's impoundment and going on indefinitely. They concluded that over the early years, when the anaerobic decomposition of the biomass in the reservoir is more present, reservoirs tend to have a larger impact on the global warming, but such impact is superseded by thermoelectric plants after the 20 years mark.

The scientific argument of whether hydroelectric or thermoelectric energy generation have a higher impact on the global warming effect went on with Fernside, i. e., (FEARNSIDE, 2004) and (FEARNSIDE, 2006), arguing that hydroelectric do in fact contribute more to the global warming effect and Rosa, i. e., (ROSA et al., 2004) and (ROSA et al., 2006) claiming that this comparison is not definitive and that thermoelectric plants on an appropriate time horizon generally have a larger impact on the global warming.

Galy-Lacaux et al. (1997) measured the methane and carbon dioxide flux during the first two years after the impoundment of the Petit-Saut reservoir in French Guiana. Total fluxes were estimated based on: diffusive fluxes measured through floating chambers, ebullitive fluxes measured through funnels, and emissions due to degassing of turbined water. Methane oxidation was also analyzed through analytical experiments, and dissolved

CH_4 and CO_2 concentration profiles were obtained through gas chromatography analysis of water samples obtained at different water levels. The results showed that carbon stored as dissolved methane and carbon dioxide in the reservoir peaked at around 78.3 tons of carbon 17 months after the dam's impoundment. Estimates showed that aside from emitting 270 $\pm$ 100 $\times$ 10^3 tons of methane in the first two years of the reservoir, the methanotrophic process is responsible for heavy oxygen consumption in the upper layers. According to the authors, the degassing process that occurs when the water leaves the turbine and goes through an artificial waterfall, releases about 92% of the dissolved methane into the atmosphere and is the main source of CH_4 to the atmosphere, surpassing both diffusive and bubbling processes.

Also by approximating the carbon budget, Galy-Lacaux et al. (1997) estimated that after 2 years of the reservoir filling about 800 $\pm$ 300 $\times$ 10^3 tons of carbon was lost. By accounting for the carbon present in the biomass and the soil prior to the dam's impoundment, the authors argue that about 10% of the initial total carbon stock was lost, both to the atmosphere and downstream of the dam. A global estimate was also calculated based on parameters developed from the Petit-Saut's measurements and latitude distributed reservoir data, which resulted in the approximation that reservoirs constitutes about 2.5 to 5% of the global methane sources, and therefore should be accounted for in global warming related works.

Using static chambers, funnels, gas chromatograph and a mass spectrometer, Lima (2005) obtained both the concentration of methane in the water, sediment and bubbles as well as its isotopic $^{13}C/^{12}C$ ratio, for the Tucuruí (deep) and Samuel (shallow) Amazonian reservoirs. The methane in the sediment presented a lower isotopic ratio than the dissolved portion, due to the fact that metanotrophic bacterias prefer lighter (^{12}C) carbon isotopes. However, due to the fact that Tucuruí is deeper than Samuel reservoir, and therefore has a larger metanotrophic oxic layer, the isotopic ratio of the emitted methane is considerably lower in Tucuruí than in Samuel. The author concludes that metanotrophic activities, are higher in Tucuruí reservoir rather than Samuel. This is in agreement with the theory that reservoirs with higher energy production per unit area, which are usually deeper, contribute less to the global warming effect.

Recently, Barros et al. (2011) performed a global assessment of the GHG emission from hydroelectric reservoirs by using data from 85 different reservoirs distributed latitudinally on the globe and 141 carbon dioxide and 89 methane measured emissions were assembled. While all the reservoirs in the data set were sources methane, the vast majority of the reservoirs were characterized as sources of carbonic gas, with only a few absorbing more CO_2 than emitting. Using the assembled data, the authors performed several correlation analysis between reservoir characteristics and methane and carbonic gas emissions. Characteristics such as age, latitude and input dissolved organic carbon to

the reservoirs were found to explain around 40% of the CO_2 flux variation, and, with the addition of the mean depth of the reservoir 54% of the variation in the CH_4 flux.

Mannich (2013) theoretically analyzed the possible errors regarding floating chamber measured diffusive fluxes. The impact of the chamber on lowering the concentration gradient at the air-water interface is increased the longer the measurement time, and therefore, measured fluxes are underestimated in this regard. The chamber also impacts the gas transfer velocity by changing the turbulence at the air-water interface, since it blocks the wind effect at the interface inside the chamber. Whether the chamber decreases the gas transfer velocity by lowering wind induced turbulence, or increases it through the movement induced by the submerged portion of its walls, is uncertain. Additionally the uncertainties regarding the sensors used to measure gas concentration are typically higher the lower the gas concentration inside the chamber. All these factors might culminate in significant errors regarding floating chamber measured CO_2 fluxes.

Mannich (2013) also measured several water quality parameters for the Vossoroca reservoir between august 2012 and march 2013. The measurements of physical and chemical parameters, such as pH, temperature, and dissolved oxygen, were taken at multiple depths to assess their vertical distribution. Diffusive CO_2 flux was measured through floating chambers and corrected to mitigate the aforementioned turbulence and gradient attenuation errors. Multiple measurements were taken at different times in each campaign to assess nictemeral characteristics of the reservoir. The results showed that both thermal and chemical stratification occur at the Vossoroca reservoir during warmer seasons. Unlike the expected photosynthesis/respiration cycle, a nightly absorption and daily emission of carbon dioxide was detected. Both absorption and emission of CO_2 were of similar magnitudes, around 500 mg/m^{2}d, indicating small daily averaged emissions.

2.3 THERMAL STRATIFICATION

Besides influencing the biochemical reaction speed, temperature is one of the main factors influencing vertical mix in water systems. Combined with the existence of a vertical temperature gradient, the fact that water density varies according to temperature creates different densities at the upper and lower layer of the reservoir. Such phenomena is commonly referred to as thermal stratification (CHAPRA, 2008).

The main cause for depth varying temperatures is the majority of the solar radiation emitted to the water body being absorbed in the upper centimeters of water. This warm and less dense upper layer, denominated *epilimnium*, is homogeneous due to being subject to wind induced mixture. The deepest layer, called *hipolimnium*, is heterogeneous and is characterized by its interaction with the bottom of the system, while the middle layer, referred to as *metalimnium* is even more heterogeneous and usually presents the largest temperature gradient (TUNDISI; MATSUMURA-TUNDISI, 2011).

The metalimnium, or *planar thermocline*, can be seen as an imaginary plane which divides the water body in two different layers: the productive, lit, mixed and oxygen rich upper layer and the low circulation, decompositive and low oxygen lower layer.

Lakes and reservoirs can be classified according to its thermal pattern, or specifically, according to the quantity of periods in which the system is not thermally stratified along one year: the *monomithic* lakes have only one, while the *dimithic* have two and the *polymithic* has three or more fully mixed period in a year. When the system does not present thermal stratification at all, it is classified as *meromithic*.

Temperature has a significant role in many carbon dynamic processes, acting in chemical kinetics, respiration of organisms , primary production rate and gas solubility. Therefore, thermal stratification can also contribute to carbon concentration vertical gradients in lakes and reservoirs (ÅBERG; JANSSON; JONSSON, 2010).

As estimated by Åberg, Jansson e Jonsson (2010), the surface CO_2 concentration, in the boreal lake of Merasjärvi in Sweden, was higher when the epilimnium was warmer and deeper and that the daily variation of carbon dioxide concentration was due to a second thermal stratification inside the upper layer.

2.4 CARBON DYNAMIC AND GHG MODELS IN LAKES AND RESERVOIRS

Due to the high spatial and temporal variations of GHG emission estimations for lakes and reservoirs, several researchers have developed numerical approaches to the biological, physical and chemical related processes (MUKHERJEE; PANDEY; SINGH, 2002)(BARRETTE; LAPRISE, 2002)(HANSON et al., 2004)(WEIPING et al., 2011)(SBRISSIA et al., 2011)(LU; GAN; DAI, 2012)(MANNICH, 2013)(MANNICH et al., 2015).

Mukherjee, Pandey e Singh (2002) utilized the producers, consumers and decomposers oriented modeling paradigm to represent carbon flux inside the reservoir. The primary production is used to represent photosynthetic processes, while consumption represents the organisms respiration and decomposition is the organic to inorganic carbon transformation. The model utilizes carbon and bicarbonate dissociation constants to calculate each of the carbonate components (H_2CO_3, HCO_3^-, CO_3^{-2}) concentrations according to pH and total inorganic carbon. These values are then used to calculate the total alkalinity which is in turn used to assess the total inorganic carbon according to the pH. However, despite the model's high chemical detail, it does not estimate the GHG fluxes to the atmospheres and analyze the different forms of organic carbon and its transformations inside the system.

Barrette e Laprise (2002) developed a vertical one-dimensional model to represent the diffusive and convective CO_2 transport between the atmosphere and the lake's sediment. A one-dimensional thermal balance is also used to assess the thermal stratification, since

the temperature effect is used to determine the diffusion coefficient in different layers. The CO_2 source is the organic matter decomposition in the sediment, which is vertically transported to the upper layers and emitted to the atmosphere. Although the advection and diffusion processes are detailed, this model does not represent the different forms of carbon and the photosynthetic processes.

The model proposed by Hanson et al. (2004), has the main goal of estimating the evasion and sedimentation of temperate lakes. It models the lake as a mixed homogeneous reactor and represent its physical variables, such as temperature and volume, as fixed parameters. The carbon present in the aquatic system is divided in 5 categories: Dissolved Organic Carbon (DOC), live Particulated Organic Carbon (POC_L), dead Particulated Organic Carbon (POC_D), Sedimented Carbon (SC) and Dissolved Inorganic Carbon (DIC). Mass transfer from one class to another is modeled as a first order chemical reaction, and kinetic parameters are used to model reaction velocity. Besides the different forms of carbon, the model accounts for variables such as Total Phosphorous (TP), which is utilized in the primary production carbon transformation calculation.

Sbrissia et al. (2011) expanded the model by Hanson et al. (2004) and included the CH_4 ebullitive emission through bubbles in the sediment that are formed by anaerobic decomposition of sedimented carbon. However, only one stationary value was used for most chemical and physical variables, such as volume, temperature and pH. The kinetic reaction parameters were calibrated, based on field monitoring, for a small hydroelectric plant in the subtropical region of Paraná, Brazil.

Mannich et al. (2015) further expanded on the same idea and developed the CICLAR model, that is short for **C**arbon **C**ycle in **LA**kes e **R**servoirs. The CICLAR model uses the same aforementioned compartments to represent different forms of carbon, but has the additional complexity of using temporal series instead of stationary values, to treat meteorological, hydrological and water quality data. Since, in CICLAR the temperature and alkalinity are not stationary, additional differential equations on time are also incorporated and numerically solved. pH values are obtained through by solving a third degree polynomial equation with constants based on different model variables, such as DIC concentration and total alkalinity. This is the main GHG emission model used in this study, and its physical and mathematical equations will be further expanded in Chapter 3.

Focusing on seawater CO_2 emission and its seasonal variation, Lu, Gan e Dai (2012) presented a 1D model that calculates the vertical distribution of dissolved inorganic carbon based partial differential equations. The study is an implementation of the Regional Ocean Modeling System integrated with the Fasham-Type ecosystem model, which is nitrogen-based and include prognostic variables such as nitrate, ammonium, Chlorophyll-a, zooplankton and phytoplankton. In order to calculate the partial carbon dioxide

pressure vertical distribution, the photosynthetic, respiration, and nitrification processes involved in the carbonate system are incorporated as half-saturated equations. The 17 model parameters were successfully adjusted using salinity, temperature, total alkalinity, dissolved inorganic carbon, nitrate, and Chlorophyll-*a* data for the SEATS region in the South China Sea. The effects of different controlling mechanisms were also analyzed and the authors concluded that, for the seasonal scale the temperature and air-water flux were the main factors, while for the diurnal scale the wind induced mixing contributed to higher variation on partial carbon dioxide pressure vertical distribution.

Weiping et al. (2011) developed a 3 dimensional carbon cycling model for Lake Taihu in China. It uses over 70 parameters and 20 partial differential equations to represent several processes regarding carbon transformation and transport that occur in aquatic systems. These modeled processes can be divided into: input, e. g., wind transported terrestrial vegetation, man-made organic waste and carbon present in inflow; output, e. g., diffusion emitted carbonic gas and, carbon outflow, and output due to fishing; and internal processes, e. g., vertical and horizontal diffusive-convective transport and zooplankton and phytoplankton predation and respiration. The carbonate system is also incorporated in a dissolved inorganic carbon compartment, however, unlike the CICLAR line of models, zooplankton, phytoplankton, fish and macroplants carbon are not modeled as a single particulated organic carbon compartment. Pore water organic and inorganic carbon compartments are also included in the model, creating a buffer effect, in which carbon from upper layers are not directly sedimented.

However, together with the fact that methane emissions are not modeled by Weiping et al. (2011), the additional parameters and equations that are necessary to implement a 3 dimensional model, may not yield an equivalent improvement in GHG fluxes estimation. The problem of finding realistic parameter values whose results are in accordance with measured data, together with the required temporal and spatial resolution of calibration data, might preclude model usage.

Mannich (2013) developed the vertical one-dimensional BCR carbon cycle model. Similarly to Hanson et al. (2004) and Sbrissia et al. (2011), the BCR model compartmentalizes different carbon forms, such as POC_L and DOC, and uses first order and saturation reactions to transfer mass between compartments. The model is based on a finite volumes discretization of first order partial differential equations. Each volume has different carbon concentrations for each compartment and exchanges mass both convectively and diffusively with its upper and lower neighbors. The upmost volume exchanges CO_2 and CH_4 with the atmosphere, while the lowest volume exchanges both carbon and dissolved oxygen with the sediment. A vertical one-dimensional temperature model is coupled with BCR to provide each discretized volume its own temperature. Both BCR and thermal model were manually calibrated with vertical distributed data at the Vossoroca reservoir, Parana,

Brasil. Results showed that the thermal model was successfully calibrated and presented a root mean square error lower than 0.5 ^{o}C. The BCR model was harder to calibrate due to the complexity of carbon dynamic processes, and the model was not able to reproduce nightly absorption of CO_2, albeit the modeled daily emission is inside the measured data confidence interval. The CH_4 ebullition model was also unsuccessful to reproduce the expected methane emission through bubbles.

Despite the different mathematical, physical and biochemical approaches of all aforementioned models, all of them use empirical parameters to encompass physical uncertainties in mathematical values. Specifically the Hanson et al. (2004) model, which culminated on the CICLAR model (MANNICH et al., 2015), represent uncertainties regarding chemical reaction and biological processes in the kinetic parameters. Since most of these unknown parameters are extremely hard or impossible to measure, a calibration process needs to be applied in order to approximate model results to field observed values.

2.5 MODEL CALIBRATION

According to Refsgaard e Henriksen (2004), the calibration of a model is the process of adjusting parameter values in order to obtain a desired model output. The performance of the calibration is as dependent on the quantity and quality of observed data and on the conceptual model itself, as it is on the calibration routine.

Several research, e. g., Madsen (2003), Ramsay et al. (2007), Maiwald e Timmer (2008) and Tarantola (2004) , refer to the process of adjusting parameter values to achieve a goal as *parameter estimation* instead of *calibration*. Parameter estimation typically is focused on the parameter values themselves and what they represent, while calibration is focused on approximating model results to observed values.

Although calibration focuses on model results, having knowledge on how the parameters relate to each other and to the output is valuable. Resende, Mannich e Fernandes (2015) analyzed the sensitivity of the CICLAR model to variations on photosynthetic and sedimentation parameters. This enables heuristics based on previously known model characteristics and expert knowledge to be applied during model calibration.

To select a calibration procedure many variables must be accounted for, such as the amount of model parameters, the number of calibration objectives and the computational cost of the model simulation. Most calibration algorithms are based on preexisting mathematical optimization methods, and therefore, problems like discontinuity of the search space and the objective function being nondifferentiable, must be addressed (BOUSSAïD; LEPAGNOT; SIARRY, 2013).

Calibration algorithms are based on minimizing an objective function f that associates sets of parameters to the quality of the corresponding model output. Typically

the quality of the model output is assessed by combining its values to observed data through metrics such as the Root Mean Square Error (RMSE) and the Nash-Sutcliffe (NS) coefficient. If more than one quality metric needs to be minimized the calibration is a Multi-objective Optimization Problem (MOP).

The calibration of the CICLAR model is a MOP since multiple outputs, such as CH_4 and CO_2 fluxes, need to fitted to observed data. Multi-objective optimization methods are usually divided into two categories: the ones that are designed specific for a given problem and usually rely on mathematical characteristics of the problem, e. g., gradient based methods and branch-and-bound methods; and the ones that are generic and not directed towards a particular problem ,e. g., artificial intelligence algorithms, usually referred to as *metaheuristics* (BLUM et al., 2011) (SHIN; RAVINDRAN, 1991).

Metaheuristic techniques were originally developed to solve complex problems, e. g., $\mathcal{NP}$-hard problems, in which the optimality of a given solution cannot be easily proved. Most metaheuristic methods are based on iteratively updating a set of viable solutions until a convergence criteria is met. Therefore, unlike exact optimization techniques, the optimality of the returned solution is not guaranteed.

Since the CICLAR calibration problem may not be solvable by an exact algorithm, a metaheuristic technique is used. This selection is based on several reasons: the high mathematical and input complexity of the CICLAR model; the high sensitivity to the input parameter values (RESENDE; MANNICH; FERNANDES, 2015), which result in discontinuous-like optimization function; and that metaheuristic algorithms have already been successful in past engineering applications, e. g., Ndiritu e Daniell (2001), Gill et al. (2006), Liu et al. (2007), Jiang et al. (2010), and Spiliopoulou et al. (2015).

There is an abundant amount of methods and algorithms on the metaheuristics class, most of them are nature-inspired, meaning they are typically based physics and biology principles. Generally metaheuristic techniques are heavily based on stochastic characteristics (random variables), and do not rely on problem specific operations, such as the objective function gradient or the Hessian matrix. However, as a consequence of being generic, most metaheuristic methods have several parameters that need to be fitted to the problem at hand (BOUSSAïD; LEPAGNOT; SIARRY, 2013).

Although metaheuristic algorithms have different principles and concepts, Wolpert e Macready (1997) proved, through the use of bayesian statistics, the No Free Lunch (NFL) theorems which relates to performance comparison between metaheuristic methods. Wolpert e Macready (1997) proved that, through the set of all possible optimization problems, all metaheuristic algorithm have the same mean performance. One direct corollary of such theorem is that if a specific algorithm is *averagely better* than another in a subset of the optimization problems, than it must be *averagely worse* than the other on the rest of the problems.

Since it was proven that a method can only be considered better than another one on a specific subset of all the optimizations problems, one good guideline for choosing a specific algorithm is through the analysis of previous implementation performances on problems with the same characteristics.

The most popular algorithms used to calibrate parameters of a differential equation system are *evolutionary* and *swarm intelligence* based. Both lie on the natural-based scope of the metaheuristic techniques and have been extensively used successfully on engineering and biology model calibration (BOUSSAïD; LEPAGNOT; SIARRY, 2013).

2.5.1 Multiple Objective Optimization

Typically, finding the set of global bests of a multi-objective optimization and proving its optimality is unachievable. Therefore, most methods that solve MO problems are based on iteratively updating a set of equally good solutions until a certain stop criteria is satisfied. This set is commonly refered to as Pareto-front, and the term true Pareto-front is used when referring to the actual Pareto-front of the problem.

According to Reyes-sierra e Coello (2006), when solving multi-objective problems, there are three main goals to achieve:

1. Variety: Obtaining the maximum number of elements in the Pareto-optimal set.

2. Quality: Minimizing the distance of the Pareto-front produced by the optimization technique and the true Pareto-front.

3. Spread: Maximizing the spread of solutions found, in order to achieve a solution's distribution as uniform and smooth as possible.

Note that goals 1 and 3 are exclusive to multiple objective, since the Pareto-front and Pareto-optimal set are not singletons, while goal 2, although simplified, is also present in single objective optimization problems. Additionally, discontinuity and local optima convergence are common in multiple objective problems, such problems are typically more computationally complex and cost-worthy than its single objectives counterparts.

2.5.2 Evolutionary Optimization

Although there are many different evolutionary metaheuristics, the *Genetic Algorithm* (GA) is arguably the most studied one, both theoretically and in practice. The GA method, whose creation is generally attributed to Holland (1975), is based on the natural selection proposed by Darwin and uses genetic operators, such as crossover and mutation, to pseudo-randomly generate new individuals, which then endure a selection based on a quality evaluation procedure. This technique have also been extensively and successfully

applied in the engineering model calibration scope, e. g., Ndiritu e Daniell (2001), Liu et al. (2007), and Spiliopoulou et al. (2015).

Ndiritu e Daniell (2001) successfully calibrated the SIXPAR rainfall-runoff model through genetic algorithms. The SIXPAR is a hydrological model that is a simplified version of the SAC-SMA model of the United States National Weather Service River Forecasting System. It uses six different parameters to model processes such as percolation and recessions.

Like many others in the field of model calibration, Ndiritu e Daniell (2001) approached the model as a function that maps the parameter space into a value that measures how well the modeled data fit observed values. In this case, the parameter space was six-dimensional and the quality measure was the sum of the least square errors. This approach is used in conjunction with global optimization methods, such as GA, since finding the function minimum is equivalent to finding the best set of parameters by which the model approximates observed data. Ndiritu e Daniell (2001) concluded that for 99% of the random simulations of the genetic algorithm, the model calibration was successful and the sum of the least square errors values was below 0.001.

Liu et al. (2007) applied the genetic algorithm technique to calibrate the diffuse PIT model for the Windrush catchment in England. The PIT model is a semi-distributed, GIS-based, non-point phosphorous model with annual time step, it uses three layers to represent the phosphorous transfer from animal manure to the soil, and ultimately to the river. By being a semi-distributed, cell-divided model, PIT has 78 parameters that needs to be calibrated, which consequently makes for a 78-dimensional search space for the best set of parameters. The model was successfully calibrated by (LIU et al., 2007), using only the phosphorous concentration in the river and model input data such as satellite-derived land cover and agricultural census data. The model was calibrated for the year 1995 and validated for the year 2000. The PIT model was recoded within Matlab in order to reduce the computational cost of the simulations. This resulted in a two-minute total calibration time, which meant 16,000 simulations required 8 milliseconds each.

Liu et al. (2007) also addressed the philosophical question that commonly arises during the calibration process: *"When multiple parameter sets are returned from calibrations that are made using potentially different observed datasets, which one of them is the right one?"* Such question is somewhat evaluated by computing a sensitivity factor for each parameter, in which the absolute difference between multiple sets is divided by its average, resulting in a scaled difference between the values of the parameters.

2.5.3 Swarm Intelligence Optimization

Particle Swarm Optimization (PSO) is one of the many global optimization techniques that is based on artificial swarm intelligence. PSO was initially proposed by

Kennedy e Eberhart (1995) as an optimization technique for nonlinear functions that is based on swarm movement such as bird flocking and fish schooling. Besides the ties to swarm intelligence, PSO is also based heavily on evolutionary computation and genetic algorithms.

According to Kennedy e Eberhart (1995) the five principles of swarm intelligence are:

1. Proximity: ability to compute simple space and time operations;
2. Quality: ability to respond to quality factor in the environment;
3. Diverse response: individuals must not respond equally to environment changes;
4. Stability: individuals must not change its behavior every time the environment changes;
5. Adaptability: individuals must be able to change their behavior if it is advantageous.

PSO is based on the movement of particles that communicate with one another regarding its personal best position, evaluated by the objective function. The algorithm is based in pseudo-aleatory value selection, which enables it to escape local optima, since movements in the search space may result in worse objective function values.

The movement of particles is dictated by their velocities, which are in turn based on the personal best position of the particle, the best position of its neighboring particles and its previous velocity. How much each of these criteria influence this movement is calculated as a product of PSO parameters and pseudo-random values. After a new position is set, the particle is re-evaluated, and its personal best updated accordingly. This process is repeated until the stop criteria is met and the best position among the personal bests of all particles (global best) is returned. (EBERHART; KENNEDY, 1995).

The manner in which particles communicate varies according to the implementation. There are many communication topologies such as: full communication, where every particle communicates with one another, and therefore neighboring personal best coincide with the global best; and the ring topology, where each particle communicate only with two previously selected particles. The impact of different communication topologies is further explored by Kennedy e Mendes (2002).

Ever since its creation, PSO has been the focus of much research, and therefore a plethora of modifications and improvements are available to choose from when designing a new application. Regarding problems in which more than one objective are optimized, Reyes-sierra e Coello (2006) presented and classified several different Multiple Objective Particle Swarm Optimization (MOPSO) implementations.

According to Reyes-sierra e Coello (2006), most MOPSO implementations fall under one of four categories:

1. Aggregated: multiple objectives are combined into a single one, through the use of aggregating functions, such as a weighted mean of the different objectives. The weights of each objective can be constant or vary over the run of the optimization.
2. Lexicographic Ordered: different objectives are ranked in an order of importance and the minimization of each one of them is done separately according to the assigned order.
3. Sub-populated: several sub-populations are used, typically one per objective. Populations also typically communicate and recombine with one another.
4. Pareto-based: a non-dominated set of solutions, which are potential swarm leaders, is kept and updated throughout the simulation. Such set, referred to external archive, ideally approaches the Pareto-front as more iterations are ran.

Early multiple objective particle swarm optimization implementations are typically under the aggregation category. They aggregate problems into a single objective to enable the use of single objective optimization methods. Recent approaches, however, focus on the combination of multiple methods such as sub-populated methods with different aggregating functions and weights.

Since without the use of an aggregating function, solutions in the Pareto-front are of equal quality, Pareto-based approaches are arguably more efficient since they potentially return the whole Pareto-front of the problem, meanwhile aggregated and lexicographic order techniques return only one solution. However, Pareto-based approaches have several additional steps, such as: selecting which particles from the external archive will be used as leaders, maintaining and updating the external archive, and promoting diversity to avoid convergence to a single solution.

Focusing on leader selection and mutation, Coello, Pulido e Lechuga (2004) developed a MOPSO variation which applies the notion of hypercubes of adaptable equal sizes that are used to increase the exploration of unpopulated areas. The leader selection is based on a Roulette-Wheel process in which the probability of each Pareto solution being selected is inversely proportional to the number of solutions that are in the same hypercube, i. e., solutions that are in less populated cubes are more likely to be selected. In order to limit the size of the archive, when a nondominated solution needs to enter a full archive, a Pareto solution is removed from the set according to a probability that is also proportional to its hypercube density. The mutation operator is based on pseudo-random number generation inside a dynamic mutation range (around the current value) that shrinks as more iterations are executed. In early stages, where exploration processes are

stimulated, this mutation range tends to be close to the actual lower and upper bound of the variable, whereas later in the simulation the range is small and centered in the previous variable value.

Coello, Pulido e Lechuga (2004) used different measures to analyze the three MOP goals mentioned in Subsection 2.5.1: the Generational Distance (GD) and the Spacing (SP). The GD value regards to the quality goal and measures the average distance between the current and the true Pareto-optimal set, i. e. it is only applicable to problems in which the true Pareto-front is already known, while SP regards to the spread property and measures the average distance between neighboring Pareto-optimal solutions. The authors also compared their algorithm performance against three other multiobjective optimization evolutionary methods using different test functions and different PSO parameter values. The main conclusion was that, averagely their MOPSO implementation outperforms the other methods and therefore is a viable alternative to solve MOPs.

Fieldsend e Singh (2002) applied the Nondominated Tree technique, to solve MOPs using multiobjective particle swarm optimization with unconstrained external archive size. According to the authors, limiting the size of the external archive may cause the Pareto-front to shrink, oscillate and retract. However an uncontrolled growth of the external archive may also present difficulties, like excessive memory usage and the computational time that is expended to search for solutions and update the archive.

To mitigate these difficulties Fieldsend, Everson e Singh (2003) developed the Nondominated and Dominated Trees data structures. In these structures Pareto-optimal solutions are also represented through composite points in the objectives space. Such points are constructed in a way that enables ordering according to the weakly-dominance relationship. The distinction between Nondominated and Dominated Trees is in the construction, based on a preexisting Pareto-front, process: to construct dominated/nondominated tree's first composite point, the unused Pareto solution with the maximum/minimum coordinate in the first objective axis is used to represent the point's first coordinate, the solution is then marked as used and the process is repeated for the second, third and n-th objectives, until all the coordinates of the point are set. The processes is then repeated until there are no unused solutions.

Although such structure enables faster queries and insertion of solutions, the dominated and nondominated trees needs to undergo a systematic cleanup processes, in which they are recreated from the current Pareto-optimal set. Such approach is best used in problems where the Pareto-front is heavily populated, otherwise the cost of the trees maintenance may outweigh the decreased search time. This technique is also not necessary in problems where most of the algorithm's computational time is spent during particle evaluations, e. g., calibration of computationally expensive models, since the time spent to query and insert Pareto-optimal solutions is irrelevant when compared to the one spent

during evaluation routine.

Alvarez-Benitez, Everson e Fieldsend (2005) presented a novel method to select the swarm leader from the external archive in order to promote diversity in the Pareto-optimal set. The technique, referred to as PROB, is based on assigning different selection probabilities to solutions in the archive, and is a combination of two other methods RAND and ROUND which are also described in the same article. Higher probabilities are attributed to solutions that dominate fewer swarm members and vice-versa. Simulation results were measured by the Generational Distance and the Volume Measure method and a successful increase in the Pareto-front diversity was noted.

In a similar way Ho et al. (2005) applied a technique, where a strength value is attributed to Pareto-front solutions that is proportional to the amount of swarm members they dominate, in order to increase the Pareto-optimal set diversity. Additionally, an age criteria is introduced to promote solutions that recently added to the Pareto-front, was also added to promote diversity.

On the single objective scope, Jiang et al. (2007) incorporated concepts from competitive evolution and complex shuffling into a particle swarm optimization technique, developing the Improved Particle Swarm Optimization (IPSO) method. IPSO is based on iteratively partitioning the population into sub-swarms that are independently optimized and subsequently combined and shuffled. The population is partitioned according to the quality of the particles, i. e. particles that initially have similar function values are in the same swarm. During each sub-swarm internal optimization only a subset of the particles are selected, with better located particles having higher probabilities of being selected, to be moved and evaluated. Such partitioning and selecting methods were developed to ensure competition among particles.

Jiang et al. (2010) later extended this concept and introduced the Master-Slave swarm Shuffling Evolution Particle Swarm Optimization (MSSE-PSO). This approach is similar to the one presented by Jiang et al. (2007), but has the addition of a master sub-swarm that uses the best position among all sub-swarms on its velocity calculation. These techniques, along with the typical PSO implementation, were analyzed using usual benchmark mathematical functions and the results showed that while the IPSO outperforms the usual implementation, the MSSE-PSO outperforms both IPSO and usual PSO implementations without significant additional computational cost.

To mitigate the premature convergence problems of PSO, Ardizzon, Cavazzini e Pavesi (2015) presented the Adaptive Search Diversification Particle Swarm Optimization (ASD-PSO) technique. The ‘explorer-settler’ approach was used, where a particle has either a role of ‘explorer’, that are more focused with searching outside the known domain, or ‘settler’, with a larger focus on local optimization. To implement such concepts the authors used previously published techniques such as adaptive control of the inertia and

acceleration weights with higher inertial weights to explorers and higher acceleration weights to settlers. Techniques such as random restart of converged particles and local uniform random search around the global best have also been implemented to avoid early convergence and enhance local search.

On the model calibration scope, Gill et al. (2006), Jiang et al. (2007), Jiang et al. (2010), Afshar, Kazemi e Saadatpour (2011) and Zambrano-Bigiarini e Rojas (2013) successfully applied variations of the standard PSO technique to automatically calibrate different hydrological and water quality models.

Gill et al. (2006) applied a MOPSO technique to calibrate the SACSMA hydrological model for the Leaf River watershed, near Collins, Mississippi. The Sacramento soil moisture accounting model (SACSMA) is a well known conceptual rainfall-runoff model, it has 16 different calibration parameters and require daily precipitation and potential evapotranspiration data series to output modeled daily runoff data. Unlike most researchers, the authors used two different but very similar quality measures (RMSE and BIAS) of the same output data as multiple objectives to optimize. While different objectives, such as flood predictions, would possibly yield better results, Gill et al. (2006) deemed the results satisfactory and that the model output for the different Pareto-front solutions showed good agreement with observed data.

Jiang et al. (2007) and Jiang et al. (2010) calibrated the IPSO and MSSE-PSO single objective methods to calibrate the Xinanjiang conceptual hydrological model for the Tianfumiao reservoir and the Huangbohe basin, both located in Hubei province of China. The Xinanjiang model has 15 parameters and requires daily rainfall and evapotranspiration data series to simulate daily runoff data, it was calibrated using five years and tested with two years of data. On average, the calibration process took around 50 minutes and the relative errors and R^2 coefficients of the comparison between modeled and observed runoff data was deemed as satisfactory.

Afshar, Kazemi e Saadatpour (2011) applied particle swarm optimization to calibrate the CE-QUAL-W2 large scale water quality model for the Karkheh Reservoir in Iran. Since the author's goal was to calibrate the model regarding both water elevation and water temperature observed data, an aggregation based MOPSO technique was used. Different aggregating weights combinations were analyzed and the one that yielded the best result, i. e., lowest errors, was used to further compare manual and automatic calibration results. Eight months of data for two different stations in the Karkheh reservoir was used in the calibration process with average absolute errors ranging from 0.5 to 2 degrees Celsius.

2.6 OVERVIEW OF LITERATURE REVIEW

Given the complexity of carbon dynamic processes and the low spatial and temporal resolution of available measured reservoir data, estimations regarding the role of these inland aquatic systems in the global climate are highly debatable. The accuracy of such estimations is subject to a plethora of uncertainties regarding: errors in point measurements due to the impact of the measuring technique itself on the system, e. g., floating chambers; extrapolation of point measurements to total estimations; generalization of estimations on short periods of times to assess both future and past data; and indexes utilized to compare both direct and indirect global warming potential of different greenhouse gases.

Mathematical models are used to simulate the processes related to the carbon cycle on both inland waters and oceans. These models vary according to different purposes and theoretical hypotheses, and therefore have different levels of complexity regarding spatial dimensionality, temporal resolution and modeled biochemical processes. All these models have numerical parameters that require adjustment to fit a given study area measured data. The process of finding values for these parameters is referred to as calibration.

Model calibration can be done by minimizing differences between measured data and the results of the model for a given set of parameters. Both exact and metaheuristic optimization methods can be used to minimize such error, but the former require certain characteristics, such as differentiability and continuity of the objective function, to be applied. Whether multiple objectives are simultaneously optimized or a single objective function is minimized impact the choice of a proper calibration algorithm. Given the complex nature of the carbon dynamic models and their calibrations, metaheuristic techniques are mainly used as optimization algorithms in this scope. Among these artificial intelligence metaheuristic techniques, the swarm intelligence based algorithms were widely used as calibration routines.

3 CICLAR MODEL AND STUDY AREA

> Far better an approximate answer to the right question, which is often vague, than an exact answer to the wrong question, which can always be made precise.
>
> John W. Tukey

3.1 MODEL CONCEPTS

CICLAR is a lumped model for carbon dynamics in lakes and reservoirs. Neither vertical nor horizontal spatial variations are modeled characterizing a fully mixed approach, in which only time variations are considered. The model is based on aggregation of different carbon forms into six compartments (Table 1). The carbon transfer from one compartment to another, when present, is modeled as a first order reaction, based on the reactant concentration. The model uses a daily time-step to compute the evolution of daily averaged physical quantities.

Table 1 – CICLAR carbon compartments

Compartment	Abbreviation
Dissolved Inorganic Carbon	DIC
Dissolved Organic Carbon	DOC
Live Particulated Organic Carbon	POC_L
Dead Particulated Organic Carbon	POC_D
Labile Sedimented Carbon	SC_L
Refractory Sedimented Carbon	SC_R

Inorganic forms of dissolved carbonic gas from the carbonate system compose the DIC (CO_2, HCO_3^- e CO_3^{2-}) compartment. Phytoplankton, zoo-plankton and other living organisms are considered in POC_L, while POC_D has a similar composition but does not contain photosynthetic organisms and, through resuspention, represent an entry for sedimented carbon. Labile and refractory sedimented carbon are separated in order to differentiate unstable, fast reacting, methane producing, labile substances from stable, refractory substances that react slowly producing less methane. The SC_R compartment is used to represent the carbon sink characteristic present in many lakes and reservoirs.

In CICLAR, methane is only emitted through ebulitive processes, while carbon dioxide is emitted through diffusive processes. The CO_2 emission is calculated through Henry's law, where the gas partial pressure in water is estimated based on DIC concentration while the input atmospheric partial pressure is set as constant 0.0003 atm.

Figure 2 displays the different carbon compartments and the mass transfer among them as boxes and arrows, respectively. The organic to inorganic carbon transformations are referred to as respiration, and occurs from the dissolved and particulated organic carbon to the dissolved inorganic carbon compartment. The inorganic to organic carbon transformation is due to photosynthetic processes that transfer carbon from the DIC to POC_L compartment.

Figure 2 – CICLAR conceptual carbon dynamic model

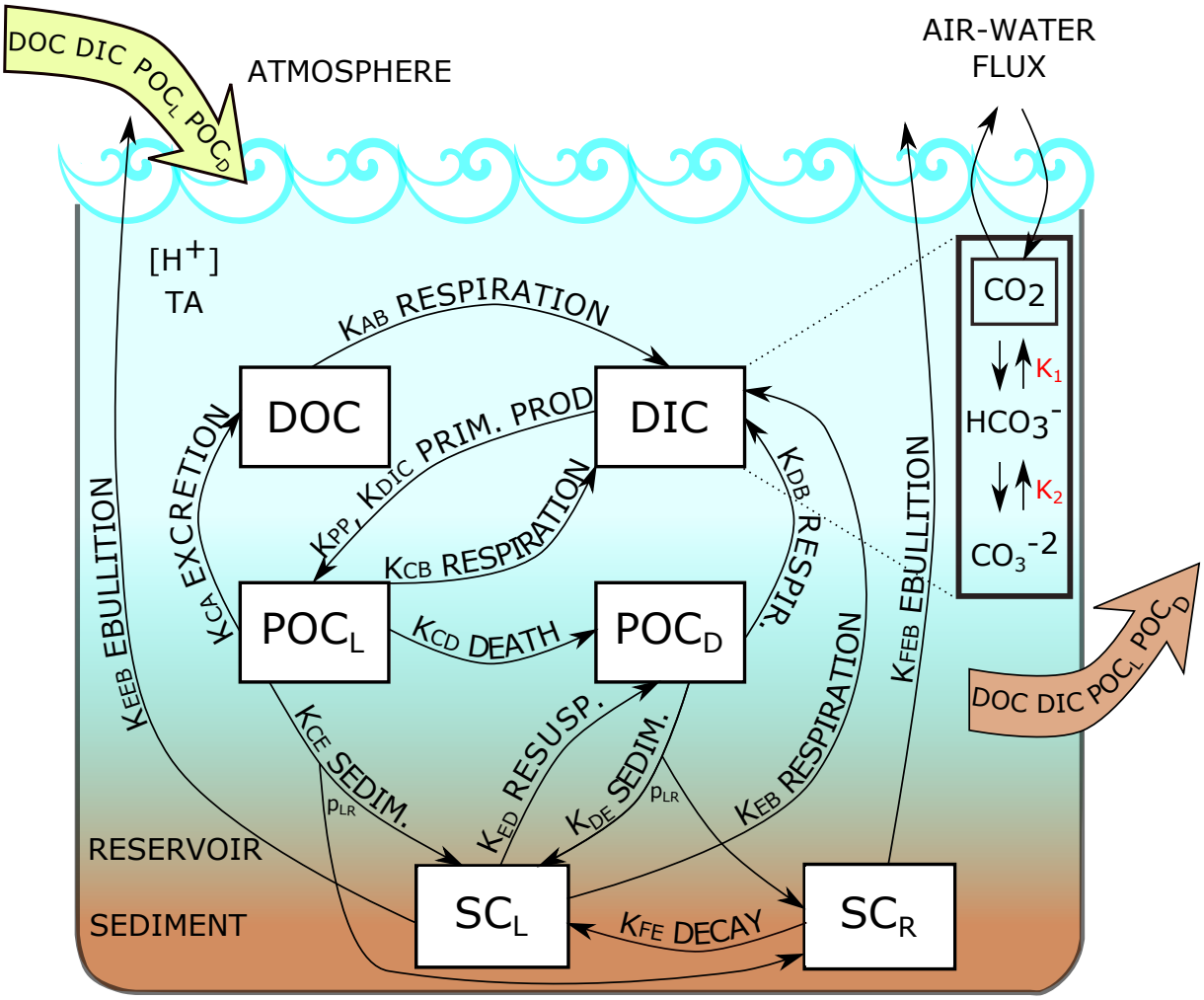

Living organisms produce dissolved organic carbon through excretion, and are subject to sedimentation and death, producing sedimented carbon and dead particulated carbon, respectively. Both, refractory and labile sedimented carbon are subject to ebullition (although with potentially different rates), but only the labile fraction is subject to resuspension to the water column while the refractory portion is gradually decayed into labile sedimented carbon. Sedimentation from dead and live particulated carbon through the K_{DE} and K_{CE} coefficients is divided between the labile and refractory compartments according to the p_{LR} parameter.

Primary production is calculated based on: the current and maximum solar

radiation, the DIC and POC_L concentrations, the primary production coefficient K_{PP} and the DIC half-saturation constant K_{DIC}. A summary of the different processes and their corresponding rates is given in Table 2.

Table 2 – CICLAR parameters

Parameter	Description	Reaction			Unit
K_{AB}	Respiration	DOC	$\rightarrow$	DIC	[d^{-1}]
K_{CA}	Excretion	POC_L	$\rightarrow$	DOC	[d^{-1}]
K_{CB}	Respiration	POC_L	$\rightarrow$	DIC	[d^{-1}]
K_{CD}	Death	POC_L	$\rightarrow$	POC_D	[d^{-1}]
K_{DB}	Respiration	POC_D	$\rightarrow$	DIC	[d^{-1}]
K_{CE}	Sedimentation	POC_L	$\rightarrow$	SC_L & SC_R	[d^{-1}]
K_{DE}	Sedimentation	POC_D	$\rightarrow$	SC_L & SC_R	[d^{-1}]
K_{ED}	Resuspension	SC_L	$\rightarrow$	POC_D	[d^{-1}]
K_{EB}	Respiration	SC_L	$\rightarrow$	DIC	[d^{-1}]
K_{EEB}	Ebullition	SC_L	$\rightarrow$	Atm.	[d^{-1}]
K_{EF}	Decay	SC_R	$\rightarrow$	SC_L	[d^{-1}]
K_{FEB}	Ebullition	SC_R	$\rightarrow$	Atm.	[d^{-1}]
K_{PP}	Primary Production	DIC	$\rightarrow$	POC_L	[d^{-1}]
K_{DIC}	DIC Half-Saturation	DIC	$\rightarrow$	POC_L	[mg/l]

Carbon enters the system through inflow (green arrow in Figure 2) both in the dissolved and particulated forms. There are three carbon outlets of the system: methane emitted through ebullition of sedimented carbon and in dissolved and particulated forms that are carried by outflow (brown arrow in Figure 2). Carbon may also enter/exit the system through diffusion at the air-water interface, when the partial pressure of dissolved CO_2 in the system is lower/higher than the atmospheric one.

CICLAR requires a variety of input data: time series of monthly averaged hydrological, meteorological and water quality data (Table 3) and reservoir data (Table 4).

Table 3 – CICLAR time series input data

Hidrological and Meteorological			Water Quality		
Var.	Name	Dim.	Var.	Name	Dim.
Q_{in}	Inflow	[m^3/s]	T_{Win}	Inflow Temperature	[^oC]
Q_{out}	Outflow	[m^3/s]	pH_{in}	Inflow pH	-
T_{air}	Air Temperature	[^oC]	DOC_{in}	Inflow DOC	[mg/l]
U	Relative air Humidity	-	DIC_{in}	Inflow DIC	[mg/l]
V_w	Wind Velocity	[m/s]	POC_{Lin}	Inflow POC_L	[mg/l]
			POC_{Din}	Inflow POC_D	[mg/l]

The time series from Table 3 are monthly averaged in climatological mean values, which are cyclically used by the model. Since the model uses a daily time-step, linear interpolations are used to extract daily averages from monthly data series.

A water budget is calculated in order to obtain reservoir volume from the input inflow and outflow series. Since CICLAR can simulate an arbitrarily long period and that it cyclically uses monthly averages, the equality of the sums of the inflow and outflow

series is required. If such restriction is not satisfied, the model automatically adjust outflow data, by multiplying each value by a factor r ($r = \sum Q_{in} / \sum Q_{out}/12$).

Table 4 – CICLAR reservoir and initial data

Reservoir Characteristics	Initial Data	
Minimum Volume [m^3]	Temperature [^oC]	DOC
Latitude	pH	DIC
Sediment Depth [m]	Soil Carbon [kg/m^2]	POC_L
CO2 Atmospheric Pressure [atm]	Vegetation Carbon [kg/m^2]	POC_D
Depth-Area Curve		

The model calculates the initial volume so that, given input inflow and outflow series, the minimum volume of the reservoir is reached at least once along the yearly cycle. This is done by finding the minimum volume of a yearly water budget with zero as initial volume and subtracting it from the minimum volume of the reservoir (Table 4).

Given the importance of temperature in biochemical reactions, a heat budget is also calculated on the model. This calculation is based both on inflow temperature (Table 3) and surface heat exchange, i. e. solar radiation, atmospheric radiation, water emitted radiation and conduction/convection induced heat exchanges.

Being a part of the carbonate system (DIC), the hydron (H^+) concentration, or pH, is also assessed. In CICLAR, the only acid-base reactions considered is the carbonate and water dissociation ones, depicted on Table 5, and the total alkalinity is calculated as the hydroxide concentration that would neutralize the solution. After the alkalinity computation, pH is obtained by solving a polynomial equation whose coefficients are based on: total alkalinity, DIC concentration, and water dissociation equilibrium constants.

Table 5 – Carbonate system reactions

$CO_2 + H_2O$	$\overset{K_1}{\rightleftharpoons}$	$H^+ + HCO_3^-$
HCO_3^-	$\overset{K_2}{\rightleftharpoons}$	$H^+ + CO_3^{-2}$
H_2O	$\overset{K_W}{\rightleftharpoons}$	$H^+ + OH^-$

3.2 MATHEMATICAL FORMULATION

Given that the CICLAR is a lumped model, all processes mentioned in Section 3.1 are treated as ordinary first order differential equations in time. The carbon concentrations

of each compartment varies over time, and are mathematically formulated as:

$$\frac{dC_{DOC}}{dt} = \frac{Q_{in}C_{DOC_{in}} - Q_{out}C_{DOC}}{V} + K_{CA}C_{POC_L} - K_{AB}C_{DOC} \tag{3.1a}$$

$$\frac{dC_{DIC}}{dt} = \frac{Q_{in}C_{DIC_{in}} - Q_{out}C_{DIC}}{V} + K_{CB}C_{POC_L} + K_{DB}C_{POC_D} + K_{AB}C_{DOC} - PP + K_{EB}C_{SC_L}\frac{V_s}{V} - \frac{A \times F_{CO_2}}{V} \tag{3.1b}$$

$$\frac{dC_{POC_L}}{dt} = \frac{Q_{in}C_{POC_{Lin}} - Q_{out}C_{POC_L}}{V} - K_{CB}C_{POC_L} - K_{CA}C_{POC_L} - K_{CD}C_{POC_L} + PP - K_{CE}C_{POC_L} \tag{3.1c}$$

$$\frac{dC_{POC_D}}{dt} = \frac{Q_{in}C_{POC_{Din}} - Q_{out}C_{POC_D}}{V} + K_{CD}C_{POC_L} - K_{DB}C_{POC_D} + K_{ED}C_{SC_L}\frac{V_s}{V} - K_{DE}C_{POC_D} \tag{3.1d}$$

$$\frac{dC_{SC_L}}{dt} = (-K_{EEB} - K_{EB} - K_{ED})C_{SC_L} + K_{FE}C_{SC_R} + p_{LR}\frac{V}{V_s}(K_{DE}C_{POC_M} + K_{CE}C_{POC_L}) \tag{3.1e}$$

$$\frac{dC_{SC_R}}{dt} = -K_{FE}C_{SC_R} - K_{FEB}C_{SC_R} + (1 - p_{LR})\frac{V}{V_s}(K_{DE}C_{POC_M} + K_{CE}C_{POC_L}) \tag{3.1f}$$

where V and V_s [m^3] indicate reservoir and sediment volumes, respectively, A [m^2] is the reservoir surface area, C_x [mg/l] is the concentration on compartment x, PP [mg/ld] is the primary production, F_{CO_2} [mg/m^2d] is the carbonic gas flux at the air-water interface and p_{LR} indicates the percentage of the sedimentation that goes to the labile sedimented carbon compartment.

DIC concentration is the sum of the inorganic carbon represented by:

$$C_{DIC} = [CO_2] + \left[HCO_3^-\right] + \left[CO_3^{-2}\right] \tag{3.2}$$

where the brackets indicate concentration [mg/l].

The effect of temperature on biochemical reaction rates is modeled by:

$$K^* = K_{20}\theta^{T-20} \tag{3.3}$$

where K_{20} [d^{-1}] is the value of the parameter at 20^{o}C, K^* [d^{-1}] is the value at a given temperature T [^{o}C] and θ is an adimensional coefficient. Equation 3.3 is applied to all parameters in Table 2, i. e., the K_{20} input value is transformed into K^*, to be used in Equations 3.1, in every time-step.

Temperature effects (PLUMMER; BUSENBERG, 1982) on the equilibrium constants of the carbonate system (K_1 and K_2 from Table 5) are also incorporated in the

model through:

$$log(K_1) = -356.3094 - 0.06091964T + 21834.37/T + 126.8339\,log(T) - 1684915/T^2 \tag{3.4a}$$

$$log(K_2) = 107.8871 - 0.03252849T + 5151.79/T + 38.92561\,log(T) - 563713.9/T^2 \tag{3.4b}$$

Primary production is calculated according to:

$$PP = K_{PP}\frac{I}{I_S}e^{1-I/I_S}\frac{C_{DIC}}{K_{DIC}+C_{DIC}}C_{POC_L} \tag{3.5}$$

where K_{PP} and K_{DIC} are parameters described on Table 2, I [W/m^2] is the solar radiation and I_S [W/m^2] is the radiation for which the the primary production is at its peak.

CO_2 flux at the air-water interface, represented by the last term of Equation 3.1b, is calculated according to Henry's law (Equation 3.6). Gas dissolution in water is proportional to the pressure it does on the liquid as:

$$F_{CO_2} = k\left([CO_2]_W - [CO_2]_E\right) \tag{3.6}$$

where k [m/s] is the gas transfer velocity, $[CO_2]_W$ and $[CO_2]_E$ are water and equilibrium carbon dioxide concentrations [mg/l], respectively (STUMM; MORGAN, 1993).

The gas transfer velocity k is mainly dependent on wind velocity and air temperature and is calculated according to the adimensional Schmidt number (Sc), which represents the ratio between water's kinematic viscosity and the gas diffusion coefficient in water. Wanninkhof (1992), developed a polynomial equation to evaluate Schmidt number's values for CO_2 in temperatures varying between 0 and 35^{o}C:

$$k = 0.39u_{10}^2\left(\frac{Sc}{660}\right)^{-0.5} \tag{3.7a}$$

$$Sc = 1911.1 - 118.11T - 3.4527T^2 - 0.041320T^3 \tag{3.7b}$$

where u_{10} [m/s] is the wind velocity at 10 meters height, T is the water temperature and the value 660 is the Schmidt number for CO_2 at 20^{o}C in salty waters.

The carbon dioxide equilibrium concentration ($[CO_2]_E$) is calculated based on the carbonic gas partial pressure and the dimensional Henry's coefficient K_H:

$$[CO_2]_E = K_H\,pCO_2\,12000 \tag{3.8a}$$

$$log(K_H) = 108.3865 + 0.01985T - 6919.53/T - 40.45154\,log(T) + 669365/T^2 \tag{3.8b}$$

where pCO_2 is the input partial CO_2 pressure in the atmosphere (Table 4) and 12000 converts mol to milligram unit. Temperature is used in K in Equations 3.7 and 3.8 (STUMM; MORGAN, 1993) (PLUMMER; BUSENBERG, 1982).

Dissolved carbon dioxide concentration ($[CO_2]_W$) is not explicitly modeled by CICLAR, and therefore is calculated based on DIC concentration, pH, and the carbonate system equilibrium constants, according to:

$$[CO_2]_W = \frac{C_{DIC}\,[H^+]^2}{[H^+]^2 + K_1\,[H^+]^2 + K_1K_2} \tag{3.9}$$

which is derived from Table 5 and Equation 3.2, and where K_1 and K_2 are the carbonate's reactions equilibrium constants (Table 5).

Total alkalinity (TA) is defined as the quantitative capacity of an aqueous solution to neutralize an acid, i. e. the quantity of electrons it can neutralize. In the scope of the carbonate and water dissociation systems (Table 5) TA can be defined according to Equation 3.10a, and expressed in terms of pH and DIC concentration as Equation 3.10b.

$$TA = \left[HCO_3^-\right] + 2\left[CO_3^{-2}\right] + \left[OH^-\right] - \left[H^+\right] \tag{3.10a}$$

$$TA = \frac{C_{DIC}}{12000}\frac{K_1\,[H^+] + 2K_1K_2}{[H^+]^2 + [H^+]\,K_1 + K_1K_2} + \frac{K_W}{[H^+]} - \left[H^+\right] \tag{3.10b}$$

Since total alkalinity is also time varying, its rate of change is also be modeled as a first order differential equation over time as

$$\frac{dTA}{dt} = \frac{Q_{in}TA_{in} - Q_{out}TA}{V} - \frac{18}{106}\sum R \tag{3.11}$$

where TA_{in} is the inflow's total alkalinity, calculated according to inflow's pH and DIC concentration, and R refers to all reactions in Equation 3.1b. The term $\frac{18}{106}$, is used to represent the phytoplankton's metabolism and organic matter degradation stoichiometry, according to Redfield, Ketchum e Richards (1963) approximation for the 106 C:18 H^+ alkalinity.

After DIC and TA values are updated, through the use of Eqs. 3.1b and 3.11, the system's pH needs to be reassessed, and to do so, Equation 3.10b is used with $[H^+]$ being the independent variable. Equation 3.12a is the transcendental equation a needs to be solved in order to determine the new hydron concentration, and Equation 3.12b is the equivalent fourth order polynomial equation.

$$f\left(\left[H^+\right]\right) = TA - \hat{C}_{DIC}\frac{K_1\,[H^+] + 2K_1K_2}{[H^+]^2 + [H^+]\,K_1 + K_1K_2} - \frac{K_W}{[H^+]} + \left[H^+\right] \tag{3.12a}$$

$$\begin{aligned} f\,(x) = x^4 + (K_1 + TA)\,x^3 + \left(K_1TA - K_1\hat{C}_{DIC} - K_1K_2 - K_2\right)x^2 + \\ \left(K_1K_2 - K_1K_W - 2K_1K_2\hat{C}_{DIC}\right)x - K_1K_2K_2 \end{aligned} \tag{3.12b}$$

where $\hat{C}_{DIC}$ is used to indicate the molar concentration of DIC, i. e. $\hat{C}_{DIC} = \frac{C_{DIC}}{12{,}000}$.

The heat budget model used in CICLAR is also based in an ordinary differential equation in time to calculate the rate of change of temperature. This calculation, based

on the combination of heat transfer through inflow, outflow, and surface heat exchange through radiation. Being a fully mixed model, vertical temperature variations that typically occur in water system and processes such as thermal stratification are not incorporated into CICLAR, and the temperature is calculated through:

$$\frac{dT}{dt} = \frac{Q_{in}T_{in} - Q_{out}T}{V} - \frac{A_S}{\rho C_P V}\left[R_{SN} + R_{AN} - (R_{BR} + R_C + R_E)\right] \tag{3.13}$$

where T_{in} [^{o}C] is the inflow's temperature (Table 4), ρ [kg/m^3] is the water density, C_P [J/kg^{o}C] is the water's specific heat. The R_{SN}, R_{AN}, R_{BR}, R_C and R_E terms represent net solar shortwave radiation, net atmospheric longwave radiation, longwave water-emitted radiation, conduction and evaporation, respectively. The surface heat exchange model is based on Chapra (2008) and is further elaborated in Appendix A.

3.3 COMPUTATIONAL IMPLEMENTATION

A fourth order Runge-Kutta method (RK4) is used to solve the ordinary differential equation system that is formed by Equations 3.13, 3.11 and 3.1. RK4 is an iterative method based on four slope estimations, it works by using sub-steps inside the original time-step, to obtain intermediate function evaluations that are later used in a weighted average that approximates the function value at the current step.

Different implementations of CICLAR were developed in two programming languages: Python, which includes a user friendly interface that facilitates both the data input and the output analysis processes and C++, which underwent optimization and enables parallel simulations. While both implementations follow about the same simulation scheme, shown in Figure 3, there are some significant differences. Since the C++ optimized version is geared towards calibration, the processes that are not impacted by the kinetic parameters are done separately, in order to reduce the computational cost of evaluating different sets of parameters.

Figure 3 shows the original CICLAR scheme that is implemented in the Python version, where the colors and forms are used to represent three different stages: the cloud represent User Interaction via the interface, the blue stages are executed separately in the optimized version and the green ones are present in both the Python and the C++ versions.

Aside from using precalculated values that are not parameter-dependent, such as temperature and geometric characteristics, the optimized implementation also minimizes the amount of computational expensive operations, e. g. logarithms, potencies and float divisions, inside the main loop by using yearly *lookup tables*.

The heat and carbon/alkalinity balances are done separately in two different Runge-Kutta runs as a consequence of the impact of temperature in the biochemical

Figure 3 – Fluxogram of the CICLAR model

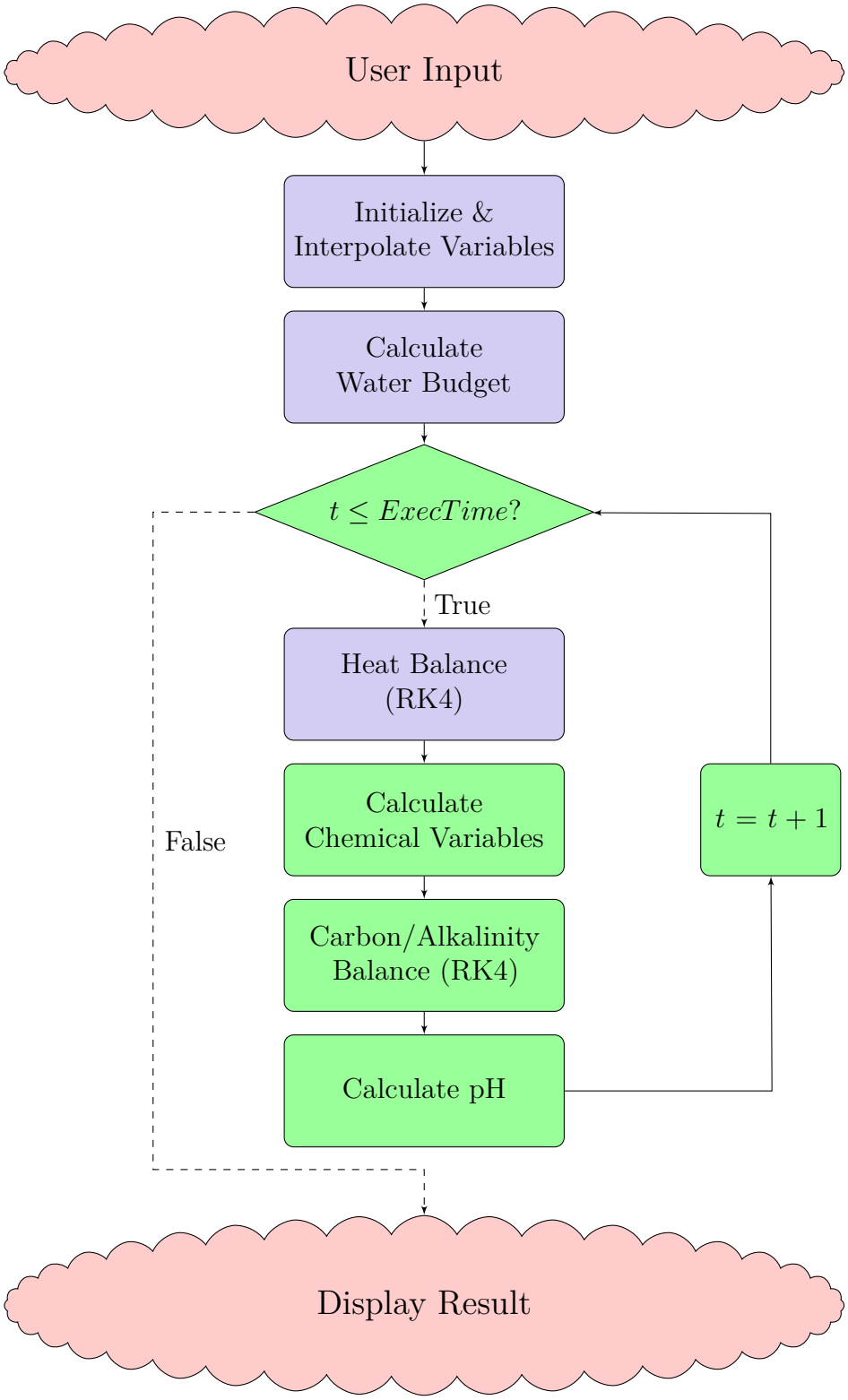

chemical reactions. The biochemical variables calculation refers to variables that are directly dependent of the temperature and the hydron concentration, such as equilibrium constants, Schmidt's number and gas transfer velocity.

Since the alkalinity variation over time is directly related to dissolved inorganic

carbon concentration and its biochemical reactions, Equation 3.11 is solved together with the carbon mass balance equations (Eqs. 3.1).

Being based on the dissolved inorganic carbon concentration, the total alkalinity and the temperature, the pH calculation represents the main loop's last step. The fourth order polynomial equation is solved through the Ferrari method in the Python implementation (via the *roots* function) and using balanced-QR reduction of the companion matrix, that is available in the GNU Scientific Library, in the C++ version.

3.4 STUDY AREA

Capivari reservoir is located, as shown in Figure 4, in the Parana state, near Curitiba City, on Brazil's southern region, and feeds the Governador Parigot de Souza Hydro-power plant, which has a 250 MW installed capacity.

Figure 4 – Capivari reservoir and sampling points locations

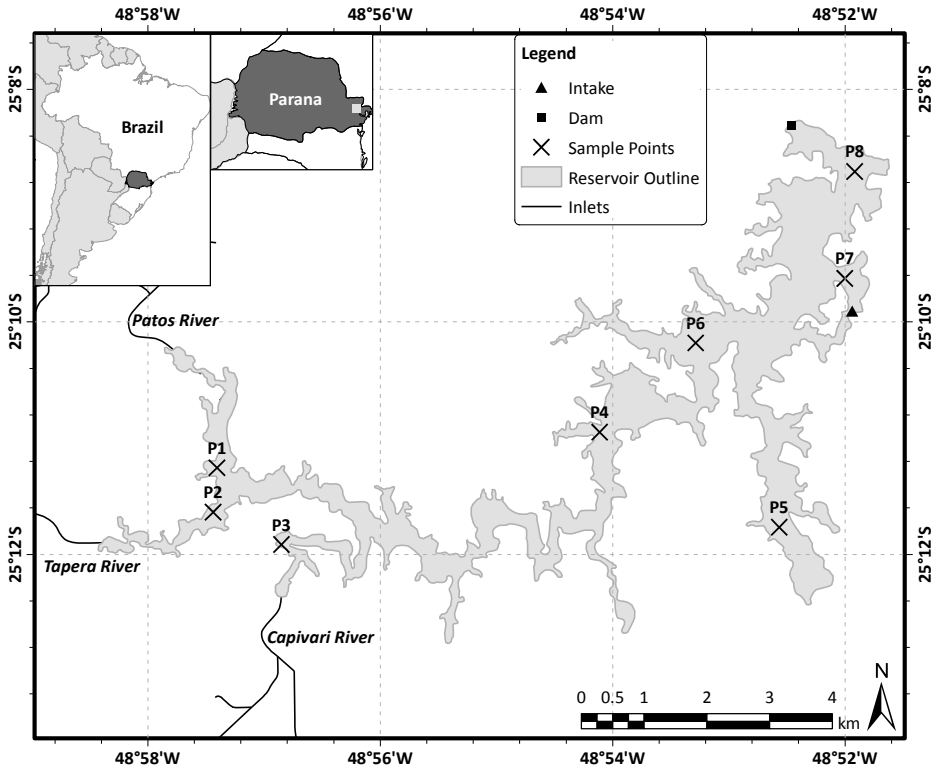

Capivari reservoir is formed mainly by Capivari, Patos and Tapera rivers. The reservoir was constructed in 1970, with 13 km^2 area and 179 hm^3 total volume. It has a 945 km^2 drainage area, 20 m$^3/s$ mean annual flow, 103 days residence time and 14 m mean depth. Less than 8% of its outflow is spilled, i. e. more than 92% of the flow is turbined. The reservoir's characteristics that are used as input for the CICLAR model are shown in Table 6.

Table 6 – Capivari geophysical characteristics

Input	Value	Input	Value
Minimum Volume	21967200.0 m^3	Sediment Depth	1.0 m
Latitude	-25^o	CO_2 Atmospheric Pressure	316 μatm

In order to model the Capivari reservoir, several input data needed to be obtained and estimated. To enable reproducibility, all required data will be displayed in the remaining of this section. Table 7 displays the initial condition of the reservoir, where the carbon concentration regarding soil and vegetation that were present prior to the dam's impoundment were estimated according to Kan et al. (2013).

Table 7 – Capivari reservoir initial data

Initial Data			
Input	Value	Input	Value
Temperature	20 ^{o}C	DOC	1.5 mgL^{-1}
pH	7	DIC	3.0 mgL^{-1}
Soil carbon	12 kgm^2	POC_L	1.0 mgL^{-1}
Vegetation carbon	12.4 kgm^2	POC_D	0.5 mgL^{-1}

The current (2015) carbon stock of the reservoir was estimated based on sediment samples, collected at the sampling points depicted on Figure 4, and on vertical profiles of DOC, DIC, POC and dissolved CH_4. The carbon stock on sediment and on water is estimated to be around 35.2 and 0.5 $kgCm^{-2}$ respectively, resulting on 35.7 $kgCm^{-2}$ current total carbon stock. Since the sediment's carbon stock is 10.8 $kgCm^{-2}$ larger than its initial soil and vegetation carbon, Capivari can be characterized as a carbon sinkhole and presents an equivalent average absorption of 720 $mgCm^{-2}d^{-1}$.

Although the CICLAR model enables the use of monthly averaged inflow's water quality data series, due to the difficulty in obtaining time varying carbon related data for Capivari's tributaries, the stationary values in Table 8 were used instead.

Table 8 – Capivari inflow water quality data

Input	Value	Input	Value
pH_{in}	6.5	POC_{Lin}	0
DOC_{in}	2.5	POC_{Din}	2.5
DIC_{in}	5.0		

Tables containing the monthly averaged meteorological and hydrological data series (Table B1), as well as the points used to interpolate the depth-area-volume curve (Table B2) are in Appendix B.

Meteorologic data shown in Table B1 were obtained from station 25254905 located in the city of Pinhais ($-25.42^oS, -49,13^oO$). Since CICLAR requires monthly averaged

data, the daily data obtained from the station had to be prepared correspondingly.

Inflow data were obtained from station 8129900 (Barragem Capivari - Montante) located in the largest tributary (Capivari river). The fluviometric station is located a few hundred meters upstream of the reservoir and, due to a waterfall, does not present backwater influence. Outflow was obtained from the dam operation company and was estimated based on the hydroelectric energy generation series. Table B1 presents the monthly averaged inflow and outflow series used and Figure 5 depicts its yearly behavior.

Figure 5 – Capivari inflow and outflow yearly cycle

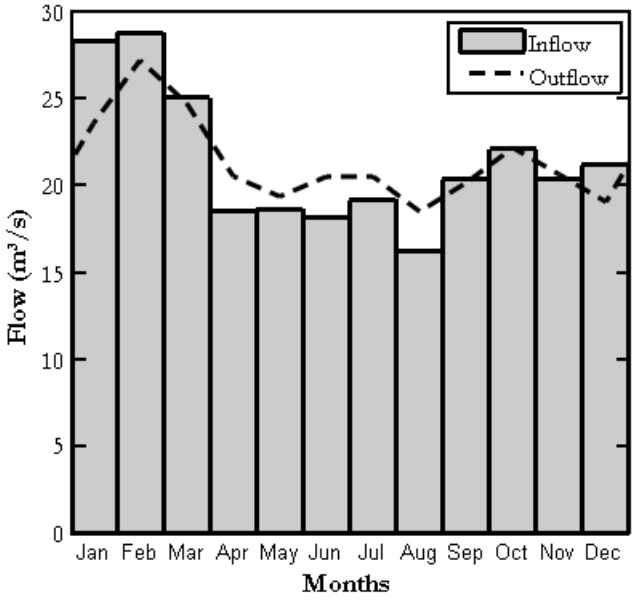

The elevation-area-volume curve of the reservoir that is used to obtain the depth and area from the water budget calculated volume, has its bathymetry points shown in Table B2 and its interpolated plot displayed in Figure 6.

The interpolated curve from Figure 6 was constructed by considering the reservoir as multiple stacked truncated cones with top and bottom circular areas directly extracted from the depth-area curve. The heights of the truncated cones are given by the difference between two adjacent point's depths. Since the volume series of the reservoir is directly calculated through the aforementioned water budget, the calculation of a surface area based on a given volume and the truncated cones interpolation is done by solving third degree polynomial equations.

The greenhouse gas fluxes for the Capivari reservoir were estimated by Mannich et al. (2015). Ebullitive CH_4 fluxes were measured using fixed circular funnels with one meter diameter, while diffusive CO_2 and CH_4 were measured through floating chambers with 23 cm^2 cross section and 1 L volume. Although the fluxes presented high spatial variability, i. e. measured values varied significantly among sample points, only its averages (Table 9) were used to calibrate CICLAR.

Figure 6 – Capivari elevation-area-volume interpolated curve. min WL and max WL denotes the minimum and maximum water level of the reservoir.

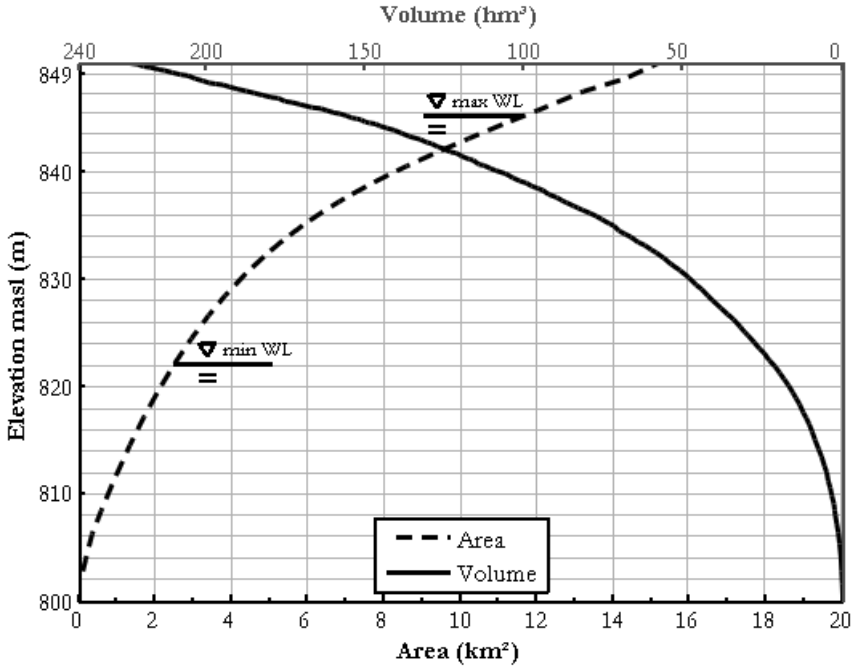

Table 9 – Estimated Capivari CO_2 and CH_4 fluxes

Measurement Dates	Fluxes	
	CO_2 $mgCO_2m^{-2}d$	CH_4 $mgCH_4m^{-2}d$
Nov/Dec 2012	−69.5	19.9
May 2013	262.8	26.6

The data on Table 9 evidences GHG seasonal variation of the emissions, with CO_2 absorption and lower CH_4 emissions during the autumn and higher CO_2 and CH_4 emissions during the spring. This characteristic is attributed to meteorological forcings, and mainly to the higher temperatures that occur in the November-December period.

4 MODEL CALIBRATION

All roads lead to Rome

Roman proverb

4.1 MANUAL CALIBRATION

The CICLAR model was applied to the Capivari reservoir and manually calibrated to fit measured data. Since the output of the model is very sensitive to input chemical kinetic parameters, and there is a lack of calibration data, the main goals during the manual calibration were, in order of importance (MANNICH et al., 2015):

- Obtaining the carbon stock close to the measured value;
- Obtaining CO_2 and CH_4 fluxes inside the measured range
- Obtaining carbon concentrations and pH close to measured intervals.

Upper and lower limits to the parameters in Table 10 were used to reduce the search space and facilitate both manual and automated calibrations. Some of these boundaries were adapted from the review of Mannich (2013), while some were set based on sensitivity analysis of the model.

Table 10 – Lower and upper limits of CICLAR parameters

Param.	Limits		Param.	Limits	
	Lower	Upper		Lower	Upper
K_{AB}[1]	0.02	0.5	K_{EEB}[2]	0	1E−5
K_{CA}[2]	0	1E−2	K_{CD}[1]	0.1	0.5
K_{CB}[1]	0.03	0.4	K_{FE}[2]	0	1E−3
K_{EB}[2]	0	1E−3	K_{FEB}[2]	0	1E−7
K_{CE}[1]	0.5	0.9	K_{DB}[1]	0.02	0.34
K_{DE}[1]	0.5	0.9	K_{PP}[1]	2	3.5
K_{ED}[2]	0	1E−5	K_{DIC}[1]	1	2

[1]Adapted from Mannich (2013)
[2]Estimated values

The calibration process was based mainly on experience with the model and the biochemical reactions that it represents, however it typically takes considerable time and effort to find acceptable values for the parameters in order to satisfy the aforementioned goals. Additionally this method does not offer flexibility, in the sense that if the model was applied to a different reservoir, the whole calibration process would need to be redone.

4.2 PARTICLE SWARM OPTIMIZATION AND CALIBRATION

The PSO algorithm is tied to swarm intelligence principles such as the ability of individuals to respond to quality changes in the environment in a diverse and stable manner. It simulates the movement of multiple particles, each with its own individual position, through a velocity variable that is calculated based on the best position found so far by the particle itself (referred to as personal best) and the one found by the whole swarm (referred to as global best or leader) (REYES-SIERRA; COELLO, 2006).

A fully connected PSO algorithm to maximize an objective function $f : \mathbb{R}^{ND} \rightarrow \mathbb{R}$, is given in Algorithm 1. Since the function domain is multidimensional, x_p^t and v_p^t are ND-dimensional vectors that represent the p-th particle position and velocity at iteration t. To reference a specific dimension d, the variables $x_p^{t,d}$ and $v_p^{t,d}$ are used. The main equations used in Algorithm 1 are:

$$v_p^{t+1} = \omega v_p^t + c_1 r_1 \left(P_{b,p}^t - x_p^t\right) + c_2 r_2 \left(G_b^t - x_p^t\right) \tag{4.1a}$$

$$x_p^{t+1} = x_p^t + v_p^{t+1} \tag{4.1b}$$

where r_1 and r_2 are pseudorandom uniform numbers $U(0,1)$,ω is the particle inertia, i. e. the influence of previous velocity in the current velocity, c_1 is the particle acceleration towards personal optimum $(P_{b,p}^t)$ and c_2 is the particle acceleration towards global best or leader (G_b^t).

Algorithm 1 PSO

```
1:  procedure PSO(f,NP,NI,c1,c2,ω)
2:      for p = 1, ..., NP do
3:          for d = 1, ..., ND do
4:              x_p^d ← RAND(LB^d, UB^d)
5:              v_p^d ← RAND(−v_max^d, v_max^d)
6:          P_{b,p} ← x_p
7:      G_b ← argmax(f(P_{b,p}), ..., (P_{b,NP}))
8:      for i = 1, ..., NI do
9:          for p = 1, ..., NP do
10:             v_p ← ωv_p + c1 r1 (P_{b,p} − x_p) + c2 r2 (G_b − x_p)
11:             x_p ← x_p + v_p
12:             f_p ← f(x_p)
13:             P_{b,p} ← argmax(f(P_{b,p}), f(x_p))
14:         G_b ← argmax(f(P_{b,p}), ..., (P_{b,NP}))
```

The set X of all NP particles is called a swarm and the total number of iterations NI is used as *stop criteria* to halt the execution of the optimization.

Velocities and positions are limited inside $[-v_{max}^d, v_{max}^d]$ and $[LB^d, UB^d]$ ranges, respectively, where v_{max}^d is the maximum modular velocity and LB^d and UB^d are the lower

and upper boundaries for each dimension d. The damping wall technique (Algorithm 2) is used to ensure that the updated position remains under the viable domain set under each boundary (HUANG; MOHAN, 2005).

Algorithm 2 Damping Walls

```
procedure DAMPING WALLS(x_p^d, v_p^d, LB^d, UB^d)
    while x_p^d + v_p^d < LB^d or x_p^d + v_p^d > UB^d do
        if x_p^d + v_p^d < LB^d then
            v_p^d ← RAND(0,1) (LB^d − x_p^d − v_p^d)
            x_p^d ← LB^d
        if x_p^d + v_p^d > UB^d then
            v_p^d ← RAND(0,1) (UB^d − x_p^d − v_p^d)
            x_p^d ← UB^d
```

The optimization function used is $f : \mathbb{R}^{14} \rightarrow \mathbb{R}^3$, where 14 is the number of chemical kinetic parameters (Table 2) and 3 is the number of objectives. Absolute difference (AD) between modeled and measured final stock values and Root Mean Square Error (RMSE) between modeled and observed CO_2 and CH_4 fluxes are the quality metrics used as objectives:

$$AD = \left| y_m^T - y_o^T \right| \tag{4.2a}$$

$$RMSE = \sqrt{\frac{\sum_{i=1}^{n} \left(y_m^i - y_o^i \right)^2}{n}} \tag{4.2b}$$

where y_m^i and y_o^i represents the i-th day modeled and observed fluxes, n is the amount of days used for calibration and T is the last day of available calibration data.

To evaluate a set of parameters, i. e. to call $f(x_p)$, the CICLAR parameters needs to be set, the model needs to be run, and the results compared against observed data, as depicted in Figure 7.

Figure 7 – Flowchart for the evaluation of a parameters set

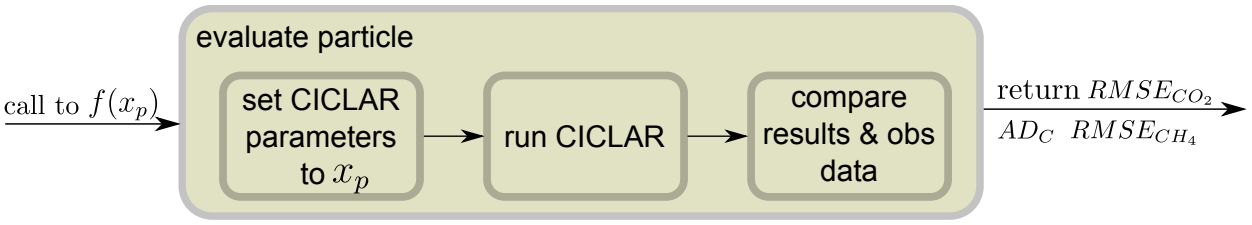

The C++ optimized version of CICLAR is used during the calibration process in order to reduce the computational cost of the algorithm. Each optimized model simulation for the 45 years period is 500 times faster than the Python simulation.

However, even with lower runtime, particle evaluation is still the most computationally expensive step of the PSO algorithm, given that the remaining steps only involve

a relatively small amount of operations. To mitigate such cost, particles are evaluated in parallel, using multiple threads in multiple processor cores, through the use of the OpenMP programming library.

4.3 AGGREGATED MULTI-OBJECTIVE PARTICLE SWARM OPTIMIZATION

To solve multi-objective problems through single objective optimization techniques, all objectives must be aggregated into a single optimizable variable. Figure 8 shows the Aggregated Multi-Objective Particle Swarm Optimization (AMOPSO) technique.

Figure 8 – Aggregated Multi-objective Particle Swarm Optimization fluxogram

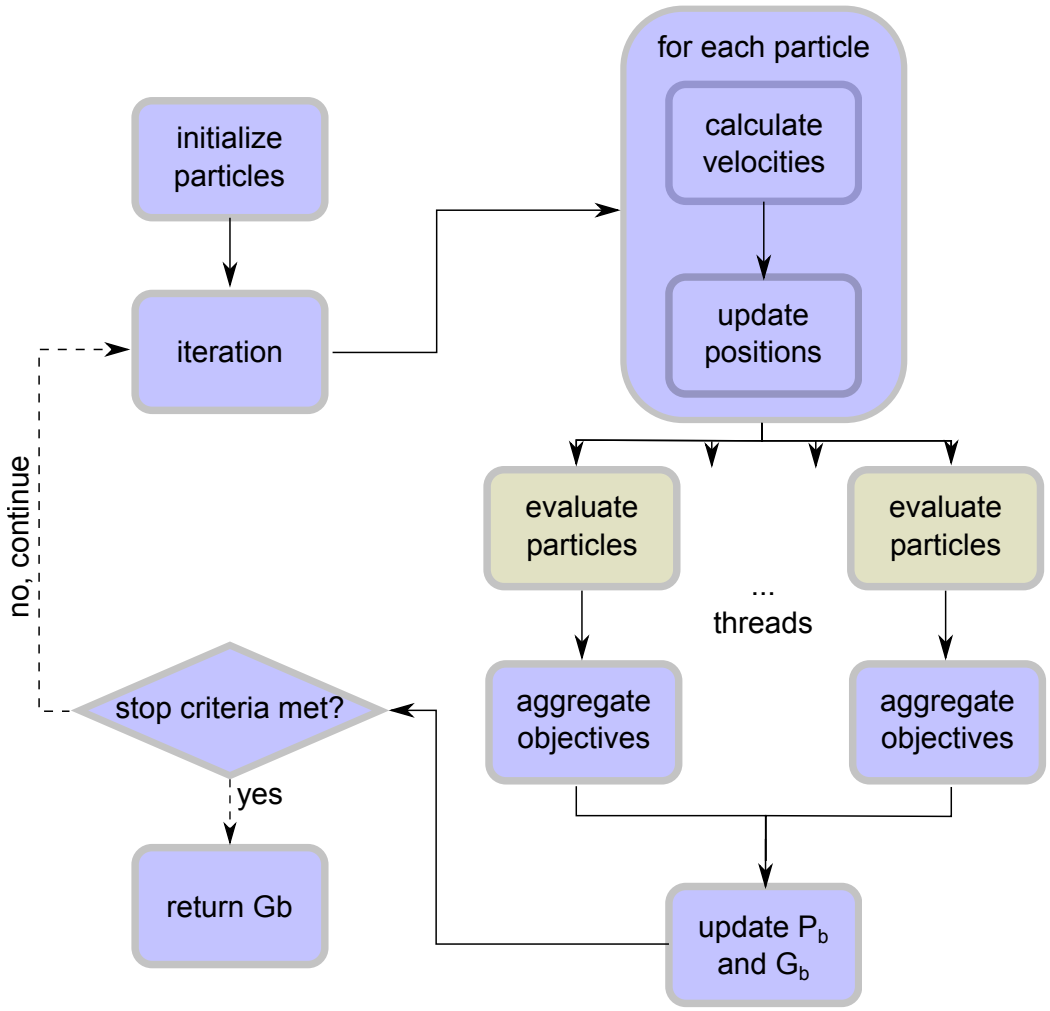

The topology used is fully connected, and so, the variable G_b holds the best solution found by the algorithm at each iteration. The velocity calculations and position updates are calculated according to Equation 4.1.

A weighted mean function was used to aggregate the objectives into a single value:

$$f = w_C AD_C + w_{CO_2} RMSE_{CO_2} + w_{CH_4} RMSE_{CH_4} \tag{4.3}$$

The weights are based on the Global Warming Potential (GWP) for a hundred years horizon:

$$GWP = 28\frac{44}{16}CH_4 + CO_2 - \frac{44}{12}C \tag{4.4}$$

where the GWP for methane and carbonic gas is 28 and 1 respectively (IPCC, 2013).

Each weight was calculated according to the contribution to the GWP index:

$$w_C = \frac{44/12}{28 \cdot 44/16 + 1 + 44/12} = 0.0449 \tag{4.5a}$$

$$w_{CO_2} = \frac{1}{28 \cdot 44/16 + 1 + 44/12} = 0.0122 \tag{4.5b}$$

$$w_{CH_4} = \frac{28 \cdot 44/16}{28 \cdot 44/16 + 1 + 44/12} = 0.9429 \tag{4.5c}$$

where only the absolute value of the stocked carbon C contribution for GWP is used.

4.4 PARETO CONCEPTS

When multiple objectives are not aggregated into a single one, the trade-offs in which the solutions that perform better in some of the objectives tend to underperform in the remaining ones, must be addressed. Such trade-off is mathematically defined in the **Pareto dominance** concepts (REYES-SIERRA; COELLO, 2006).

Definition 1 A multi-objective optimization problem can be generally defined as the **minimization** of an **objective function** $f : \mathbb{R}^{ND} \rightarrow \mathbb{R}^{NO}$, where $\mathbb{R}^{ND}$ represents the decision space and $\mathbb{R}^{NO}$ the objectives space. A vector $\vec{x} \in \mathbb{R}^{ND}$ is referred to as a **solution**.

Definition 2 Given two vectors $\vec{a}, \vec{b} \in \mathbb{R}^{NO}$, it is defined that $\vec{a} \leq \vec{b}$ if, and only if, $\vec{a}_i \leq \vec{b}_i$ for $i = 1, \ldots, NO$. Also that $\vec{a}$ **dominates** $\vec{b}$ (denoted by $\vec{a} \prec \vec{b}$) if $\vec{a} \leq \vec{b}$ and $\vec{b} \neq \vec{a}$. The domination concept is also extended to the decision space so that $f(\vec{x}) \prec f(\vec{x}') \implies \vec{x} \prec \vec{x}'$.

Definition 3 A solution $\vec{x} \in \mathcal{P} \subset \mathbb{R}^{ND}$ is **non-dominated** with respect to $\mathcal{P}$, if, and only if, $f(\vec{x}) \leq f(\vec{x}')$, for all $\vec{x}' \in \mathcal{P}$. A set $\mathcal{P}$ is said to be **non-dominated** if every solution $\vec{x} \in \mathcal{P}$ is non-dominated with respect to $\mathcal{P}$.

Definition 4 A solution $\vec{x}^* \in \mathbb{R}^{ND}$ is **Pareto-optimal** if it is non-dominated with respect to $\mathbb{R}^{ND}$. The **Pareto-optimal Set** $\mathcal{P}^*$ is defined such as:

$$\mathcal{P}^* = \left\{ \vec{x} \in \mathbb{R}^{ND} | \, \vec{x} \text{ is Pareto-optimal} \right\}$$

The **Pareto-front** $\mathcal{F}^*$ is defined by the evaluation of the Pareto-optimal set:

$$\mathcal{F}^* = \left\{ f(\vec{x}) \in \mathbb{R}^{ND} | \, \vec{x} \in \mathcal{P}^* \right\}$$

Note that, by definition, the Pareto-optimal set is a non-dominated set, since it is a subset of the search space and that if $f(\vec{x}') \not\prec f(\vec{x})$ for all $\vec{x}' \in \mathbb{R}^{ND}$ then the same is valid for all $\vec{x}' \in \mathcal{P}^*$. When the objective space is one dimensional these definitions default to single objective optimization nomenclature: the domination relationship becomes less-then, Pareto-optimal solutions become global optima.

Figure 9 illustrates Definitions 6 to 8 for a generic optimization problem with two objectives f_1 and f_2, i. e. $NO = 2$. The plotted points only represent different solutions after its evaluation (in the objectives spaces), and so, in this case, the decision dimension ND is irrelevant.

Figure 9 – Dominated and non-dominated solutions exemplification

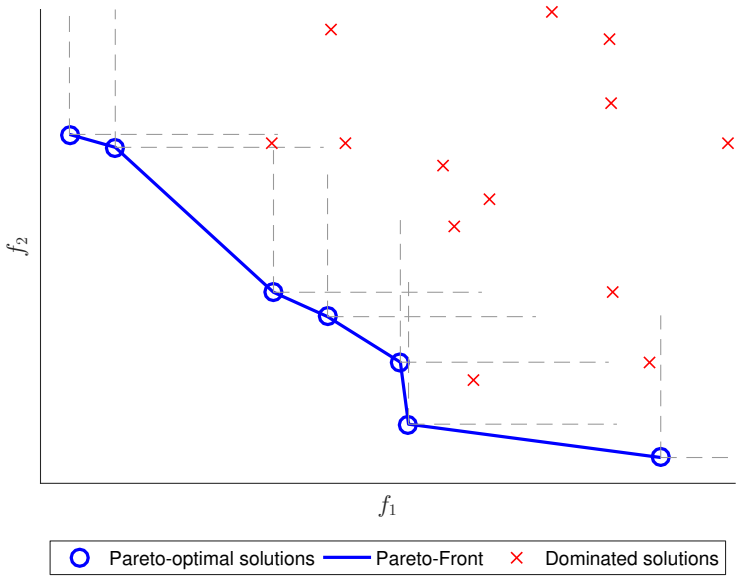

To be part of the Pareto-front, a solution must not be dominated, i. e. above the horizontal or to the right of the vertical dotted lines of Figure 9. Note that while dominated solutions might dominate one another, they cannot dominate Pareto-optimal solutions.

4.5 COMBINED PARETO MULTI-OBJECTIVE PARTICLE SWARM OPTIMIZATION

The main hindrance regarding non aggregated multiple objective is that, instead of maintaining a single optimal solution, an iterative update of a non-dominated set of solutions is required. In the multi-objective PSO such set is commonly stored in an external archive A that has three basic operations: insertion of a new solution, leader selection, and solution removal.

To ensure that the archive remains a non-dominated set, the insertion operation first goes through the entire external archive and, for each stored solution, performs a dominance check that yields one of three cases: 1) the stored solution dominates the new

one, halting the insertion procedure; 2) the new solution dominates the stored one and the stored solution is removed; 3) both are non-dominated, nothing happens and the next archived solution is checked. If the checking process cover the whole archive without halting, the new solution is inserted.

Each solution in the archive is non-dominated and 'equally good'. Therefore, selecting a stored solution as leader in Equation 4.1 requires careful consideration. The proposed Combined Pareto Multi-Objective Particle Swarm Optimization (CPMOPSO), whose concept is given in Figure 10, is a combination of different leader selection criteria and adapted single objective techniques, such as: Master-Slave subswarms PSO (JIANG et al., 2010); Adaptive Search Diversification PSO (ASD-PSO) (ARDIZZON; CAVAZZINI; PAVESI, 2015); and particle mutation (COELLO; PULIDO; LECHUGA, 2004).

Figure 10 – Combination of different PSO extensions into a single method

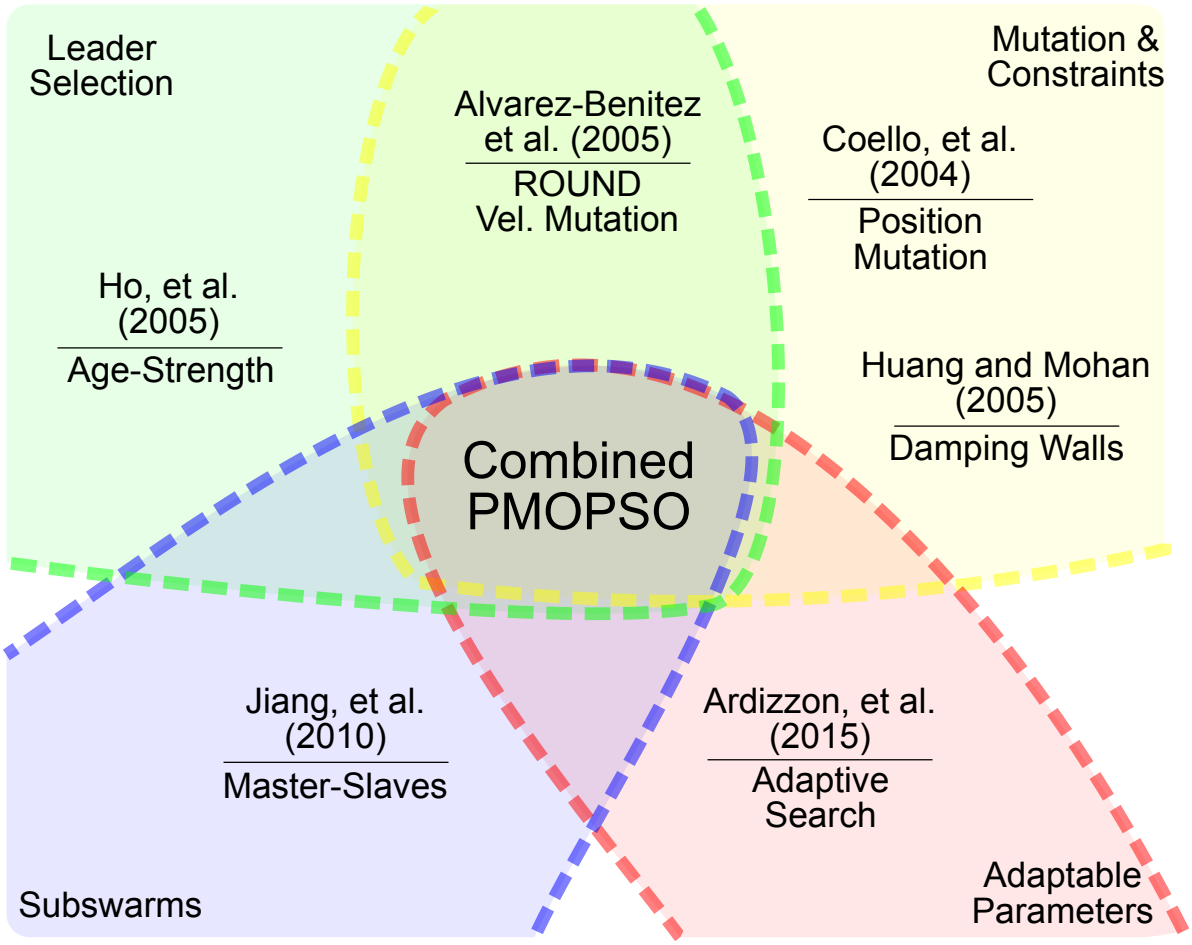

4.5.1 Mutation

Two types of mutation are employed to enhance local search and avoid local minima: the velocity and the position mutation. The velocity mutation, adapted from Alvarez-Benitez, Everson e Fieldsend (2005), is implemented through an additional term

e_k in Equation 4.1a, resulting in:

$$v_p^{t+1} = \omega v_p^t + c_1 r_1 \left(P_{b,p}^t - x_p^t\right) + c_2 r_2 \left(G_b^t - x_p^t\right) + e_k \tag{4.6}$$

and

$$e_k = \begin{cases} \mathcal{N}\left(\mu = 0, \sigma = \dfrac{x_{max} - x_{min}}{2}\right) & \text{if } r \leq p_m^{vel} \\ 0 & \text{otherwise} \end{cases} \tag{4.7}$$

where $\mathcal{N}(\mu, \sigma)$ is the normal distribution with mean μ and standard deviation σ and r is a pseudorandom uniform number $U(0, 1)$, and $p_m^{vel} \in [0, 1]$ is the velocity mutation probability used to select whether the velocity mutation will be applied or not.

The position mutation enhances exploration during early PSO iterations through a mathematical function that rapidly decreases as more iterations are executed. The probability function used was $(1 - i/NI)^{5/mr}$, where i is the current PSO iteration, NI is the total number of iterations, and mr is the mutation rate parameter which controls how fast the function decreases (COELLO; PULIDO; LECHUGA, 2004).

Algorithm 3 presents the full positional mutation process as follows: 1) if the probability function is 'satisfied', a dimension d in the ND-dimensional position vector x_p is randomly selected; 2) the mutation lower and upper boundaries are calculated based on the probability function and on the lower (LB) and upper (UB) boundaries of the selected dimension; 3) the mutated value for the d-th dimension of the x_p position vector is randomly selected between the mutated lower and upper boundaries.

Algorithm 3 Mutate

1: **procedure** MUTATE($x_p, ND, i, NI, mr, LB, UB$)
2: $r \leftarrow \text{RAND}(0, 1)$
3: **if** $r \leq (1 - i/NI)^{5/mr}$ **then**
4: $d \leftarrow$RAND_INT$(1, ND)$
5: $mrange \leftarrow \left(UB^d - LB^d\right)(1 - i/NI)^{5/mr}$
6: $lb \leftarrow \max\left(x_p^d - mrange, LB^d\right)$
7: $ub \leftarrow \min\left(x_p^d + mrange, UB^d\right)$
8: $x_p^d \leftarrow \text{RAND}(lb, ub)$

4.5.2 Leader selection

Each swarm member selects its own leader as a member of the external archive, and therefore the leader G_b^t in Equation 4.6 becomes $G_{b,p}^t$. This process is divided in two steps: the constraining of the set of selectable solutions and probability Roulette-Wheel selection of weighted archive solutions.

The Roulette-Wheel selection, formally defined as *Fitness proportionate selection*, is commonly used in evolutionary algorithms to select 'good' individuals with higher

probabilities. Given a n-dimensional ordered probabilities vector p, so that $\sum_{i=1}^{n} p_i = 1$, $p_i \geq 0$ and $p_i > p_{i+1}$, the selection process chooses an element i according to Algorithm 4.

Algorithm 4 Roulette-Wheel

```
1: function RouletteWheel(p, n)
2:     r ← RAND(0, 1)
3:     for i = 1, ..., n do
4:         if r ≤ p_i then
5:             return i
6:         else
7:             r ← r − p_i
```

Each archive member has a different probability of being selected by each particle. These probabilities are assigned according to different criteria that are described in the remaining of this section.

4.5.2.1 Dominator leader

For each particle x_p the subset $S_{x_p} \subseteq A$ is formed by all solutions in the external archive that dominate x_p. If such set is empty, i. e., the particle itself is a member of the archive, than the whole archive is used, according to:

$$S_{x_p} = \begin{cases} \{a \in A | a \prec x_p\} & \text{if } x_p \notin A \\ A & \text{if } x_p \in A \end{cases} \tag{4.8}$$

Each leader $G_{b,p}^{t} \in S_{x_p}$ is then selected from this constricted subset of the external archive in order to enhance the convergence of the algorithm (ALVAREZ-BENITEZ; EVERSON; FIELDSEND, 2005).

4.5.2.2 Weighted selection

After the constriction of the archive to the S_{x_p} subset, a discrete probability distribution is set. Each archived solution has a different probability of being selected as leader. The probability distribution is calculated based on the number of iterations that the solution a has been in the archive, the amount of swarm particles that it dominates, and its GWP weighted function value.

The age criteria is implemented through the variable age^a calculated according to the number of iterations k_a that the archive member a persisted in the archive:

$$age_a = \min\Big(1.02^{k_a}, 100\Big) \tag{4.9}$$

where, in contrast to the original implementation of Ho et al. (2005), the upper boundary of 100 was added to prevent the maintenance of obsolete solutions in the archive.

The domination criteria, represented by the dom_a variable, is the amount of swarm members that are dominated by the archive member a, i. e., $dom_a = |\{x_p \in X | a \prec x_p\}|$. To incorporate the global warming potential of the different modeled substances, a criteria based on the aggregated function (Equation 4.3) is also used, so that $GWP_a = f(a)$ (ALVAREZ-BENITEZ; EVERSON; FIELDSEND, 2005).

The goal of these criteria is to promote diversity, spread and low GWP impact of solutions in the archive. Since each swarm member has a different subset of eligible leaders, the selection criteria must be adjusted to fit a probability distribution. The discrete probability distribution is calculated based on adimensionalized criteria regarding each S_{x_p} that are inverted to promote members with lower criteria values:

$$p_{x_p}(a) = \begin{cases} 1 & \text{if } a \in S_{x_p} \text{ and } \left|S_{x_p}\right| = 1 \\ \dfrac{w_{dom}\left(1 - \frac{dom_a}{T_{x_p}^{dom}}\right) + w_{age}\left(1 - \frac{age_a}{T_{x_p}^{age}}\right) + w_{GWP}\left(1 - \frac{GWP_a}{T_{x_p}^{GWP}}\right)}{\left|S_{x_p}\right| - 1} & \text{if } a \in S_{x_p} \text{ and } \left|S_{x_p}\right| > 1 \\ 0 & \text{if } a \notin S_{x_p} \end{cases} \tag{4.10}$$

where $T_{x_p}^{age} = \sum_{a \in S_{x_p}} age_a$, $T_{x_p}^{dom} = \sum_{a \in S_{x_p}} dom_a$, $T_{x_p}^{GWP} = \sum_{a \in S_{x_p}} GWP_a$, w_{dom}, w_{age} and w_{GWP} are the weights to promote solutions in less populated locations, newer solutions and solutions with lower GWP errors, respectively. These weights need to satisfy $w_{dom} + w_{age} + w_{GWP} = 1$ so that Equation 4.10 characterize a discrete probability distribution function, i. e., $\sum_{a \in A} p_{x_p}(a) = 1$ and $p_{x_p}(a) \geq 0$ for all $x_p \in X$ and $a \in A$.

Therefore, the archive updating process (Figure 11) in CPMOPSO is as follows: first the new solutions are inserted, then the selection criteria are calculated for each archived solution and the dominant subset is constructed for each swarm particle, and finally the discrete probability distribution for each particle is calculated.

Figure 11 – CPMOPSO archive updating process

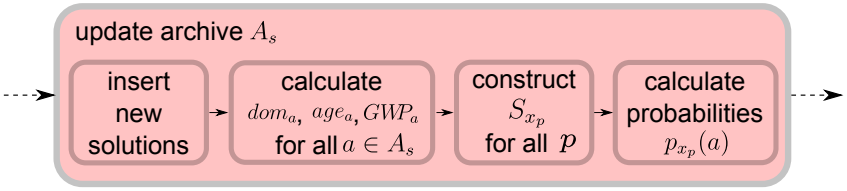

4.5.3 Adaptive parameters

The Adaptive Search Diversification (ASD) single objective PSO technique, has the goal of enforcing the cooperation of swarm members by enabling settler-explorer relationships among particle.

The settler-explorer mechanic is achieved in ASD by dynamically lowering global optimum influence and enhancing the effect of personal experience of a particle as further away it is from the current global best position. This promotes exploration on particles farther from the current solution, avoiding premature convergence, and boosts local search around the best solution by particles close to it (ARDIZZON; CAVAZZINI; PAVESI, 2015).

However, the ASD technique is based on a single global guide and therefore must be adapted so that a potentially different leader is selected from the external archive for each particle in each iteration. In this MO adaptation, instead of using the distance to the global best to set different parameters values in each dimension, there is no distinction for each dimension and a single value is used for each parameter and each particle based on the distance from the particle to the current Pareto-front. This distance d_p is calculated as the distance between the position of a particle (in the objective space) to the line segment between the two closest (also in the objective space) archive members.

The ASD parameters are then constructed to enhance particle cooperation, by dynamically adjusting each particle to explorer or settler roles, and to maintain the convergence of the algorithm. Upper and lower limits, i. e., $c_{1_{max}}$, $c_{2_{min}}$, $c_{2_{max}}$, ω_{min} and ω_{max}, are used to ensure that the parameters remains inside a reasonable domain. A maximum distance $d_{max} = \max(d_1, \ldots, d_{NP})$, is used to adjust quadratic functions so that the relationships in Figure 12 are achieved.

Figure 12 – Behavior of the Adaptive Search Diversification parameters

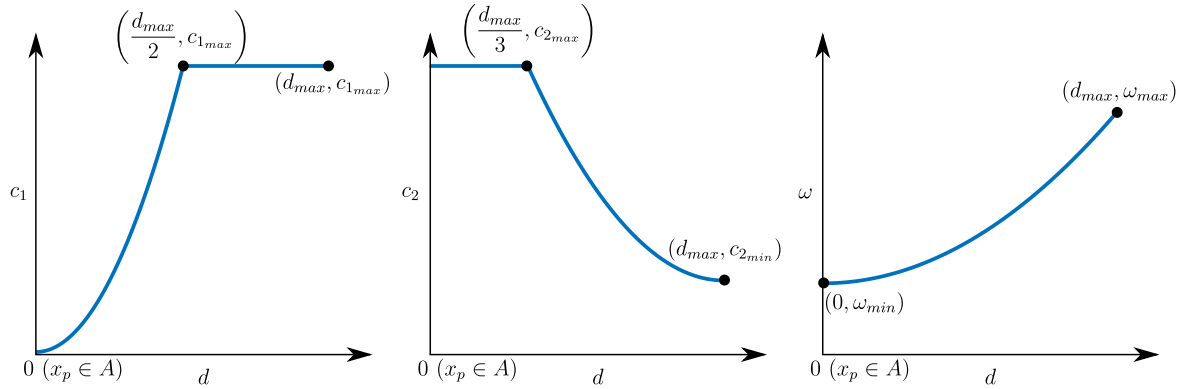

Solving the quadratic equations to find the proper coefficients yields the following formulas to calculate adaptive PSO parameters:

$$c_1^p = \min\left(\frac{4c_{1_{max}}}{d_{max}^2} d_p^2, c_{1_{max}}\right) \tag{4.11a}$$

$$c_2^p = \min\left[\frac{9\left(c_{2_{max}} - c_{2_{min}}\right)}{4d_{max}^2}\left(d_p^2 - 2d_{max}d_p + \frac{5}{9}d_{max}^2\right), 0\right] + c_{2_{max}} \tag{4.11b}$$

$$\omega^p = \frac{\omega_{max} - \omega_{min}}{d_{max}^2}\left(d_p^2 - d_{max}^2\right) + \omega_{max} \tag{4.11c}$$

The full particle updating process for the CPMOPSO method (Figure 13) is applied to each particle in each iteration.

Figure 13 – CPMOPSO particle updating process

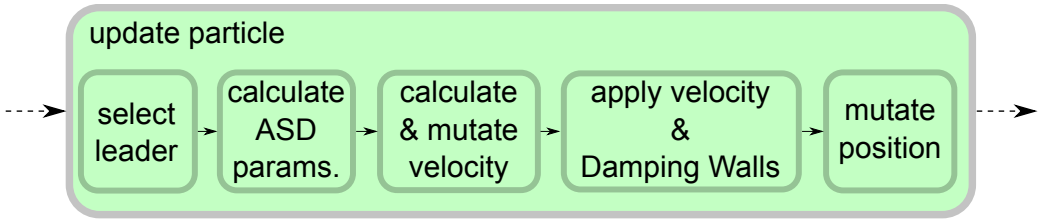

4.5.4 Subswarms

The CPMOPSO implementation of subswarms is based on the Master-slave Swarms Shuffling Evolution PSO (JIANG et al., 2010) and on the explorer-settler dynamic (ARDIZZON; CAVAZZINI; PAVESI, 2015). In CPMOPSO, each subswarm performs one of three roles: (i) master subswarm whose archive A_{master} is the non-dominated set of the best solutions found, (ii) the slave-explorer subswarm, which is optimized completely independently from each other and only 'feeds' solutions to the master subswarm, and (iii) the slave-settler swarm whose archive is periodically cleared and populated with solutions from the master swarm. The algorithm uses a total of $NSS = 1 + NSS_{set} + NSS_{exp}$ subswarms, where $NSS_{set} = \left\lfloor \frac{NSS-1}{2} \right\rfloor$ is the number of settlers and $NSS_{exp} = \left\lceil \frac{NSS-1}{2} \right\rceil$ is the number explorer swarms.

Each subswarm is optimized using the same PSO algorithm, with potentially different parameters, e. g., $c_{1_{max}}$ and w_{dom}, and merges (Algorithm 5) periodically occurring in every $M = NI/10$ iterations.

Algorithm 5 Merge

```
1: procedure MERGE(A_master, SS_settler)
2:     [A^1_master, ..., A^NSS_set_master] ← partition (A_master)
3:     i ← 1
4:     for each s ∈ SS_settler do
5:         reset(s)
6:         for each x_p ∈ A^i_master do
7:             insert(A_s, x_p)
8:         i ← i + 1
```

The merge procedure uses the *partition* function that divides the master archive into multiple NSS_{set} partition sets. These sets are used to replace the archives of settler subswarms, while the current position and velocity of each settler particle is randomly reinitialized by the *reset* function. Since each solution that is inserted in slave archives is also inserted in the master archive, no solution is lost by replacing these sets with master

partitions. Explorer subswarms are not affected in the merge routine and are independently optimized.

The periodic reinitialization of particles in the merge algorithm is intended to promote Pareto-front diversity by exploring different locations in the search space. Aside from solutions being inserted in the master archive, explorer slave subswarms are optimized without the interference of other subswarms. These explorer swarms are utilized to examine regions that are potentially far from the current Pareto-front.

4.5.5 Solution filtering

A filter is applied to remove solutions that are undesirably off regarding certain objectives from the non-dominated external archive. Since this optimization method is used to calibrate the CICLAR model and that some solutions might, for instance, accurately predict the final stock but fail to model the methane emissions, solutions are filtered through the Nash-Sutcliffe coefficient (NS):

$$NS = 1 - \frac{\sum_{i=1}^{n} \left(y_m^i - y_o^i\right)^2}{\sum_{i=1}^{n} \left(y_o^i - \bar{y_o}\right)^2} \tag{4.12}$$

where y_m^i and y_o^i represents the i-th day modeled and observed fluxes, $\bar{y_o}$ is the mean flux and n is the number of days used to calibrate the model.

The NS coefficient for the calibration data is calculated for both methane and carbon dioxide fluxes and the solutions whose values for NS_{CH_4} or NS_{CO_2} are lower than 0.95 are removed from the non-dominated set.

4.5.6 Calibration Outline

Figure 14 presents the complete CPMOPSO scheme. The internal loop runs one particle swarm optimization for master and slave subswarms indiscriminately. The external loop controls the number of iterations, the stop criteria, and whether the merge procedure is applied. The particle evaluation, archive update, and particle update steps are detailed in Figures 7, 11, and 13, respectively.

4.6 VALIDATION OF THE OPTIMIZATION ALGORITHM

By combining several PSO based optimization methods, the CPMOPSO algorithm offered a parametrizable approach in which the strengths of these individual techniques can be combined to achieve better results. This algorithm was validated and compared to other MOPSO methods through the use of the DTLZ1 and DTLZ3 mathematical benchmark functions that were designed by Deb et al. (2002). Unlike other methods, the CPMOPSO resulted in solutions extremely close to the true Pareto-front for the fifteenth dimensional test problems.

Figure 14 – CPMOPSO flowchart

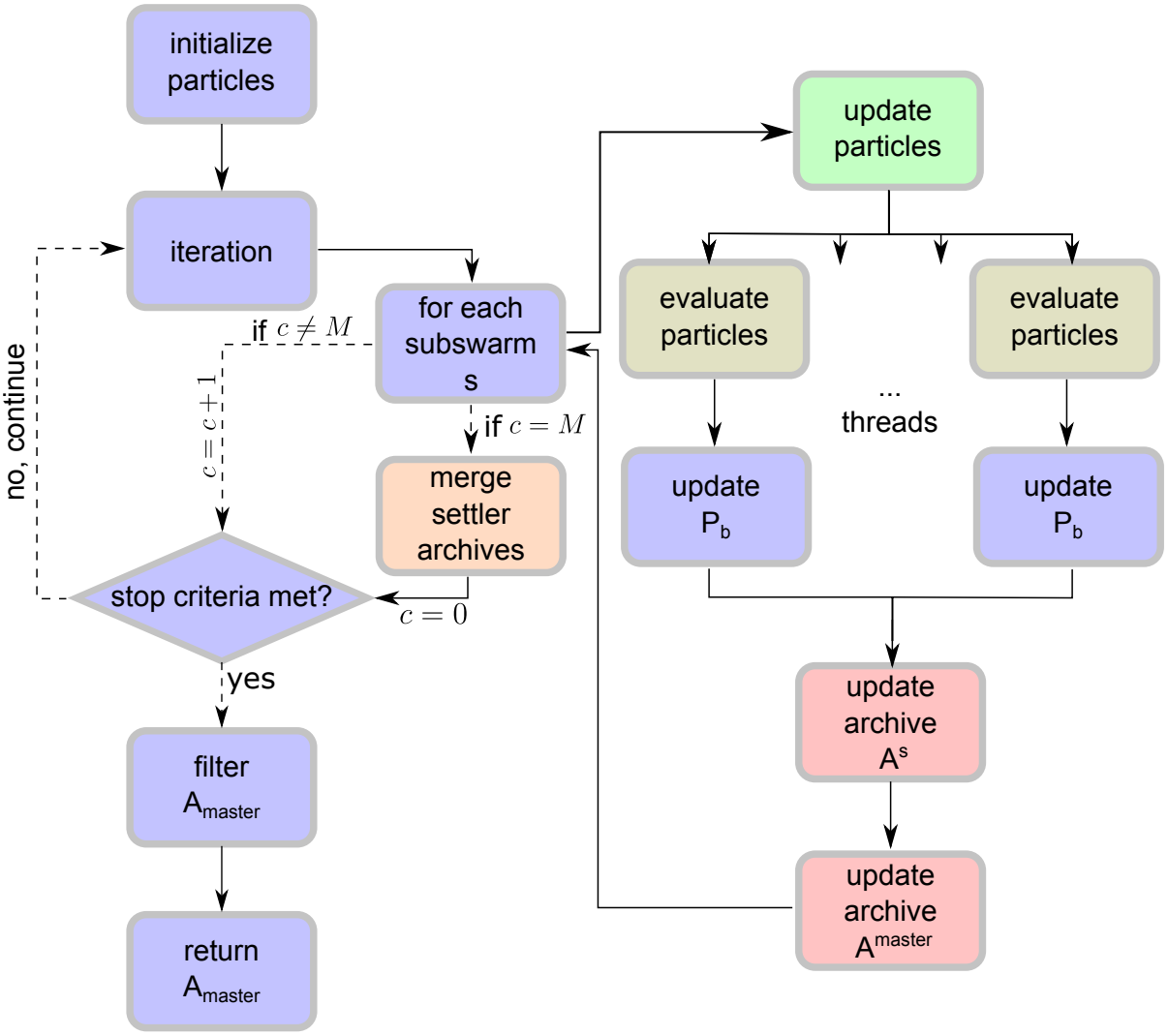

The analysis on Appendix C revealed that, although the CPMOPSO algorithm increases the computational cost by around 100 times, it achieves results that are at least three order of magnitudes better than other approaches. However, the No-Free-Lunch theorem by Wolpert e Macready (1997) highlights that the performance of the algorithm when solving these test functions cannot be generalized to untested problems.

4.7 CALIBRATION DATA DISTRIBUTION

To assess the performance of the calibration under different conditions, the full (1970-2015) simulation output of the manually calibrated CICLAR model is divided into different scenarios that are shown in Figure 15.

The four calibration scenarios, that were designed under different data availability and disposition, have the following characteristics:

1. Evaluative: divides the full 45 years range into 66% calibration and 34% validation

data. Used to compare and validate the different calibration methods;

2. Ideal: where observed data is well distributed and the calibrated model is potentially used to estimate intermediary data, i. e. used to analyze the ability to fill gaps of data;

3. Retrospective: used to estimate the retrospective capabilities of the calibration. Evaluates the ability to generate past data using present observed values, similar to the idea used by Mannich et al. (2015);

4. Prospective: used to assess the prognostic capabilities of the calibration, i. e., the impact of using initial data on the spread of different calibrated parameters and fluxes.

Figure 15 – Different calibration scenarios

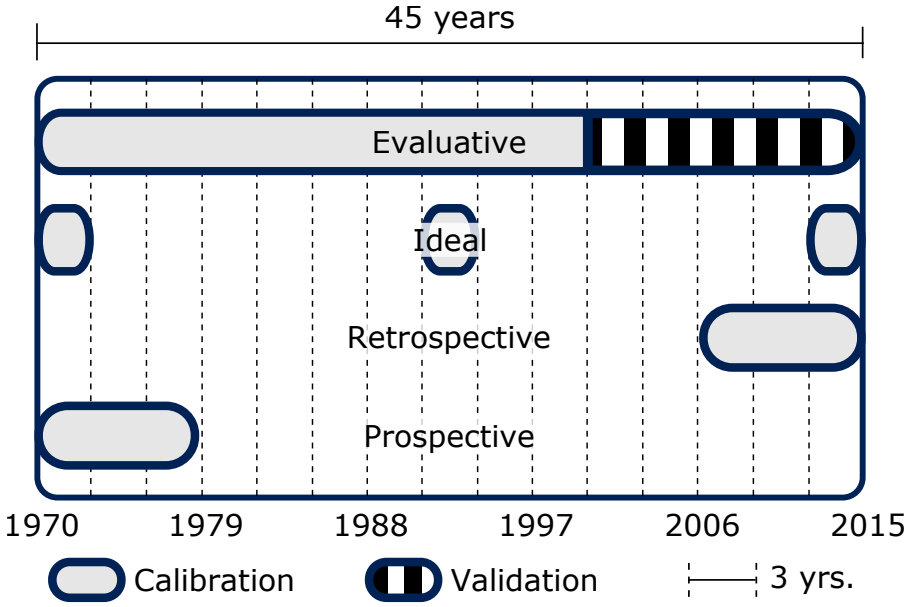

The evaluative scenario is used to validate the calibration of both AMOPSO and CPMOPSO techniques. The method that has the best performance is then calibrated under the ideal, retrospective, and prospective scenarios.

5 RESULTS

Absence of evidence is not evidence of absence

Carl Sagan

5.1 MANUAL CALIBRATION

The CICLAR model was manually calibrated to achieve the goals depicted in Section 4.1 by using the total carbon stock and GHG flux data (Section 3.4). The trial-and-error manual calibration was guided by expert knowledge of the modeled carbon dynamic processes and its results are on Table 11 (MANNICH et al., 2015).

Table 11 – Manually calibrated parameters

Parameter	Value	Parameter	Value
K_{AB}	0.05 d^{-1}	K_{EB}	0.00015 d^{-1}
K_{CA}	0.002 d^{-1}	K_{EEB}	1E−6 d^{-1}
K_{CB}	0.4 d^{-1}	K_{FE}	1E−6 d^{-1}
K_{CD}	0.4 d^{-1}	K_{FEB}	5E−8 d^{-1}
K_{DB}	0.3 d^{-1}	K_{PP}	3.0 d^{-1}
K_{CE}	0.8 d^{-1}	K_{DIC}	1.8 mgL^{-1}
K_{DE}	0.9 d^{-1}	I_S	250 Wm^{-2}
K_{ED}	0	$\%_{LR}$	0.2

The 45 year model simulation, under the input data presented on Section 3.4 and Appendix B, yielded the daily GHG flux displayed in Figure 16.

Figure 16 – Modeled and measured CO_2 and CH_4 fluxes. Black dots indicate data estimated based on field measurements

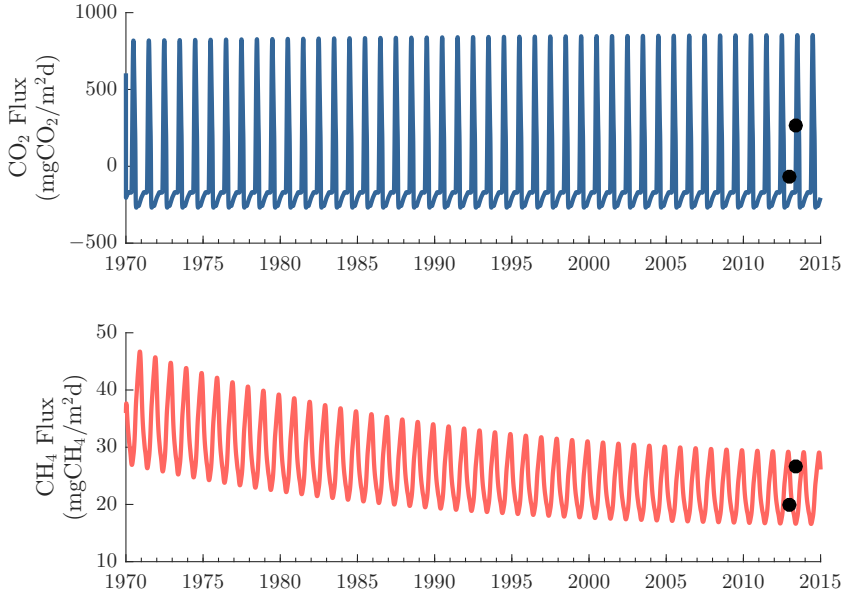

The calibrated total carbon stock is approximately 35 $kgCm^{-2}$, which is within the expected uncertainty range of the 35.5 $kgCm^{-2}$ value estimated from point measured data. Along with the manually calibrated final total carbon stock, the 45 years of modeled GHG flux are used as data for the automated calibration routines. Therefore, the ability of the calibration to redeem the parameter values in Table 11 is analyzed.

5.2 AUTOMATED CALIBRATION

To produce multiple solution with the aggregated multi-objective particle swarm optimization method, 20 simulations with different pseudorandom seed were executed for each calibration scenario. Aside from the seed, all the parameters (Table 12) were the same across all simulations.

Table 12 – AMOPSO parameters

NP	NI	c_1	c_2	ω
100	100	2	2	0.9

Since it is Pareto based, the CPMOPSO produces multiple solutions without the need of multiple simulations with different pseudorandom seeds. This enables the use of multiple subswarms without a significant increase in the runtime when compared to the 20 simulations of the AMOPSO. All 20 subswarms used the same values for the Adaptive Search Diversification and Leader Selection parameters (Table 13).

Table 13 – CPMOPSO parameters

PSO			Adaptive Search Diversification					Leader Selection			Mutation	
NP	NI	NSS	$c_{1_{max}}$	$c_{2_{min}}$	$c_{2_{max}}$	ω_{min}	ω_{max}	w_{age}	w_{age}	w_{GWP}	mr	p_m^{vel}
100	100	20	1.5	0.5	2	0.2	0.5	0.1	0.1	0.8	1	0.1

All computations regarding both PSO implementations and the CICLAR simulations were performed on a 3.40 Hz AMD FX-4100 Quadcore processor to keep the average runtime comparable between simulations. Both CICLAR and CPMOPSO were compiled by GCC with binary optimization to reduce computational costs.

5.2.1 Evaluative scenario

Resulting fluxes of the 20 AMOPSO calibrations under the evaluative scenario and a histogram of the total carbon stock are plotted on Figure 17. Each AMOPSO calibration performed about 10,000 simulations of the CICLAR model using threads in multiple processor cores and required around 2 minutes.

Figure 17 – GHG flux and total carbon stock for AMOPSO calibration on the evaluative scenario. Solid and dashed black lines indicate calibration and validation data respectively

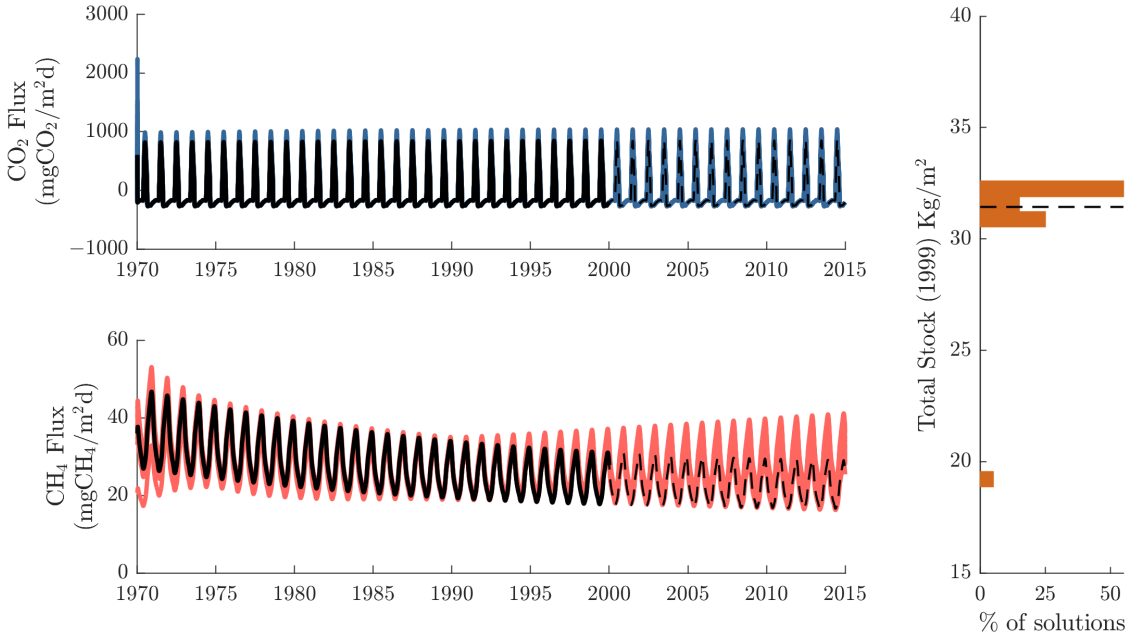

Disregarding the initial instability of modeled CO_2 flux, the aggregated calibration was able to reproduce the yearly trend of absorbing carbonic gas during warmer seasons ans emitting it on the winter (Figure 18). Most solutions had a total carbon stock at the end of the last calibration year (1999) close to the goal value of 31.44 kg/m^2. Although most solutions reproduced methane fluxes relatively well for the calibration period, all of them overestimated the CH_4 emission for the validation period, as shown in Figure 18 which focuses on the 1990 and 2010 fluxes of Figure 17.

Figure 18 – Yearly GHG flux for AMOPSO/evaluative calibration. Solid and dashed black lines indicate calibration and validation data respectively

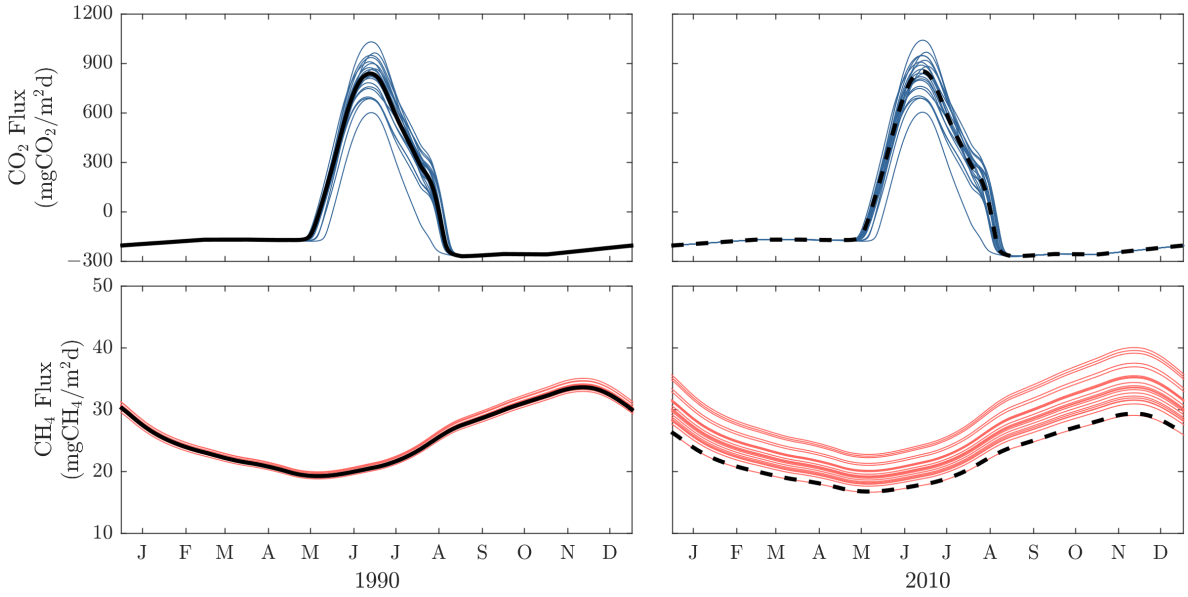

The CPMOPSO calibration of the evaluative scenario yielded 52 non-dominated solutions. The solutions were then filtered, and only 4 solutions presented low *NS* values and were consequently removed from the Pareto-front. The resulting GHG flux and total carbon stock for the CPMOPSO calibration are displayed on Figure 19. The method performed around 220,000 parallel evaluations of the CICLAR model and required around 50 minutes.

Figure 19 – GHG flux and total carbon stock for CPMOPSO calibration on the evaluative scenario. Solid and dashed black lines indicate calibration and validation data respectively

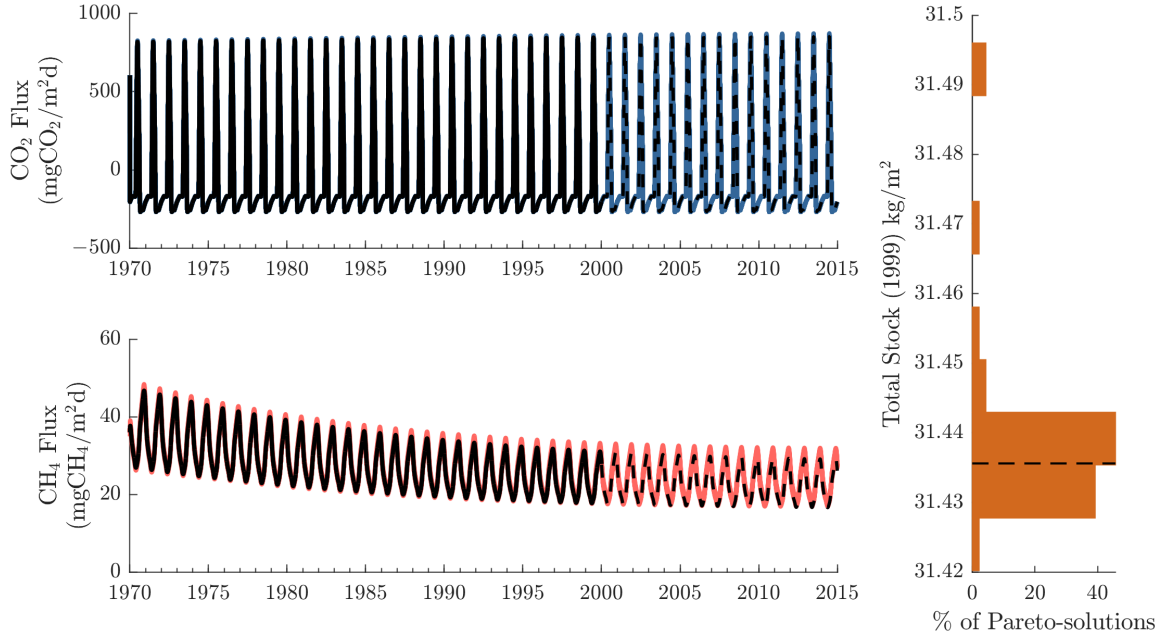

The data displayed on Figure 19 show that the CPMOPSO algorithm outperformed the aggregated approach on all objectives: better CO_2 and CH_4 fluxes for both the calibration and the validation periods and better total carbon stock estimations. All solutions were able to model extremely well the yearly carbonic gas cycle (Figure 20) while the methane emission was slightly overestimated for the validation period.

To analyze the randomness effect on the performance of the CPMOPSO calibration, five different simulations were executed with different random seeds. The RMSE values for the Pareto solutions of each calibration, along with the 20 AMOPSO solutions, for both methane and CO_2 fluxes are shown on the stacked histogram of Figure 21.

Most of CPMOPSO solutions presented RMSEs values less than 2/12 for modeled methane/carbon dioxide fluxes, while for the AMOPSO calibration these errors were 2-6 and 18-60, respectively. Although the CPMOPSO-1 calibration, which was displayed on Figs. 19 and 20, yielded better results, the simulations using different seeds were also satisfactory considering the length of the series used to calibrate the model.

The errors in predicting the total carbon stock at the end of 1999 were also

Figure 20 – Yearly GHG flux for CPMOPSO/evaluative calibration. Solid and dashed black lines indicate calibration and validation data respectively

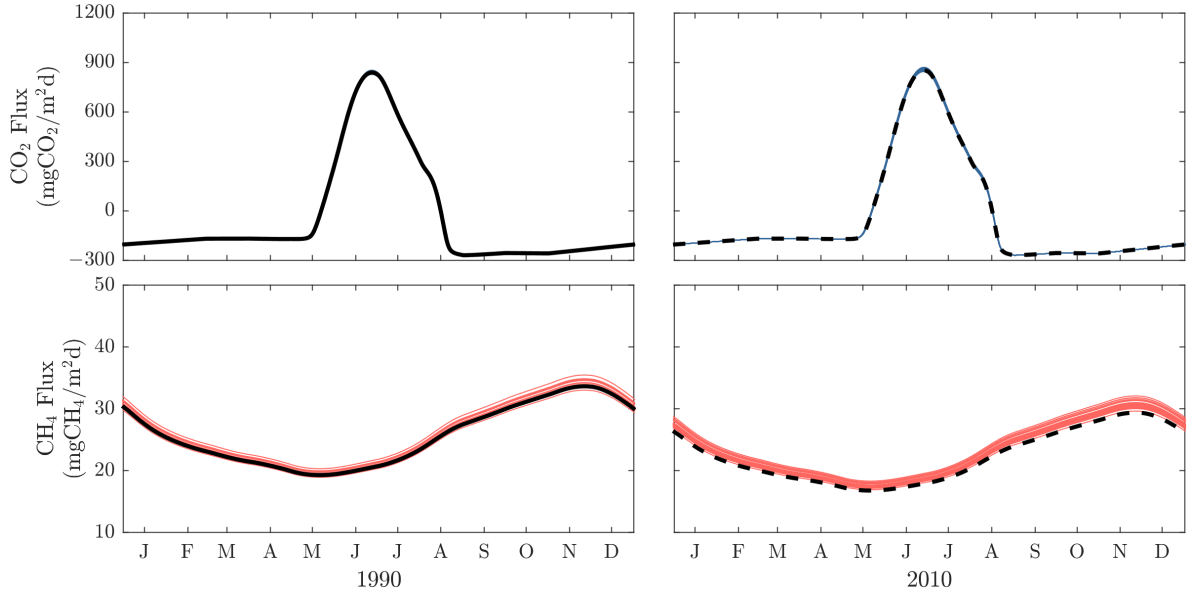

Figure 21 – Stacked histogram of Root Mean Square Error of GHG fluxes for the calibration period of the evaluative scenario

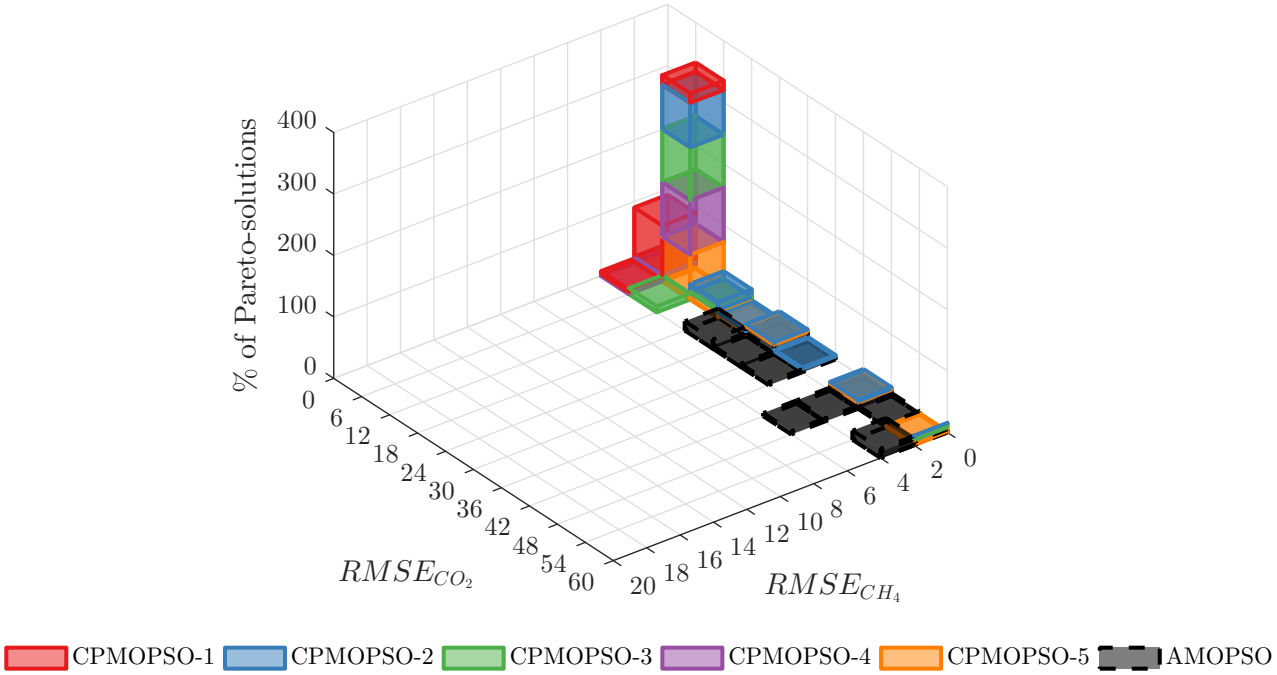

analyzed for the simulations using different random seeds. The stacked histogram for the errors is shown in Figure 22 where the errors with absolute values larger than 0.1 kg/m^2 are assembled in the extremes of the x axis.

Aside from having lower errors regarding gas fluxes, the CPMOPSO was also able to better reproduce the total carbon stock. Around 70% of all the solutions of each of the 5 simulations were able to model with errors lower than 10 g/m^2, and 90% had errors lower

Figure 22 – Stacked histogram of total carbon stock error for the calibration period of the evaluative scenario

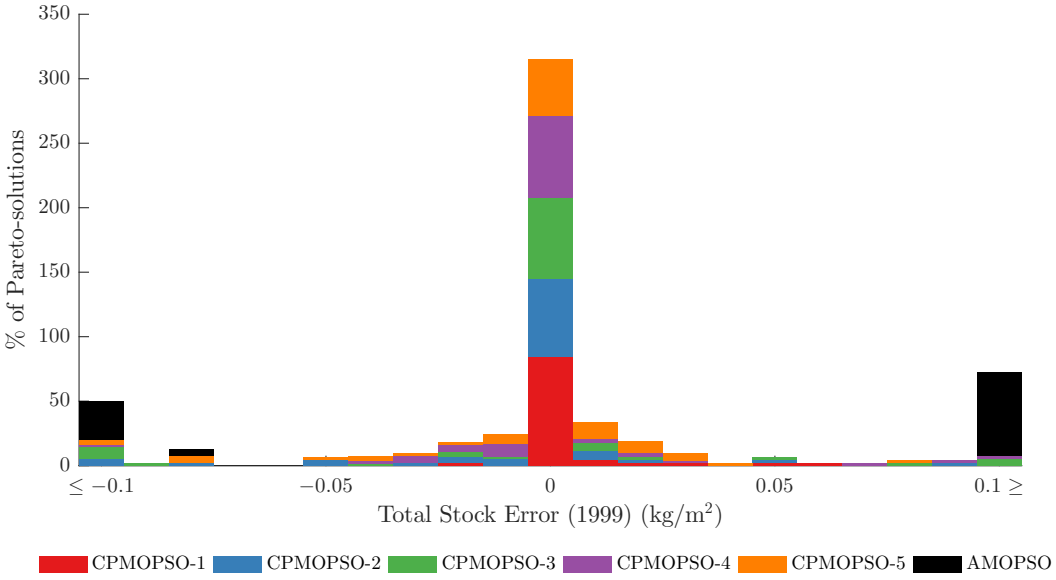

than 50 g/m^2. For AMOPSO, 95% of the solutions presented errors higher than 100 g/m^2.

Nash-Sutcliffe coefficients and stock errors for the validation period for AMOPSO and all 5 CPMOPSO simulations were calculated. Each solution had a different NS value for both CH_4 and CO_2 fluxes and a total stock error for the end of the validation period (2015) and the sets of solutions were sorted accordingly. These sets were then plotted on Figure 23 to form a cumulative distribution of the three different validation metrics.

Figure 23 – Cumulative distribution of stock errors and Nash-Stucliffe coefficients of GHG fluxes for the validation period of CPMOPSO and AMOPSO calibrated solutions

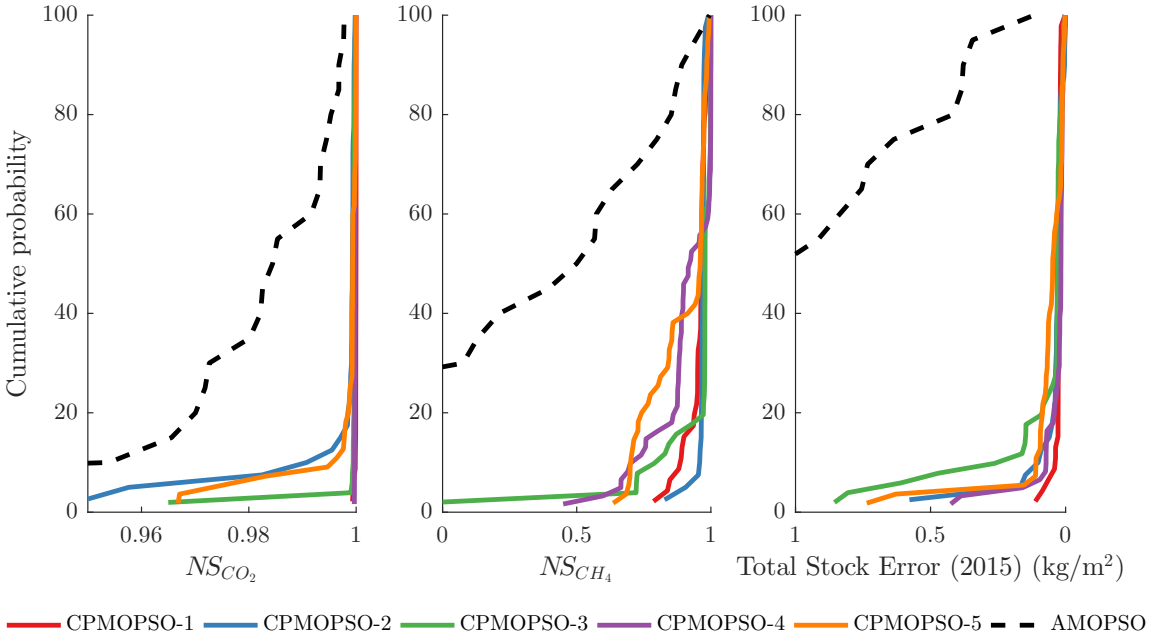

Given that the carbon dioxide flux series used to calibrate the model is periodically

stable (Figure 16), the NS coefficient for the validation period of CO_2 flux for 95% of solutions is higher than 0.98 for all CPMOPSO solutions. Although the model had a higher difficulty of predicting methane emissions, only around 20% of CPMOPSO solutions presented NS values lower than 0.8. The aggregated method had a significant lower performance on all three objectives.

Solutions obtained through CPMOPSO algorithm had significantly better validation Nash-Sutcliffe coefficient values (Figure 23), lower total carbon stock errors (Figure 22), and lower RMSE values (Figure 21) for the calibration period . The computational cost of the combined Pareto multi-objective PSO simulation is 25% bigger than the 20 AMOPSO simulations. Since the increased performance outweighs the additional computational cost, the remaining calibration scenarios are only analyzed with the CPMOPSO algorithm.

The values of the automatically calibrated CICLAR parameters are shown on Figure 24. The parameters were normalized according to $K_i^* = \frac{K_i - LB_i}{UB_i - LB_i}$ and organized in boxplots to analyze their position on the viable domain. All 5 calibrations of the evaluative scenario using different seeds were analyzed for each of the 14 biochemical parameters.

The calibration found a wide distribution of values for some parameters, e. g., K_{CA}, K_{DE}, K_{ED} and K_{DB}, that did not differ significantly regarding resulting GHG fluxes and total carbon stock. The fact that these different set of parameters have similar results may be evidence that inner relationships between parameters can be explored to simplify the CICLAR model. This is also consequence that the equation system has more equations than parameters, although this does not imply that the system is indeterminate, since each carbon concentration varies over time.

Since the parameters represented in Figure 24 were normalized, variations that are relatively high may not be as significant in the absolute scale, such as the resuspension rate K_{ED} whose lower and upper limits are 0 and 10^{-5}. The automatically calibrated values for the decay rate K_{FE} and ebullition rate of labile sedimented carbon K_{EEB} were very similar to the values used to generate the calibration data.

The organic and inorganic dissolved carbon concentrations for all 46 solutions of the CPMOPSO-1 calibration are displayed on Figure 25. Both DOC and DIC concentrations varied seasonally but remained stable throughout the 45 simulated years. This stability may be attributed to the monthly climatic averaged input data for carbon entering the system and the fact that the reservoir absorbs carbon from the atmosphere during warmer seasons and emits it during the winter.

Aside from the seasonal variation, a slight decay of the modeled particulated organic carbon concentration occurs over the years (Figure 26). POC_L carbon has higher concentrations in the early stages of the simulation but decays faster than POC_D since its only input is primary production, while its outputs are excretion, breathing, death and

Figure 24 – Normalized CICLAR parameters resulted from CPMOPSO calibrations using 5 different seeds. Gray lines indicate the manually calibrated parameters that were used to generate calibration data

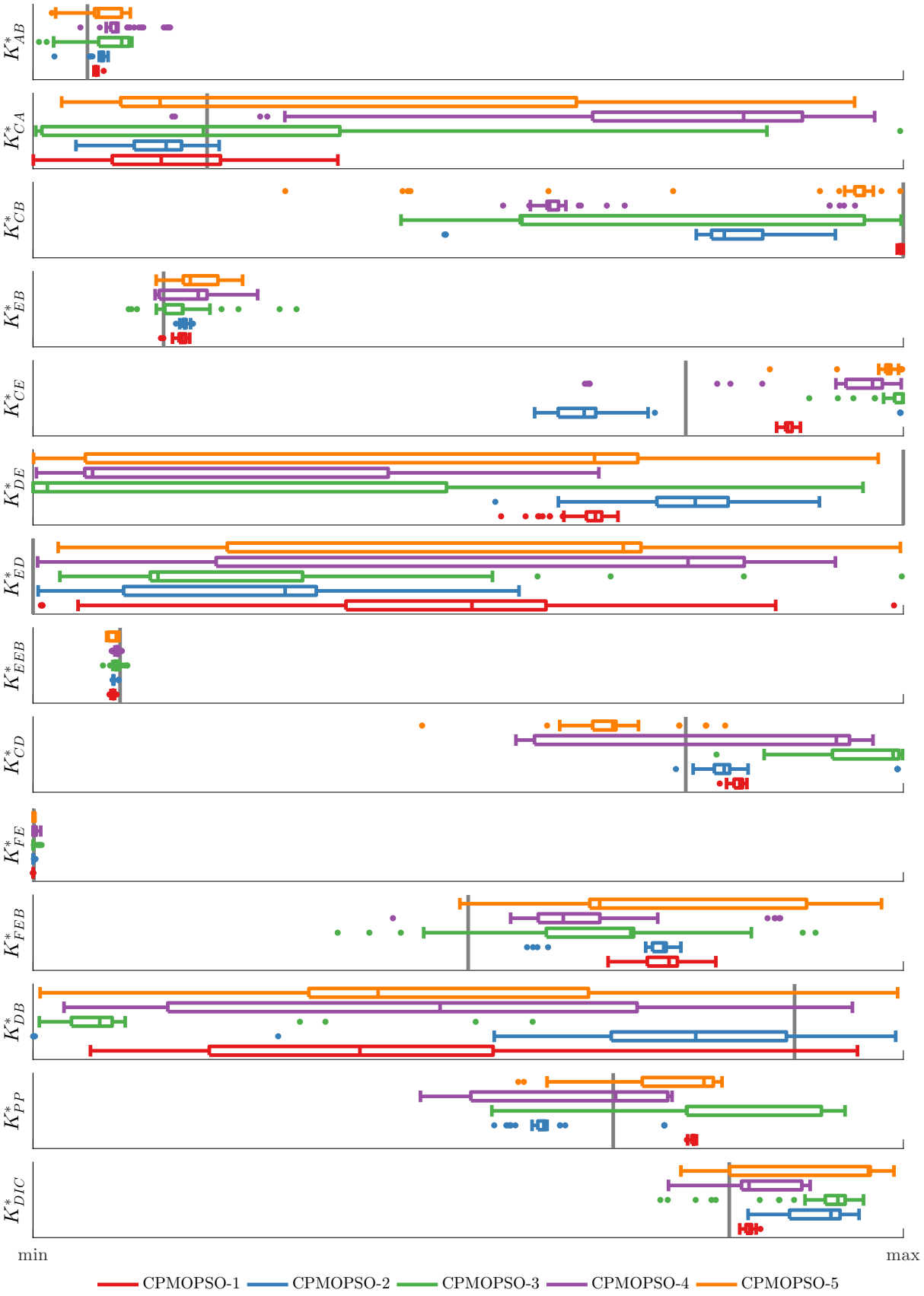

Figure 25 – Modeled DOC and DIC concentrations of CICLAR calibrated for evaluative scenario. Lines and circles indicates daily and yearly averages respectively

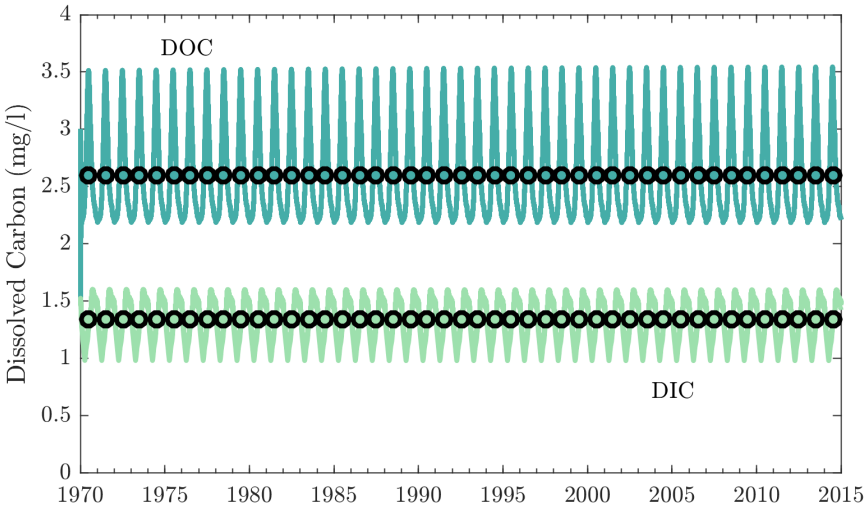

sedimentation.

Figure 26 – Modeled POC_L and POC_D concentrations of CICLAR calibrated for evaluative scenario. Lines and circles indicates daily and yearly averages respectively

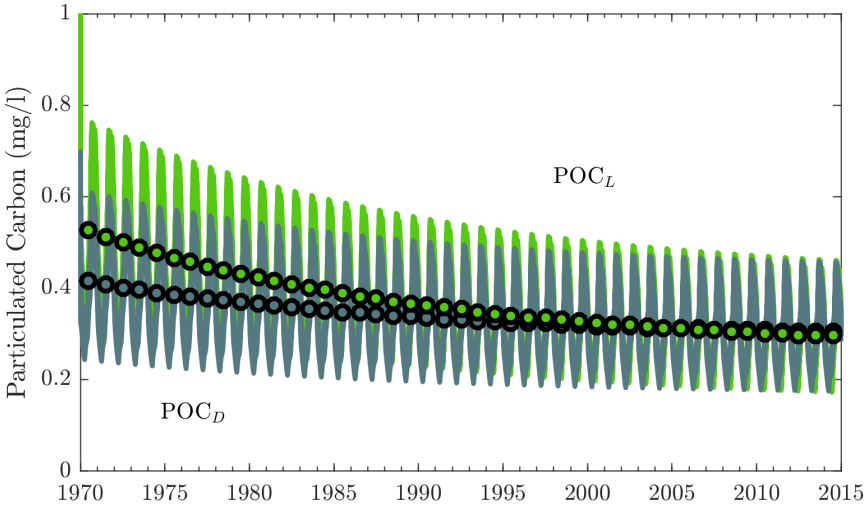

While the labile portion of the sediment is consumed, the refractory carbon concentration and total carbon stock increase throughout the years (Figure 27). Since sedimentation of particulated carbon form both refractory and labile carbon, what characterizes the consumption of the labile portion is higher ebullition rates (K_{EEB}), low decay rates (K_{FE}) and the presence of resuspension (K_{ED}).

5.2.2 Ideal scenario

The CPMOPSO calibration of the CICLAR model for the ideal scenario (Fig. 15) yielded 80 solutions, all of which had *NS* coefficients higher than 0.95 and, therefore, the filtering of the non-dominated set did not remove any solution. Resulting methane and

Figure 27 – Modeled total carbon stock and SC_L and SC_R concentrations of CICLAR calibrated under the evaluative scenario

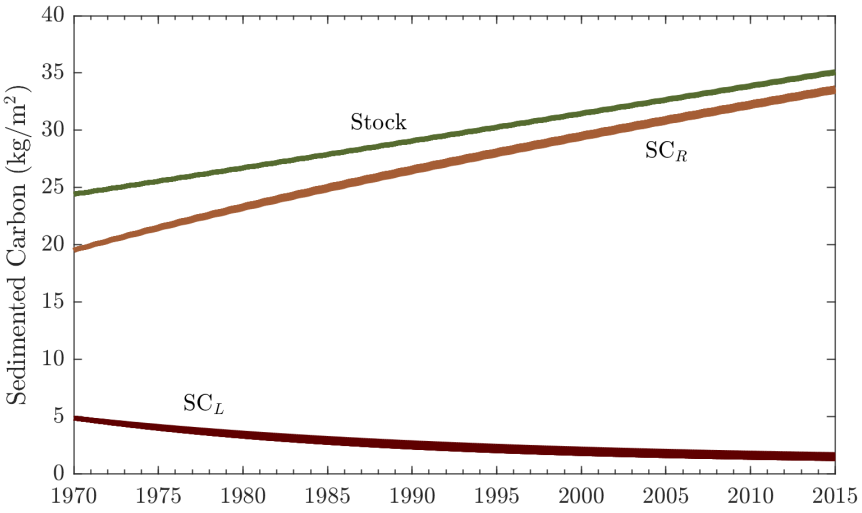

carbon dioxide fluxes, as well as the final total carbon stock, for all solutions are shown in Figure 28.

Figure 28 – GHG flux and total carbon stock for CPMOPSO calibration on the ideal scenario. Solid and dashed black lines indicate calibration and validation data respectively

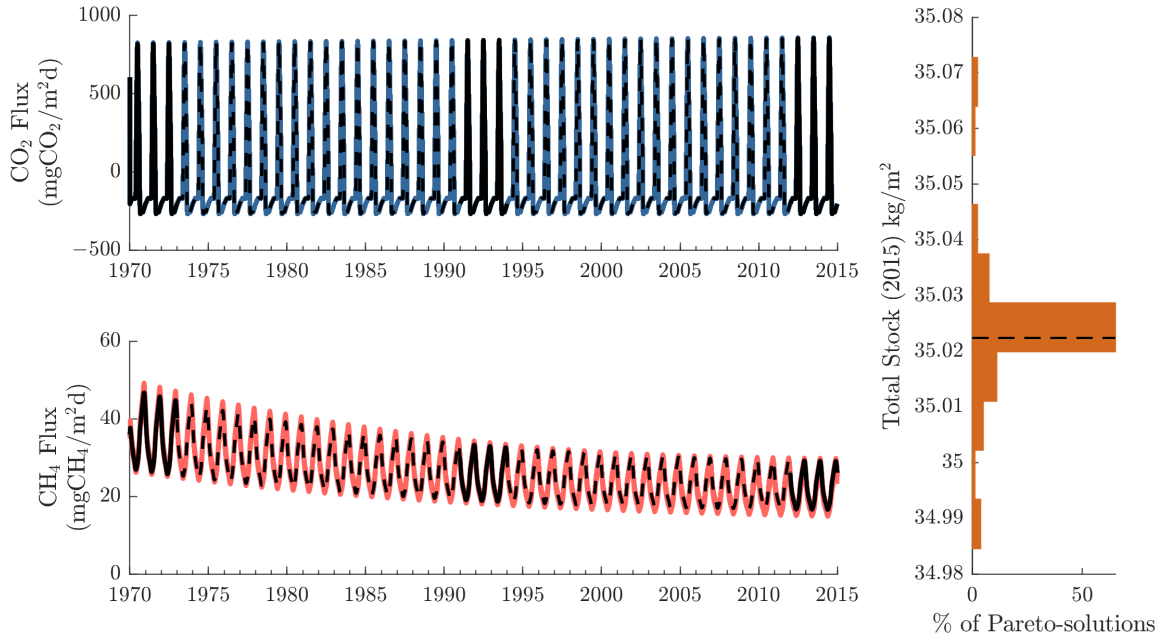

By using nine years of data: three at the beginning, three at the middle and three at the end of the simulation, the calibration had better results than under the evaluative scenario, which used the initial 30 years to calibrate the model. All CPMOPSO solutions modeled the yearly cycles of carbon dioxide and methane flux with precision, with some solutions slightly underestimating the overall methane emission (Figure 29).

Figure 29 – Yearly GHG flux for CPMOPSO calibration under the ideal scenario. Dashed black lines indicate validation data

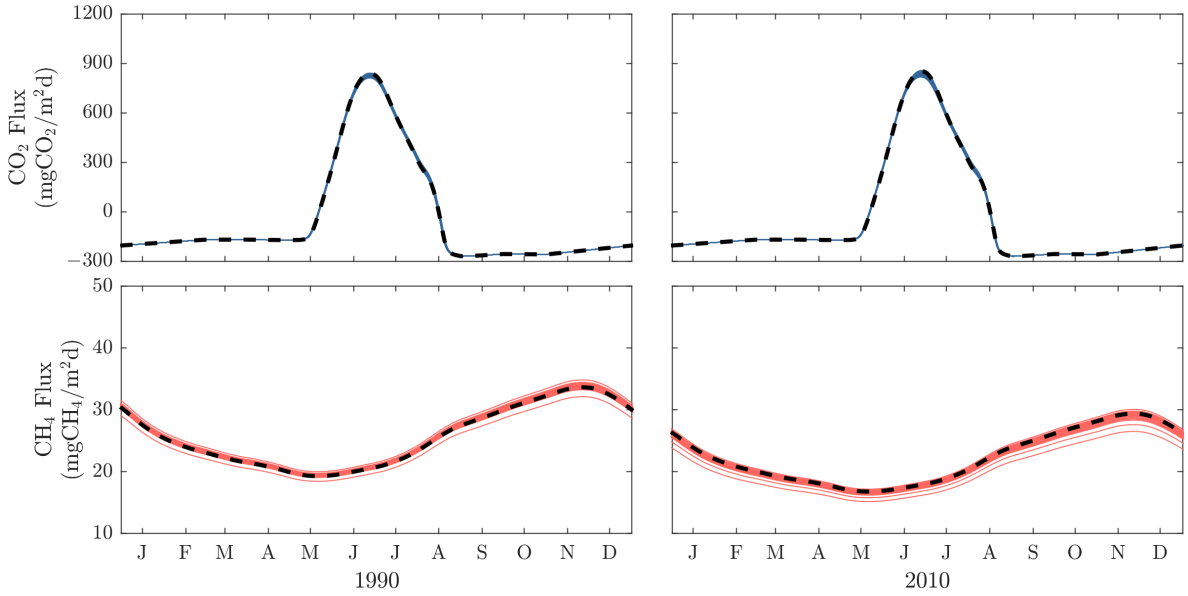

5.2.3 Retrospective scenario

The ability of the model of estimating past emissions by calibrating using only present data is assessed through the retrospective scenario. The CPMOPSO calibration resulted in 55 solutions, of which only 48 remained after the *NS* coefficient filter. Resulting GHG fluxes and final total carbon stock for all solutions are displayed in Figure 30.

Figure 30 – GHG flux and total carbon stock for CPMOPSO calibration on the retrospective scenario. Solid and dashed black lines indicate calibration and validation data respectively

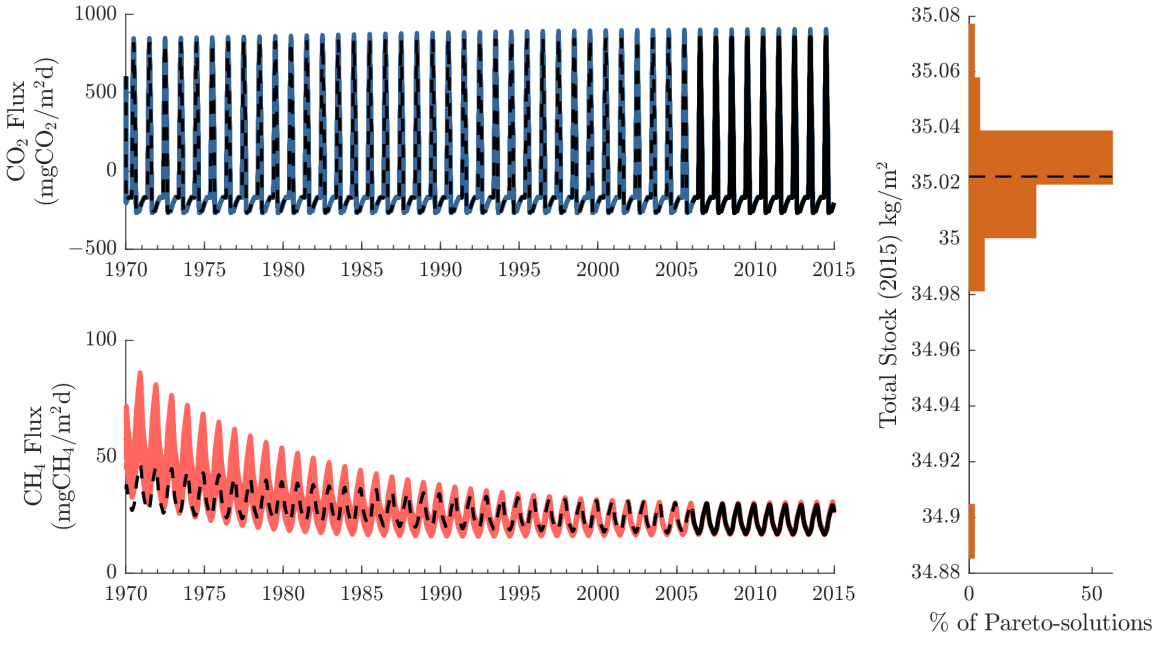

Even though the length of the calibration data of the ideal and retrospective scenarios are the same, the results of the retrospective calibration were worse than the one

with better distributed data. Although the estimation of the carbon dioxide flux cycle was accurate, the methane emission was increasingly overestimated the further they were into the past. Figure 31 shows that some solutions presented methane emissions 50% larger than the original series.

Figure 31 – Yearly GHG flux for CPMOPSO calibration under the retrospective scenario. Solid and dashed black lines indicate calibration and validation data respectively

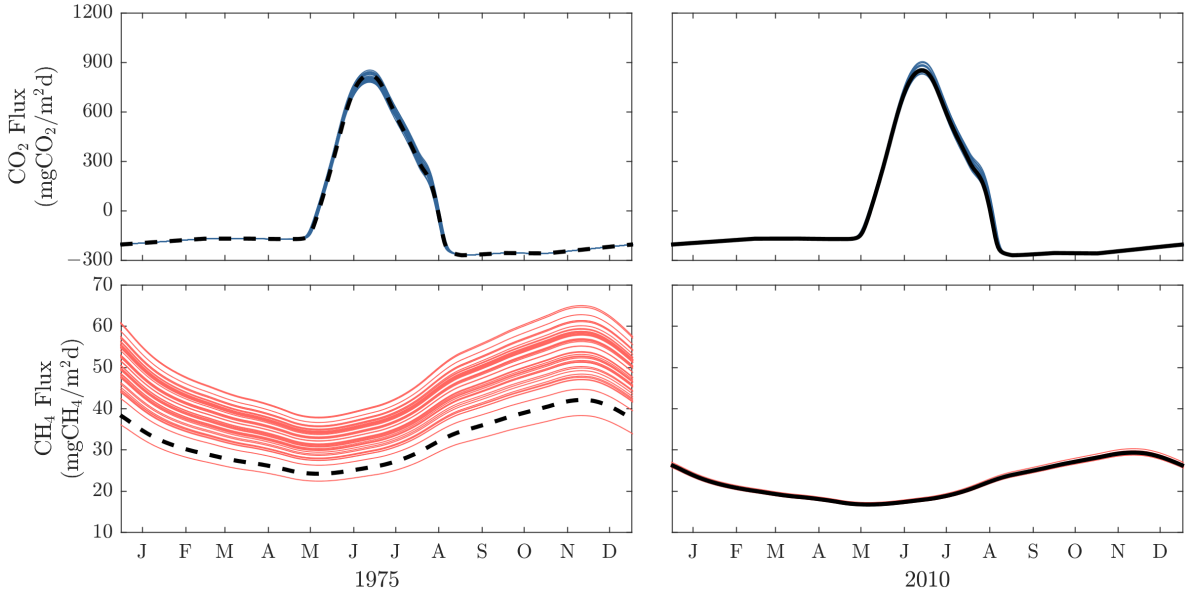

The fact that the solutions overestimated methane emissions but had, for the most part, total carbon stock errors lower than 20 g/m^2 is due to the model stocking more carbon in the refractory portion of the sediment and increasing the ebullition rate K_{EEB} from the labile sedimented carbon compartment, as shown in Figure 32.

Figure 32 – Modeled total carbon stock and SC_L and SC_R concentrations of CICLAR calibrated under the retrospective scenario

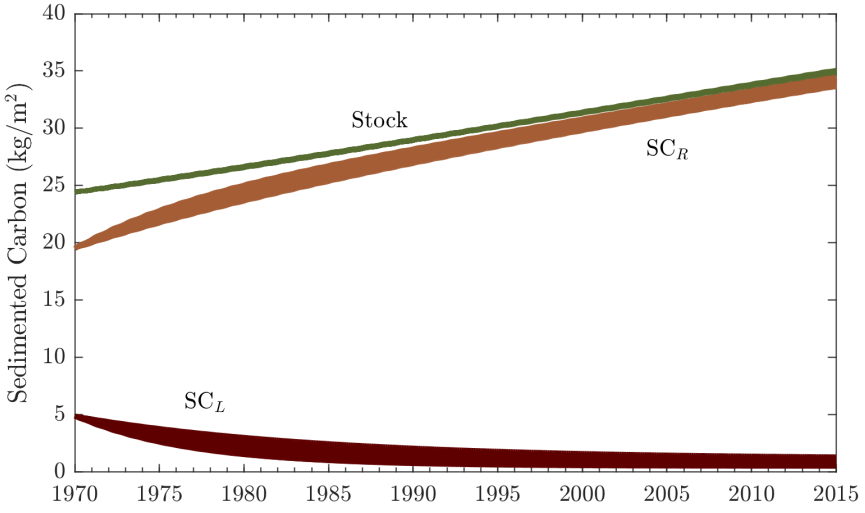

Ebullition rates for all CPMOPSO solutions for the retrospective scenario are shown in Figure 33. By increasing the ebullition of labile sedimented carbon, the model

quickly depleted the SC_L compartment, producing larger methane emissions in the early stages of the reservoir. After the labile portion is depleted, all CH_4 emissions are from the refractory portion, which typically has lower ebullition rates. Therefore lower fluxes are produced at the calibration period, which is at the end of the simulation.

Figure 33 – CPMOPSO calibrated ebullition rates for the retrospective scenario. Gray bars indicate the manually calibrated parameters that were used to generate calibration data

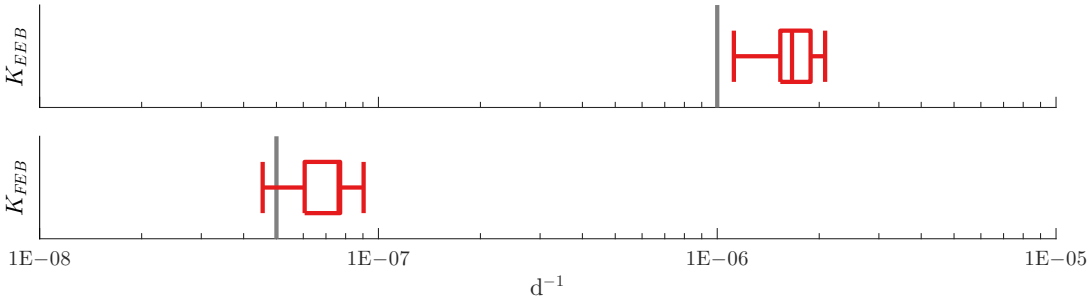

5.2.4 Prospective scenario

The GHG fluxes and total carbon stock in Figure 34 depicts the prognostic capabilities of the CICLAR model calibrated using only data at the early stages of the reservoir. The CPMOPSO algorithm returned 51 non-dominated solutions which were then filtered to 45 sets of CICLAR parameters.

Figure 34 – GHG flux and total carbon stock for CPMOPSO calibration on the prospective scenario. Solid and dashed black lines indicate calibration and validation data respectively. The total stock used for calibration was the value at the end of the calibration period

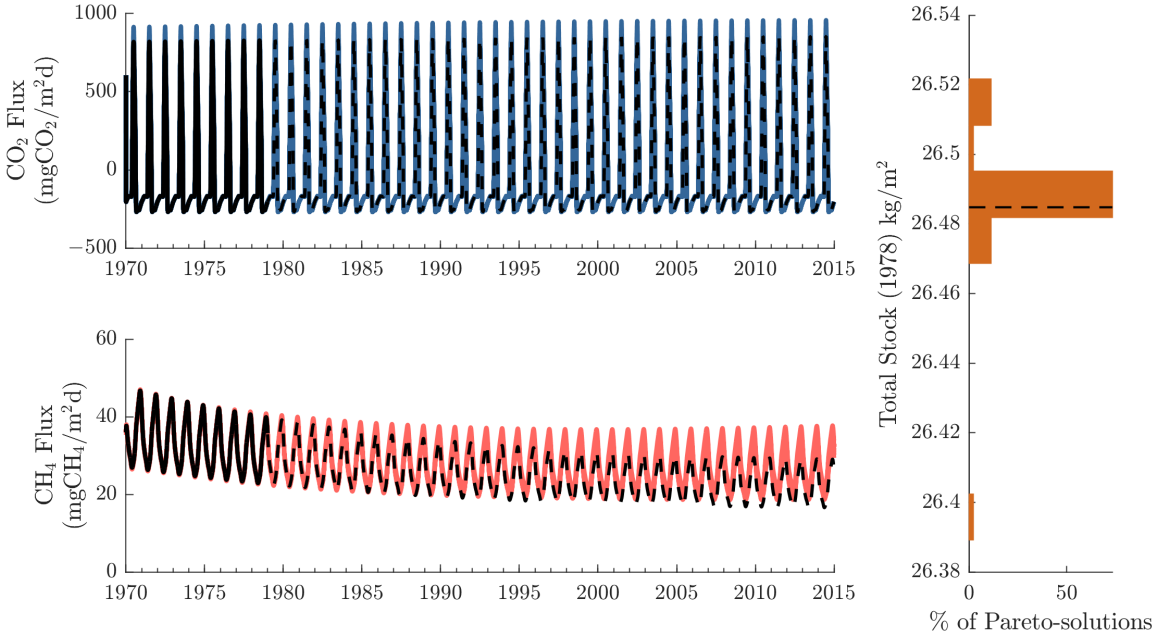

The model calibration under the prospective scenario also shows a tendency of overestimating methane emissions, however not as much as the retrospective calibration.

The modeled yearly cycle of carbon dioxide flux also presents some discrepancies regarding the original series during the winter (Figure 35). The values for the total carbon stock objective are on the same scale than the ones from other calibration scenarios, even though the interval between the start of the simulation and the end of the calibration period is about a tenth of other scenarios.

Figure 35 – Yearly GHG flux for CPMOPSO calibration under the prospective scenario. Dashed black lines indicate validation

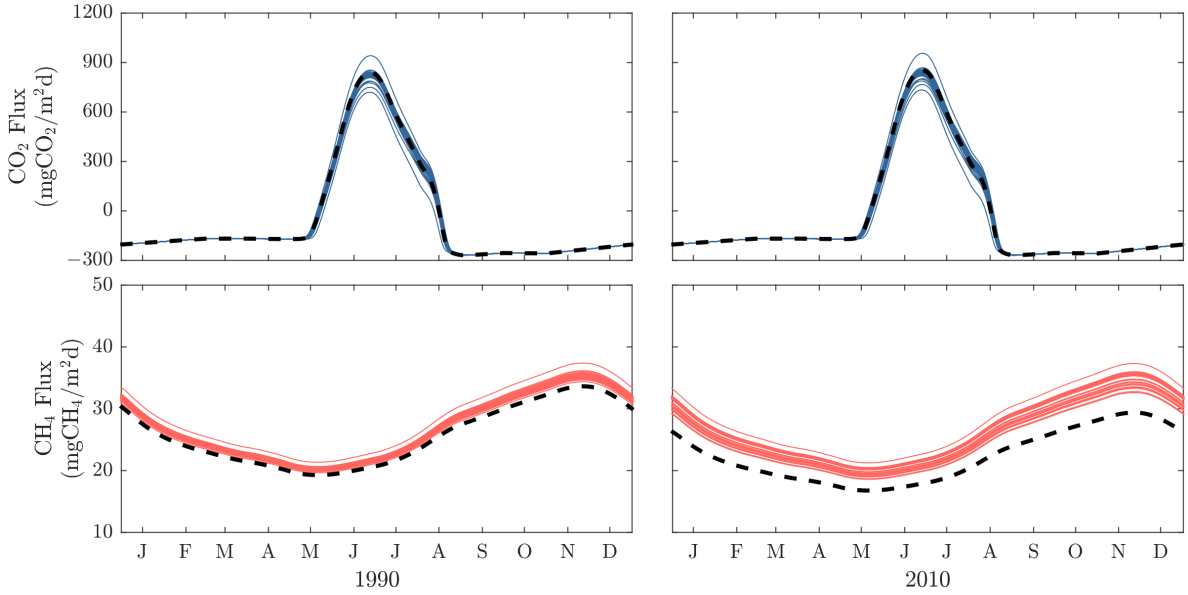

For the parameters calibrated under the prospective scenario, methane emissions remained more stable throughout the simulation than the results for the ones calibrated under other scenarios. This is due to higher ebullition rates for the refractory portion of the sediment which is, even with higher emissions, gradually increased over time. Such increase in refractory carbon ebullition compensates the decrease of methane emission from the labile portion of the sediment, which is consumed over time. The ebullition rates for all CPMOPSO solutions are shown in Figure 36, in which the decrease of K_{EEB} and increase of the K_{FEB} labile and refractory carbon ebullition rates compensate early methane emissions but result in larger emissions for latter periods.

Figure 36 – CPMOPSO calibrated ebullition rates for the prospective scenario. Gray lines indicate the manually calibrated parameters that were used to generate calibration data

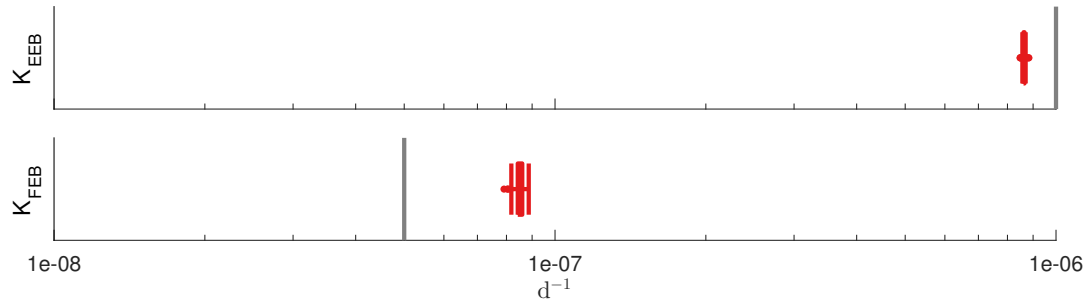

5.2.5 Scenarios Overview

The calibration under different scenarios differed mainly regarding the methane emission, while the carbon dioxide flux was modeled more evenly throughout scenarios. To analyze these different results, the cumulative distribution of the average global warming potential (Equation 4.4) for each scenario is shown in 37.

Figure 37 – Impact of different calibration scenarios on the GWP cumulative distribution function. Dashed line indicate the average GWP of the calibration data

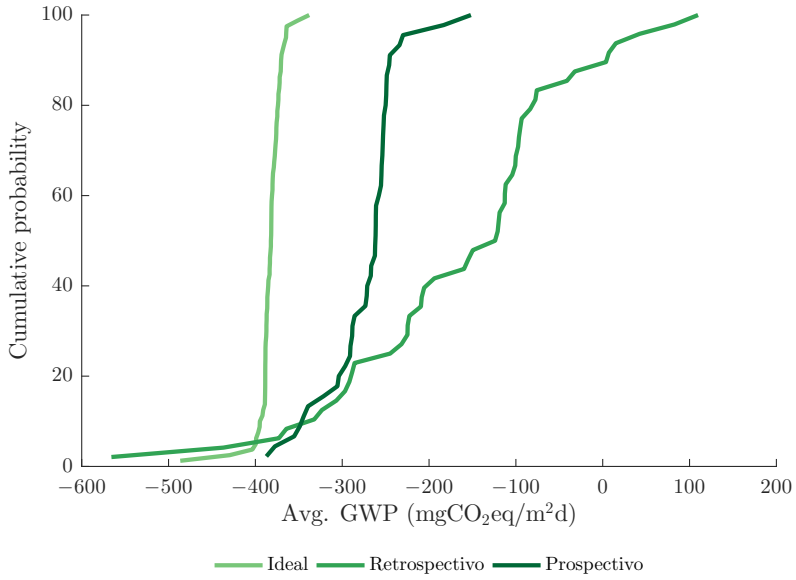

The overestimated methane emissions of the retrospective and prospective scenarios resulted in larger global warming potentials when compared to the value of -383.5 mgCO$_2$eq/m^{2}d for the calibration data. The solutions for the ideal calibration scenario presented average GWPs between -486.5 and -338.0 mgCO$_2$eq/m^{2}d without bias to over or under estimating the global warming impact.

Even though the calibrations had a tendency to overestimate methane emissions and global warming impact of the reservoir, only 6 of the 173 calibrated set of parameters would result in the reservoir having a positive GWP. Therefore, only 3% of the solutions would classify the Capivari reservoir as being a source of equivalent CO_2 to the atmosphere.

According to the cumulative distribution of average GWP, for 50% of calibrated solutions the reservoir absorbs at least 62.9, 16.4 and 42.1 Gg of equivalent carbon dioxide for the ideal, retrospective and prospective scenarios respectively. A histogram for the total absorption of equivalent carbon dioxide for solutions from all scenarios is displayed on Figure 38.

Although for most solutions the model accumulated great amounts of carbon in the refractory of the sediment, such increase in refractory carbon concentration may produce increasing methane emissions for simulations with more than 45 years.

Figure 38 – Absorbed equivalent CO_2 for solutions calibrated under the alternative stock for both ideal and retrospective scenarios. Negative values indicate emission of equivalent CO_2

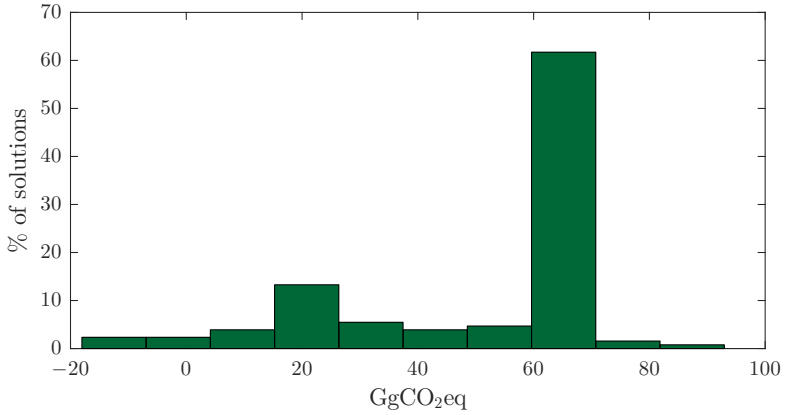

5.3 AUTOMATED CALIBRATION UNDER ALTERNATIVE STOCK

An alternative total carbon stock estimate, for both before and after the dam impoundment is presented by Bernardo et al. (2017). The pre-impoundment carbon stock was estimated as 9.0 ± 3.0 kgC/m^2 on the soil and 3.5 kgC/m^2 on vegetation, with a total carbon stock of 12.5 ± 3.0 kgC/m^2. The final total carbon stock was estimated as 26.55 ± 8.6 kgC/m^2.

To calibrate the CICLAR model using these different stock estimations, the initial conditions of the model were changed to adjust the pre-impoundment carbon stock. The same GHG fluxes for the ideal and retrospective scenarios were used, along with the alternative final total carbon stock, were used to calibrate the model. Since the initial condition of the model was modified, unlike the previous calibrations, there may be no set of parameters whose results fit the calibration data, i. e. a previously known solution.

5.3.1 Ideal Scenario

The resulting GHG fluxes and total carbon stocks of the CPMOPSO calibration of the CICLAR model under the ideal scenario are shown on Figure 39. The calibration yielded 1724 solutions that were reduced to 62 by the NS filter. The fact that 96% of the solutions were removed by having low NS values may be evidence that the 100 iterations of the optimization algorithm were not enough and that the method had not yet converged.

Although all calibrated solutions underestimated the final total carbon stock by at least 700 gC/m^2, all estimations remained inside the 26.55 ± 8.6 kgC/m^2 estimated range. Calibrated solutions were able to model both CO_2 stationary flux and CH_4 decaying emissions. The yearly GHG fluxes cycle is presented on Figure 40.

Although solutions were able to model the yearly cycle of winter emission and spring-autumn absorption of CO_2, errors of up to 300 mgCO_2/m^{2}d for the peak emission at

Figure 39 – GHG flux and total carbon stock for the ideal scenario calibration using alternative carbon stock

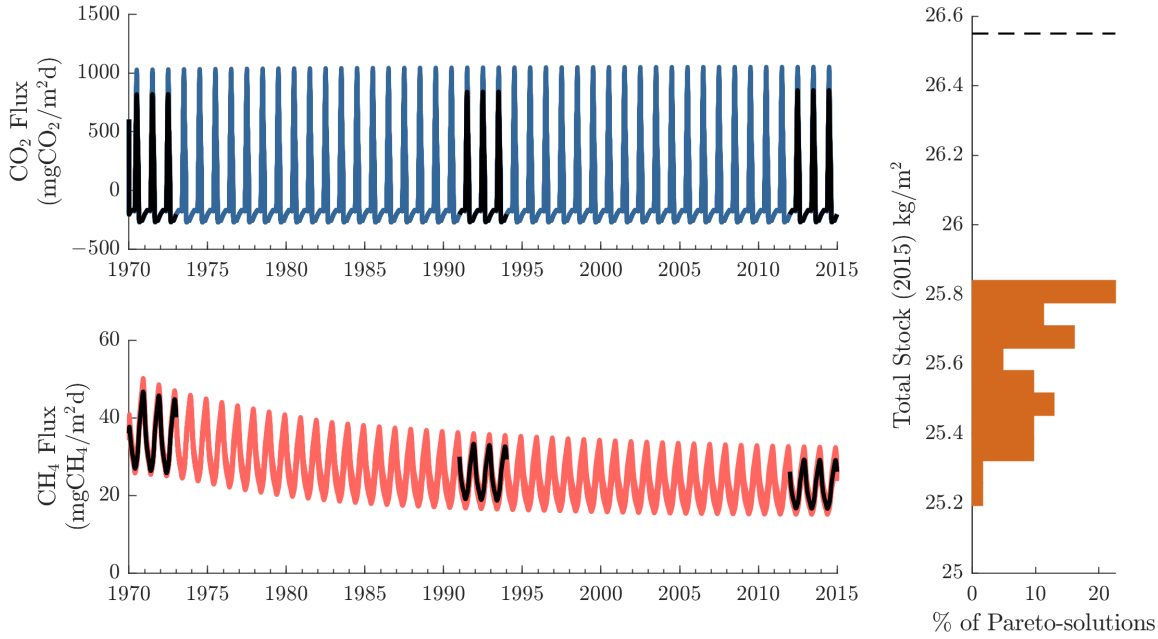

Figure 40 – Yearly GHG flux for ideal scenario calibration with alternative stock

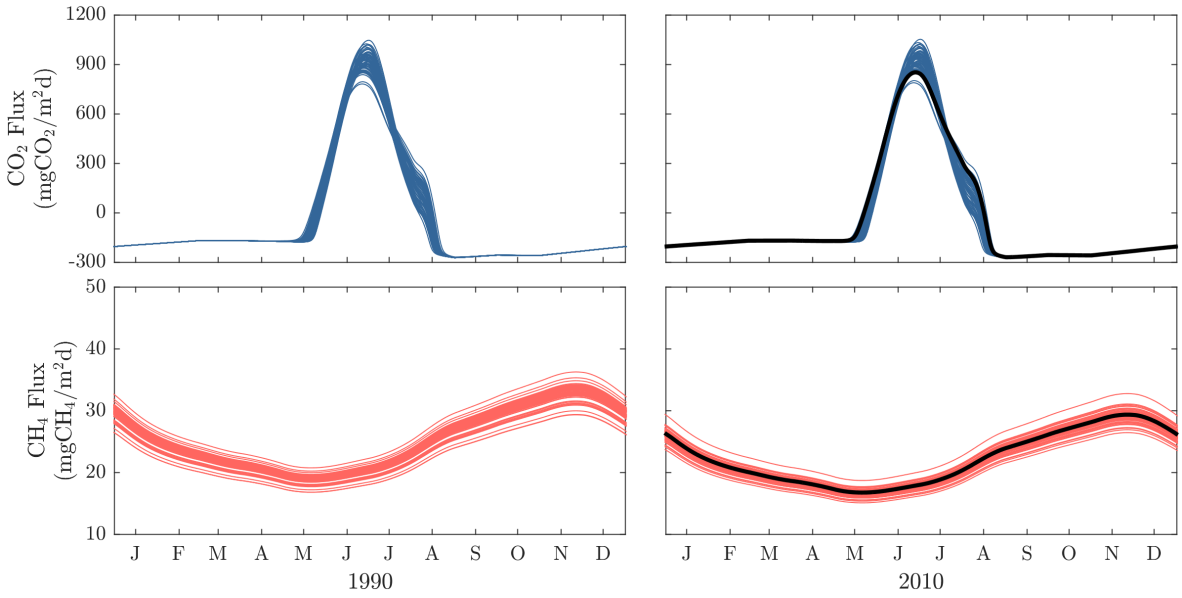

the end of June occurred. Solutions also underestimated carbon dioxide emissions by up to 250 $mgCO_2/m^2d$ at the beginning of August. Methane emissions modeled by CPMOPSO solutions presented errors around 2.5 $mgCH_4/m^2d$ without over or underestimation biases.

The resulting sedimented carbon and total stock for the CPMOPSO calibration under the ideal scenario and alternative stock is shown in Figure 41.

The initial 12.5 kgC/m^2 carbon stock is increased to values around 25.5 kgC/m^2 through sedimentation to the refractory portion of the sediment. Meanwhile the labile portion is gradually consumed over time reaching values lower than 100 gC/m^2.

Figure 41 – Modeled total carbon stock and SC_L and SC_R concentrations of CICLAR calibrated under the ideal scenario and alternative stock

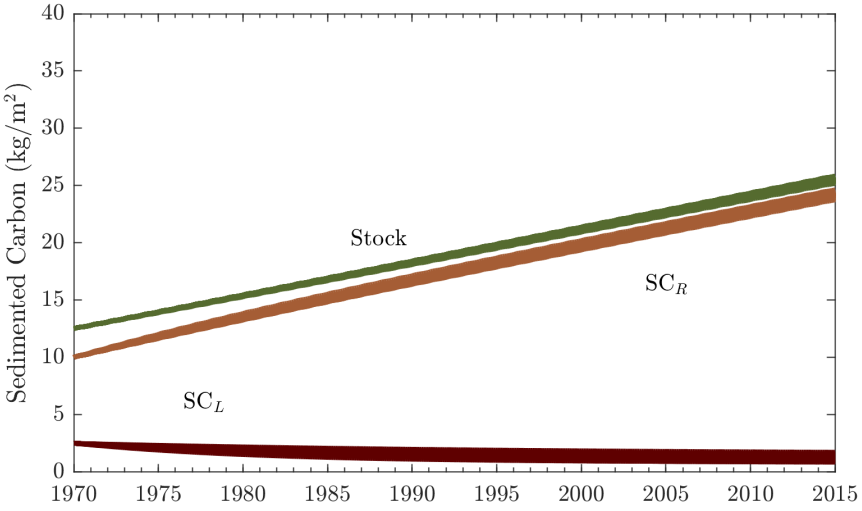

5.3.2 Retrospective Scenario

The process of calibrating the CICLAR model under the retrospective scenario using the stock estimated by Bernardo et al. (2017) is similar to the calibration on Mannich et al. (2015) in the sense that present data is used to estimate past fluxes. Since no previous solution to the calibration is known to exist, and therefore no validation data is available, all solutions that fit the calibration data to a certain degree are considered correct.

The CPMOPSO calibration using the alternative carbon stock estimation and the retrospective scenario yielded 1461 solutions. The application of the NS filter reduced the number of Pareto solutions to 73, indicating that the algorithm did not converge on only 100 iterations. GHG fluxes and final total carbon stocks for all filtered solutions are shown in Figure 42.

Although calibrated methane emissions had good fit for the calibration period ($NS \geq 0.95$) they significantly diverged on the remaining period. Some solutions attributed high emissions of up to 150 $mgCH_4/m^2d$ during the early ages of the reservoir, while some estimated low emissions of 10 $mgCH_4/m^2d$ that were gradually increased over time to fit the calibration values. GHG fluxes for the years of 1975 and 2010 are displayed in Figure 43.

Errors in modeled CO_2 flux for the calibration period are similar to the ones found for the ideal scenario calibration and reach absolute relative values of up to 30% during early and late July. The spread of modeled methane emissions for years closer to the impoundment of the dam, and therefore further from the calibration period, is evident on the 1975 plot in Figure 43.

Such divergence in modeled methane emissions are due to differences in labile and refractory sedimented carbon concentrations, as shown in Figure 44. Since solutions did

Figure 42 – GHG flux and total carbon stock for CPMOPSO calibration on the prospective scenario

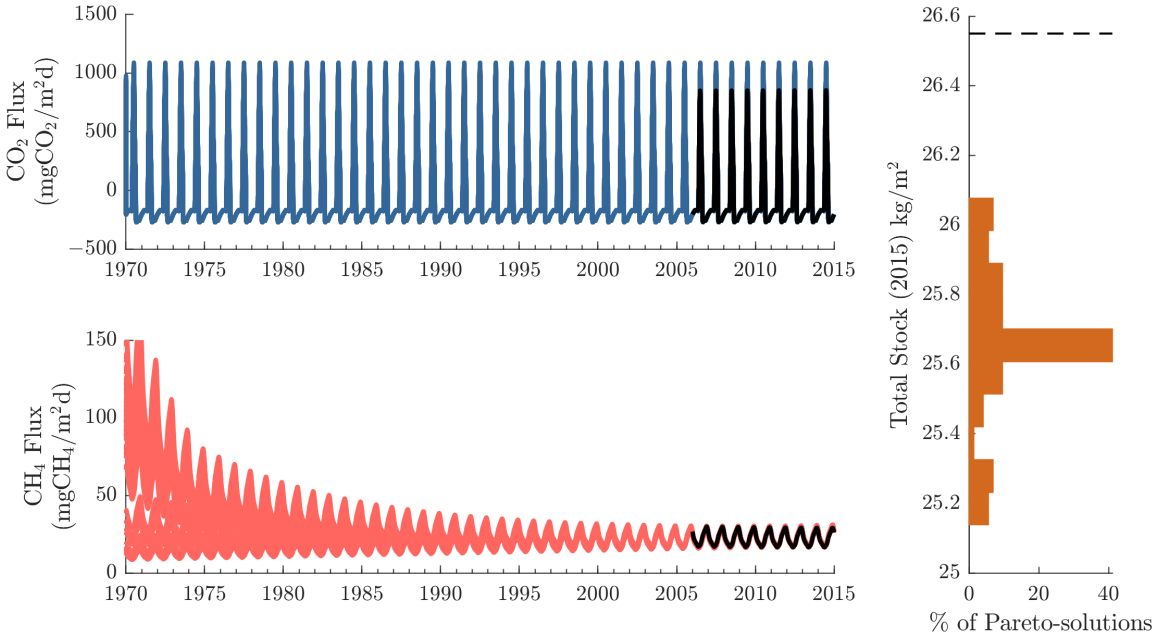

Figure 43 – Yearly fluxes for retrospective scenario calibration with alternative stock

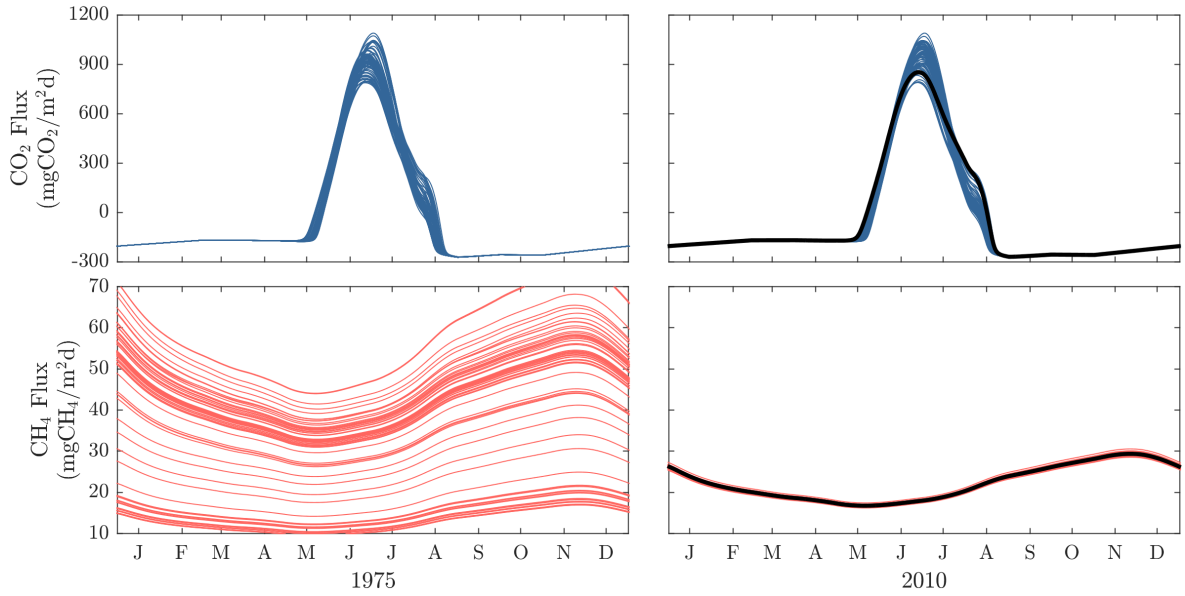

not diverge regarding the final total carbon stock, solutions with more labile sedimented carbon had less refractory sedimented carbon, and vice versa.

Unlike previous results, some calibrated solutions modeled an increase of labile sedimented carbon over time. These solutions compose about 30% of the filtered solution set. Since modeled refractory sedimented carbon concentration increases over time as well, these solutions modeled methane emissions with a positive temporal trend. Although those results dissent from the theory that methane emissions are larger in the early ages of the reservoir, they are expected when calibrating the model without using a better spread of calibration data.

Figure 44 – Modeled total carbon stock and SC_L and SC_R concentrations of CICLAR calibrated under the retrospective scenario and alternative stock

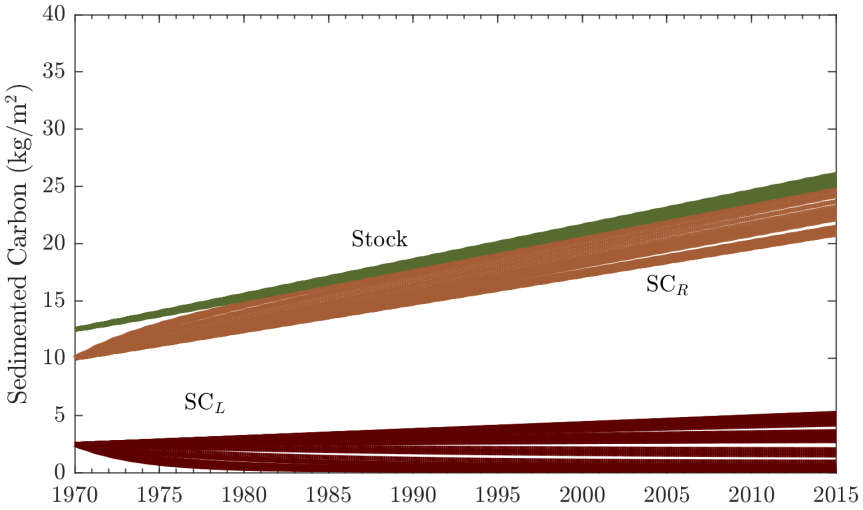

5.3.3 Scenarios Overview

The average GWPs for each solution for both scenarios using alternative carbon stock estimation were calculated using Equation 4.4. The cumulative distribution for the GWP of filtered solutions for each scenario is shown in Figure 45.

Figure 45 – Average GWP cumulative distribution for the calibration of ideal and retrospective scenarios under alternative stock

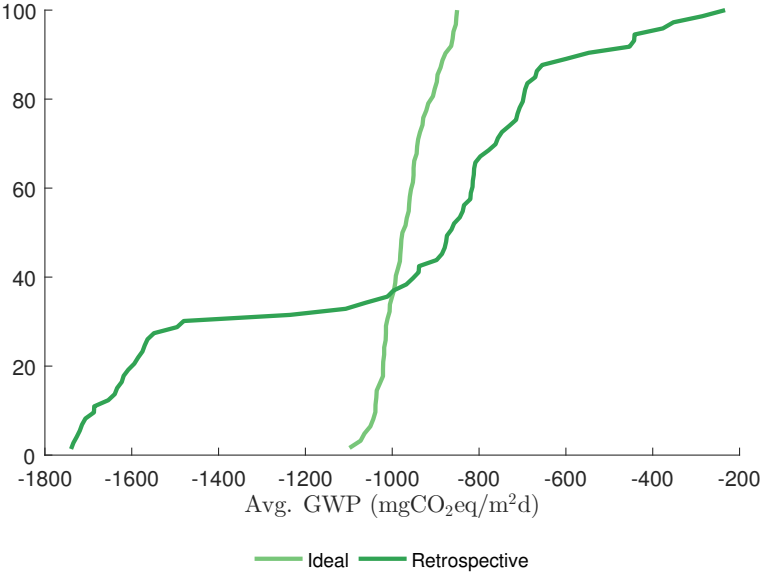

For solutions calibrated using the ideal scenario these GWP values varied between -1100 and -850 $mgCO_2eq/m^2d$. 50% of these calibrated solutions estimated that the reservoir absorbs at least 1 gram of equivalent carbon dioxide per square meter per day, with a total absorption of around 164.2 Gg of CO_2eq over the 45 simulated years.

Due to uncertainties regarding methane emissions for solutions calibrated under the retrospective scenario, the resulting average GWPs varied more (between -1750 and

-200 mgCO_2eq/m^{2}d) when compared to the calibration of the ideal scenario. Although the retrospective calibration yielded solutions with high methane emissions, the median average GWP indicates an absorption of 0.85 g equivalent carbon dioxide per square meter per day. Figure 46 presents a histogram of the total absorbed equivalent carbon dioxide of both ideal and retrospective scenarios.

Figure 46 – Absorbed equivalent CO_2 for solutions calibrated under the alternative stock for both ideal and retrospective scenarios

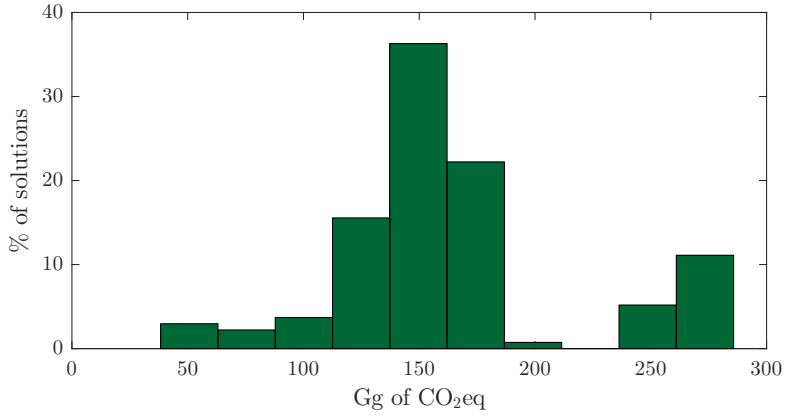

The calibration under the alternative stock estimation yielded solutions with higher equivalent carbon dioxide absorption, when compared to the standard calibration. Also in contrast to the standard calibration, no solutions calibrated under the alternative stock modeled the Capivari reservoir as a source of equivalent CO_2 to the atmosphere.

6 CONCLUSION

The fact that a novel metaheuristic algorithm was developed in the process of automating the calibration of the CICLAR model is in accordance with the recent trend of utilizing artificial intelligence methods throughout engineering research. These metaheuristic algorithms were made possible by advances in computer machinery and are only expected to grow in popularity and applicability as further progress is made in computer engineering.

The CPMOPSO technique combines different particle swarm optimization implementations into a single parametrizable method. The combined approach had a better performance than the aggregated when calibrating the CICLAR model by offering both better coverage and better quality of resulting sets of parameters. The CPMOPSO algorithm also performed better than simpler techniques when solving different complex multidimensional mathematical test functions (Appendix C).

The evaluative scenario calibration showed that aside from having good performances for the calibration period ($NS \geq 0.95$), all solutions for the five different CPMOPSO calibrations successfully predicted carbon dioxide fluxes for the validation period. The CPMOPSO algorithm had difficulties calibrating parameters to fit modeled methane emissions, due to being non-stationary, unlike modeled CO_2 flux. Despite that, over 50% of all solutions for the 5 calibrations of the evaluative scenario had Nash-Sutcliffe coefficient values of over 0.95 for the validation period for both methane and carbon dioxide fluxes, while the absolute errors in modeled total carbon stock were lower than 100 grams of carbon per square meter.

Even though the retrospective, prospective and ideal scenarios all use nine years of data to calibrate the model, the solutions that used the ideal scenario had a better performance on modeling the data. This is evidence that the spread of data is more important than its quantity when calibrating the CICLAR model. The calibration under the ideal scenario had better results even when compared to the ones under the evaluative scenario that used 30 years of unevenly spread data.

Both retrospective and prospective calibrations tended to overestimate methane emission on periods where no calibration data was used. The yearly cycle of absorbing CO_2 during spring-autumn seasons and emitting it during the winter was achieved in each calibration scenario. Most solutions had relative errors lower than 1% when modeling the total carbon stock. Although the calibrations yielded some parameter sets with good objective values, the previously known solution that was used to generate calibration data was not found by any scenario.

Even with the overestimation of methane emissions, 97% of the calibration results for all scenarios implied that the Capivari reservoir is a sinkhole of equivalent carbon dioxide. This classification was done by calculating the cumulative distribution of the average GWP for each scenario, where only a few solutions calibrated under the retrospective scenario classified the reservoir as a source of equivalent CO_2. More than 50% of solutions indicated that the reservoir absorbs at least 15 Gg of equivalent CO_2 over the 45 simulated years.

The alternative carbon stock estimate developed by Bernardo et al. (2017) offered a framework for the calibration in which no previous solution was known. To use this estimate the initial state of the model was adjusted to the alternative pre-impoundment data. Since the GHG fluxes used to calibrate the model were generated using the previous initial carbon stock, which was over 100% larger than alternative one, the resulting rates regarding ebullition were considerably lower.

The CPMOPSO calibration using alternative stock estimates and the GHG fluxes from the ideal scenario yielded stable solutions that did not diverge from one another regarding any of the 3 objectives. Although the solutions reproduced the yearly cycle of CO_2, errors of up to 30% occurred during peak emissions at the end of July. The decreasing trend of methane emissions was also reproduced by the calibrated solutions without any over or underestimation bias. Although errors of up to 1.5 kg of final total stocked carbon were detected, all solutions remained within the uncertainty error of the calibration stock.

Solutions calibrated under the retrospective scenario and alternative stock significantly diverged regarding methane emissions at the early ages of the reservoir. While some solutions modeled emissions of up to 150 $mgCH_4/m^2d$ after the impoundment of the dam, others had lower emissions of 10 $mgCH_4/m^2d$ that were gradually increased and matched the values between 20 and 25 $mgCH_4/m^2d$ close to the end of the simulation. These drastic differences regarding methane emissions are due the dynamic between the labile and refractory portions of the sediment and its respective ebullition rates.

The fact that calibrated solutions fitted the data at the calibration period and differed from one another on the remaining period is due to the versatility of the CICLAR model. It is also evidence that the model requires well spread data to perform a better calibration with lower divergence among solutions. This also delineates the risks of generalizing results obtained through single objective or aggregated calibration in which only one solution is returned, since a solution with higher/lower methane emissions can classify the reservoir as a carbon source/sinkhole.

On the other hand, the calibration found many different set of parameters that resulted in very similar GHG fluxes and total carbon stock estimations. Further investigation of relationships between inner CICLAR parameters is required to assess whether this characteristic enables model simplification. Since CPMOPSO is a metaheuristic technique it does not guarantee optimality of the returned Pareto-front. Relationships between

parameters may be analyzed to provide further inside regarding these different values that result in similar GHG fluxes and whether the true Pareto-front is finite.

The CICLAR model and CPMOPSO calibration combination offer a tool to be used in data management and GHG assessment on both preexisting and future reservoirs. By properly addressing uncertainties regarding both, the theoretical simplifications of the carbon dynamic model, and the errors regarding measurement and extrapolation of water quality and flux data, this tool can be applied to other reservoirs and used to assess whether they have a positive or negative impact on the global warming effect.

FUTURE RECOMMENDATIONS

The near equivalence between different parameter sets indicate that the CICLAR model needs to be improved regarding its theoretical model. The incorporation of processes like thermal stratification by modeling the epilimnion and hipolimnion as two mixed layers that exchange mass and energy with each other is a possibility. The addition of dissolved methane and oxygen as compartments within the model can be used to improve the modeling of the carbon cycle dynamics and estimate process such as CH_4 diffusion.

Although the results showed that the spread is more important than the amount of calibration data, further analysis of the performance of the model under different scenarios might provide insight regarding what is required to properly calibrate the model. Different scenario might also be helpful when deciding upon future field measurement campaigns. Additional data such as pH and dissolved carbon concentration might also be used to calibrate the CICLAR model by adjusting the number of objectives and the leader selection criteria of CPMOPSO.

Even though the average GWP was used to aggregate multiple solutions into discrete cumulative probabilities, more advanced techniques such as Bayesian aggregation methods can be used to provide better probabilistic estimations. The Generalized Likelihood Uncertainty Estimation or GLUE by Beven e Binley (1992) could also be used to quantify uncertainties regarding both model and parameter errors through multiple Monte Carlo simulations.

Further analysis regarding the CPMOPSO parameters and how they impact the calibration performance is also possible. Using more subswarms and more particles might reduce the susceptibility of the algorithm to local minima at the cost of computational time. Enabling the algorithm to perform more iterations might also improve the results, mainly regarding the alternative stock calibrations, in which the low quality of multiple Pareto solutions is detected.

BIBLIOGRAPHY

AFSHAR, A.; KAZEMI, H.; SAADATPOUR, M. Particle Swarm Optimization for Automatic Calibration of Large Scale Water Quality Model (CE-QUAL-W2): Application to Karkheh Reservoir, Iran. *Water Resources Management*, v. 25, n. 10, p. 2613–2632, 2011. ISSN 09204741.

ALBUQUERQUE FILHO, J. L.; SAAD, A. R.; ALVARENGA, M. C. d. Considerações Acerca dos Impactos Ambientais Decorrentes da Implantação de Reservatorios Hidrelétricos com Ênfase nos efeitos ocorrentes em aquíferos livres e suas consequências. *Geociênc. (São Paulo)*, scieloppegeo, v. 29, p. 355 – 367, 00 2010. ISSN 0101-9082.

ALRASHIDI, M.; EL-HAWARY, M. A Survey of Particle Swarm Optimization Applications in Electric Power Systems. *IEEE Transactions on Evolutionary Computation*, v. 13, n. 4, p. 913–918, 2009. ISSN 1089-778X.

ALVAREZ-BENITEZ, J. E.; EVERSON, R. M.; FIELDSEND, J. E. A mopso algorithm based exclusively on pareto dominance concepts. In: *Proceedings of the Third International Conference on Evolutionary Multi-Criterion Optimization*. Berlin, Heidelberg: Springer-Verlag, 2005. (EMO'05), p. 459–473. ISBN 3-540-24983-4, 978-3-540-24983-2.

ARDIZZON, G.; CAVAZZINI, G.; PAVESI, G. Adaptive acceleration coefficients for a new search diversification strategy in particle swarm optimization algorithms. *Information Sciences*, Elsevier Inc., v. 299, p. 337–378, 2015. ISSN 00200255.

BARRETTE, N.; LAPRISE, R. Numerical modeling: A complementary tool for studying co2 emissions from hydroelectric reservoirs. *Global Biogeochemical Cycles*, v. 16, n. 4, p. 75–1–75–11, 2002. ISSN 1944-9224. 1128.

BARROS, N. et al. Carbon emission from hydroelectric reservoirs linked to reservoir age and latitude. *Nature Geoscience*, Nature Publishing Group, v. 4, n. 9, p. 593–596, 2011. ISSN 1752-0894.

BASTVIKEN, D. et al. Fates of methane from different lake habitats: Connecting whole-lake budgets and ch4 emissions. *Journal of Geophysical Research: Biogeosciences*, v. 113, n. G2, p. n/a–n/a, 2008. ISSN 2156-2202. G02024.

ÅBERG, J.; JANSSON, M.; JONSSON, A. Importance of water temperature and thermal stratification dynamics for temporal variation of surface water co2 in a boreal lake. *Journal of Geophysical Research: Biogeosciences*, v. 115, n. G2, p. n/a–n/a, 2010. ISSN 2156-2202. G02024.

BERNARDO, J. W. Y. et al. A method for the assessment of long-term changes in carbon stock by construction of a hydropower reservoir. *Ambio*, p. 1–12, 2017. ISSN 1654-7209.

BEVEN, K.; BINLEY, A. The future of distributed models: Model calibration and uncertainty prediction. *Hydrological Processes*, John Wiley & Sons, Ltd, v. 6, n. 3, p. 279–298, 1992. ISSN 1099-1085.

BLUM, C. et al. Hybrid metaheuristics in combinatorial optimization: A survey. *Applied Soft Computing*, v. 11, n. 6, p. 4135 – 4151, 2011. ISSN 1568-4946.

BOUSSAïD, I.; LEPAGNOT, J.; SIARRY, P. A survey on optimization metaheuristics. *Information Sciences*, v. 237, p. 82 – 117, 2013. ISSN 0020-0255. Prediction, Control and Diagnosis using Advanced Neural Computations.

CHAPRA, S. C. *Surface water-quality modeling*. [S.l.]: Waveland press, 2008.

COELLO, C. A. C.; PULIDO, G. T.; LECHUGA, M. S. Handling multiple objectives with particle swarm optimization. *IEEE Transactions on Evolutionary Computation*, v. 8, n. 3, p. 256–279, June 2004. ISSN 1089-778X.

COELLO COELLO, C. A.; LECHUGA, M. S. MOPSO: A proposal for multiple objective particle swarm optimization. *Proceedings of the 2002 Congress on Evolutionary Computation, CEC 2002*, v. 2, p. 1051–1056, 2002.

COLE, J. et al. Plumbing the global carbon cycle: Integrating inland waters into the terrestrial carbon budget. *Ecosystems*, Springer-Verlag, v. 10, n. 1, p. 172–185, 2007. ISSN 1432-9840.

DEAN, W. E.; GORHAM, E. Magnitude and significance of carbon burial in lakes, reservoirs, and peatlands. *Geology*, v. 26, n. 6, p. 535–538, 1998.

DEB, K. et al. Scalable multi-objective optimization test problems. *Proceedings of the 2002 Congress on Evolutionary Computation, CEC 2002*, v. 1, n. i, p. 825–830, 2002. ISSN 1619-7127.

DOWNING, J. A. et al. The global abundance and size distribution of lakes, ponds, and impoundments. *Limnology and Oceanography*, v. 51, n. 5, p. 2388–2397, 2006. ISSN 1939-5590.

DUCHEMIN, E. et al. Production of the greenhouse gases ch4 and co2 by hydroelectric reservoirs of the boreal region. *Global Biogeochemical Cycles*, v. 9, n. 4, p. 529–540, 1995. ISSN 1944-9224.

EBERHART, R.; KENNEDY, J. A new optimizer using particle swarm theory. In: *Micro Machine and Human Science, 1995. MHS '95., Proceedings of the Sixth International Symposium on*. [S.l.: s.n.], 1995. p. 39–43.

EPE. *Balanço Energetico Nacional 2015 - Ano base 2014: Relatório Síntese*. [S.l.], 2015.

FEARNSIDE, P. M. Hydroelectric Dams in the Brazilian Amazon as Sources of 'Greenhouse' Gases. *Environmental Conservation*, v. 22, n. 01, p. 7, 1995. ISSN 0376-8929.

FEARNSIDE, P. M. Greenhouse gas emissions from hydroelectric dams: Controversies provide a springboard for rethinking a supposedly "clean" energy source. *Climatic Change*, v. 66, n. 1-2, p. 1–8, 2004. ISSN 0165-0009.

FEARNSIDE, P. M. Greenhouse gas emissions from hydroelectric dams: Reply to Rosa et al. *Climatic Change*, v. 75, n. 1-2, p. 103–109, 2006. ISSN 01650009.

FIELDSEND, J. E.; EVERSON, R. M.; SINGH, S. Using unconstrained elite archives for multiobjective optimization. *IEEE Transactions on Evolutionary Computation*, v. 7, n. 3, p. 305–323, June 2003. ISSN 1089-778X.

FIELDSEND, J. E.; SINGH, S. *A Multi-Objective Algorithm based upon Particle Swarm Optimisation, an Efficient Data Structure and Turbulence.* 2002.

GALY-LACAUX, C. et al. Gaseous emissions and oxygen consumption in hydroelectric dams: A case study in french guyana. *Global Biogeochemical Cycles*, v. 11, n. 4, p. 471–483, 1997. ISSN 1944-9224.

GIANNIOU, S. K.; ANTONOPOULOS, V. Z. Evaporation and energy budget in lake vegoritis, greece. *Journal of Hydrology*, v. 345, n. 3–4, p. 212 – 223, 2007. ISSN 0022-1694.

GILL, M. K. et al. Multiobjective particle swarm optimization for parameter estimation in hydrology. *Water Resources Research*, v. 42, n. 7, p. n/a–n/a, 2006. ISSN 1944-7973. W07417.

HANSON, P. C. et al. A model of carbon evasion and sedimentation in temperate lakes. *Global Change Biology*, Blackwell Science Ltd, v. 10, n. 8, p. 1285–1298, 2004. ISSN 1365-2486.

HO, S. L. et al. A particle swarm optimization-based method for multiobjective design optimizations. *IEEE Transactions on Magnetics*, v. 41, n. 5, p. 1756–1759, May 2005. ISSN 0018-9464.

HOLLAND, J. *Adaptation in Natural and Artificial Systems.* Ann Arbor, MI, USA: University of Michigan Press, 1975.

HUANG, T.; MOHAN, A. S. A hybrid boundary condition for robust particle swarm optimization. *IEEE Antennas and Wireless Propagation Letters*, v. 4, p. 112–117, 2005. ISSN 1536-1225.

I, I. W. G. Climate change 1995 the science of climate change. In: _____. [S.l.]: IPCC, 1995.

IPCC. Climate change 1990 the science of climate change. In: _____. [S.l.]: The Intergovernmental Panel on Climate Change, 1990.

IPCC. Climate change 1992: The supplementary report to the ipcc scientific assessment. In: _____. Cambridge, United Kingdom and New York, NY, USA: Cambridge University Press, 1992.

IPCC. Climate change 1994: Radiative forcing of climate change and an evaluation of the ipcc is92 emission scenarios. In: _____. Cambridge, United Kingdom and New York, NY, USA: Cambridge University Press, 1994.

IPCC. Climate change 2001: The physical science basis. contribution of working group i to the fourth assessment report of the intergovernmental panel on climate change. In: _____. Cambridge, United Kingdom and New York, NY, USA: Cambridge University Press, 2001.

IPCC. Climate change 2007: The physical science basis. contribution of working group i to the fourth assessment report of the intergovernmental panel on climate change. In: _____. Cambridge, United Kingdom and New York, NY, USA: Cambridge University Press, 2007.

IPCC. Book. *Climate Change 2013: The Physical Science Basis. Contribution of Working Group I to the Fifth Assessment Report of the Intergovernmental Panel on Climate Change.* Cambridge, United Kingdom and New York, NY, USA: Cambridge University Press, 2013. 1535 p. ISBN ISBN 978-1-107-66182-0.

JIANG, Y. et al. An improved particle swarm optimization algorithm. *Applied Mathematics and Computation*, v. 193, n. 1, p. 231–239, 2007. ISSN 00963003.

JIANG, Y. et al. Improved particle swarm algorithm for hydrological parameter optimization. *Applied Mathematics and Computation*, v. 217, n. 7, p. 3207 – 3215, 2010. ISSN 0096-3003.

KAN, A. et al. *Proposta de metodologia para monitoramento e avaliação de gases de efeito estufa em reservatórios de usinas hidrelétricas brasileiras*. [S.l.], 2013.

KENNEDY, J.; EBERHART, R. Particle swarm optimization. In: *Neural Networks, 1995. Proceedings., IEEE International Conference on*. [S.l.: s.n.], 1995. v. 4, p. 1942–1948 vol.4.

KENNEDY, J.; MENDES, R. Population structure and particle swarm performance. In: *Evolutionary Computation, 2002. CEC '02. Proceedings of the 2002 Congress on*. [S.l.: s.n.], 2002. v. 2, p. 1671–1676.

KOTSOPOULOS, S.; BABAJIMOPOULOS, C. Analytical estimation of modified penman equation parameters. *Journal of Irrigation and Drainage Engineering*, v. 123, n. 4, p. 253–256, 1997.

LIMA, I. B. T. Biogeochemical distinction of methane releases from two Amazon hydroreservoirs. *Chemosphere*, v. 59, n. 11, p. 1697–1702, 2005. ISSN 00456535.

LIU, S. et al. Using genetic algorithms to calibrate a water quality model. *The Science of the total environment*, v. 374, p. 260–272, 2007. ISSN 0048-9697.

LOUIS, V. L. S. et al. Reservoir surfaces as sources of greenhouse gases to the atmosphere: A global estimate. *BioScience*, v. 50, n. 9, p. 766–775, 2000.

LOZOVIK, P. A. et al. Allochthonous and autochthonous organic matter in surface waters in karelia. *Water Resources*, v. 34, n. 2, p. 204–216, 2007. ISSN 1608-344X.

LU, Z.; GAN, J.; DAI, M. Modeling seasonal and diurnal pco2 variations in the northern south china sea. *Journal of Marine Systems*, v. 92, n. 1, p. 30 – 41, 2012. ISSN 0924-7963.

MADSEN, H. Parameter estimation in distributed hydrological catchment modelling using automatic calibration with multiple objectives. *Advances in Water Resources*, v. 26, n. 2, p. 205 – 216, 2003. ISSN 0309-1708.

MAIWALD, T.; TIMMER, J. Dynamical modeling and multi-experiment fitting with potterswheel. *Bioinformatics*, v. 24, n. 18, p. 2037–2043, 2008.

MANNICH, M. *ESTIMATIVA DE EMISSÕES DE GASES DE EFEITO ESTUFA EM RESERVATÓRIOS E LAGOS – CONTRIBUIÇÕES PARA O MONITORAMENTO E MODELAGEM 1D - VERTICAL*. Tese (Doutorado) — Programa de Pós Graduação em Engenharia de Recursos Hídricos e Ambiental - Universidade Federal do Paraná, Department of Environmental Engineering, Federal University of Parana, Curitiba 81531-990, Brazil, 3 2013.

MANNICH, M. et al. CICLAR: Modelo 0d para dinâmica de carbono em lagos e reservatórios. *Revista Brasileira de Recursos Hídricos*, Associacao Brasileira de Recursos Hidricos - ABRH, v. 20, n. 1, p. 237–248, 2015.

MENDONÇA, R. F. et al. Greenhouse gas emissions from hydroelectric reservoirs: What knowledge do we have and what is lacking? In: GUOXIANG, L. (Ed.). *Greenhouse gases: emission, measurement and management*. Rijeka: InTech, 2012. p. 55–78. ISBN 9789535103233.

MUKHERJEE, B.; PANDEY, P.; SINGH, S. Mathematical modelling and system analysis of inorganic carbon in the aquatic environment. *Ecological Modelling*, v. 152, n. 2–3, p. 129 – 143, 2002. ISSN 0304-3800.

MYHRE, G. et al. Anthropogenic and natural radiative forcing. In: _____. *Climate Change 2013: The Physical Science Basis. Contribution of Working Group I to the Fifth Assessment Report of the Intergovernmental Panel on Climate Change*. Cambridge, United Kingdom and New York, NY, USA: Cambridge University Press, 2013. book section 8, p. 659–740. ISBN ISBN 978-1-107-66182-0.

NDIRITU, J. G.; DANIELL, T. M. An improved genetic algorithm for rainfall-runoff model calibration and function optimization. *Mathematical and Computer Modelling*, v. 33, n. 6–7, p. 695 – 706, 2001. ISSN 0895-7177.

PLUMMER, L. N.; BUSENBERG, E. The solubilities of calcite, aragonite and vaterite in CO2-H2O solutions between 0 and 90C, and an evaluation of the aqueous model for the system CaCO3-CO2-H2O. *Geochimica et Cosmochimica Acta*, v. 46, n. 6, p. 1011–1040, 1982. ISSN 00167037.

POLI, R. An Analysis of Publications on Particle Swarm Optimisation Applications. *Journal of Artificial Evolution and Applications*, v. 2008, n. 2, p. 1–57, 2007. ISSN 1744-8050.

RAMSAY, J. O. et al. Parameter estimation for differential equations: a generalized smoothing approach. *Journal of the Royal Statistical Society: Series B (Statistical Methodology)*, Blackwell Publishing Ltd, v. 69, n. 5, p. 741–796, 2007. ISSN 1467-9868.

REDFIELD, A. C.; KETCHUM, B. H.; RICHARDS, F. A. *The Influence of Organisms on the Composition of Sea Water*. 1963. 26–77 p.

REFSGAARD, J. C.; HENRIKSEN, H. J. Modelling guidelines—terminology and guiding principles. *Advances in Water Resources*, v. 27, n. 1, p. 71 – 82, 2004. ISSN 0309-1708.

RESENDE, J. F.; MANNICH, M.; FERNANDES, C. V. S. Análise de sensibilidade do modelo ciclar para dinâmica de carbono em lagos e reservatórios. *Anais do XXI Simpósio Brasileiro de Recursos Hídricos*, 2015.

REYES-SIERRA, M.; COELLO, C. A. C. Multi-objective particle swarm optimizers: A survey of the state-of-the-art. *INTERNATIONAL JOURNAL OF COMPUTATIONAL INTELLIGENCE RESEARCH*, v. 2, n. 3, p. 287–308, 2006.

ROSA, L. P. et al. Scientific errors in the Fearnside comments on greenhouse gas emissions (GHG) from hydroelectric dams and response to his political claiming. *Climatic Change*, v. 75, n. 1-2, p. 91–102, 2006. ISSN 01650009.

ROSA, L. P. et al. Greenhouse Gas Emissions From Hydroelectric Reservoirs in Tropical Regions. *Climatic Change*, v. 66, n. 1, p. 9–21, 2004. ISSN 02583127.

ROSA, L. P.; SCHAEFFER, R. 95/04170 Global warming potentials. The case of emissions from dams. *Fuel and Energy Abstracts*, v. 36, n. 4, p. 294, 1995. ISSN 01406701.

ROTHLAUF, F. Optimization methods. In: _____. *Design of Modern Heuristics: Principles and Application*. Berlin, Heidelberg: Springer Berlin Heidelberg, 2011. p. 45–102. ISBN 978-3-540-72962-4.

RUDD, J. et al. Are hydroelectric reservoirs significant sources of greenhouse gases? *Ambio.*, v. 22, p. 246–248, 1993.

SBRISSIA, R. C. et al. Estimativa de emissões de gases de efeito estufa em reservatórios a partir da dinâmica da matéria orgânica na coluna da Água: Estudo de caso pch salto natal, campo mourão — paraná. *Revista Brasileira de Recursos Hídricos*, v. 16, n. 13, p. 59–69, 2011. ISSN 1414-381X.

SHI, Y.; EBERHART, R. C. Empirical study of particle swarm optimization. In: *Proceedings of the 1999 Congress on Evolutionary Computation-CEC99 (Cat. No. 99TH8406)*. [S.l.: s.n.], 1999. v. 3, p. 1950 Vol. 3.

SHIN, W. S.; RAVINDRAN, A. Interactive multiple objective optimization: Survey i—continuous case. *Computers and Operations Research*, v. 18, n. 1, p. 97 – 114, 1991. ISSN 0305-0548.

SPILIOPOULOU, A. et al. Macroscopic Traffic Flow Model Calibration Using Different Optimization Algorithms. *Transportation Research Procedia*, Elsevier B.V., v. 6, n. June 2014, p. 144–157, 2015. ISSN 23521465.

STUMM, W. E.; MORGAN, J. J. e. *Aquatic Chemistry: Chemical Equilibria and Rates in Natural Waters*. [S.l.: s.n.], 1993. Third. 1022 p. ISSN 00167037. ISBN 0471511846.

TARANTOLA, A. *Inverse Problem Theory and Methods for Model Parameter Estimation*. Philadelphia, PA, USA: Society for Industrial and Applied Mathematics, 2004. ISBN 0898715725.

TRANVIK, L. J. et al. Lakes and reservoirs as regulators of carbon cycling and climate. *Limnology and Oceanography*, v. 54, n. 6part2, p. 2298–2314, 2009. ISSN 1939-5590.

TREMBLAY, A.; LAMBERT, M.; GAGNON, L. Do hydroelectric reservoirs emit greenhouse gases? *Environmental Management*, Springer-Verlag, v. 33, n. 1, p. S509–S517, 2004. ISSN 0364-152X.

TUNDISI, J.; MATSUMURA-TUNDISI, T. *Recursos Hídricos no Século XXI*. [S.l.]: Oficina de Textos, 2011. ISBN 9788579750694.

WANNINKHOF, R. Relationship between wind speed and gas exchange over the ocean. *Journal of Geophysical Research: Oceans*, v. 97, n. C5, p. 7373–7382, 1992. ISSN 2156-2202.

WEIPING, H. et al. A model on the carbon cycling in lake taihu, china. *Ecological Modelling*, v. 222, n. 16, p. 2973 – 2991, 2011. ISSN 0304-3800. Non-equilibrium Thermodynamics in Ecology.

WOLPERT, D. H.; MACREADY, W. G. No free lunch theorems for optimization. *Trans. Evol. Comp*, IEEE Press, Piscataway, NJ, USA, v. 1, n. 1, p. 67–82, abr. 1997. ISSN 1089-778X.

ZAMBRANO-BIGIARINI, M.; ROJAS, R. A model-independent Particle Swarm Optimisation software for model calibration. *Environmental Modelling and Software*, Elsevier Ltd, v. 43, p. 5–25, 2013. ISSN 13648152.

APPENDIX A – HEAT BUDGET MODEL

Shortwave radiation is based on the total hours of insolation, which is calculated according to the region's latitude (Table 4) and the day of the year, according to Equations A1. θ and ω represent, respectively, the Sun's declination and angle at sunrise, N represent the amount of hours of insolation, RD represent the Earth's relative distance to the Sun, SR_{atm} and SR represent the total solar radiation at the top of the atmosphere and the water surface, respectively and R_{SN} is the net shortwave radiation absorption (GIANNIOU; ANTONOPOULOS, 2007) (KOTSOPOULOS; BABAJIMOPOULOS, 1997).

$$\theta = 0.4093 \sin\left[\frac{2\pi(284+d)}{365}\right] \tag{A1a}$$

$$\omega = \cos^{-1}\left[-\tan\left(\frac{2\pi \text{lat}}{360}\right)\tan(\theta)\right] \tag{A1b}$$

$$N = \frac{24\omega}{\pi} \tag{A1c}$$

$$RD = 1 + 0.033\cos\left(\frac{2\pi d + 2\pi}{365}\right) \tag{A1d}$$

$$SR_{atm} = \frac{1440\,GSC\,RD}{\pi}\omega \sin\left(\frac{2\pi \text{lat}}{360}\right)\sin(\theta) + \cos\left(\frac{2\pi \text{lat}}{360}\right)\cos(\theta)\sin(\omega)) \tag{A1e}$$

$$SR = \left(0.25 + 0.5\frac{6}{N}\right) SR_{atm} \tag{A1f}$$

$$R_{SN} = SR(1-a) \tag{A1g}$$

where d is the day of the year, lat is the region's latitude, GSC is the solar constant (set as 82,000) and a is the water Albedo constant (set as 0.07).

Longwave atmospheric radiation is represented as a modification of the Stefan-Boltzmann law and calculated by Equation A2c. The air vapor pressure, in mmHg, is calculated according to dew temperature, which is in turn based air temperature and relative humidity (Table 4), as seen in Eqs. A2a and A2b (CHAPRA, 2008).

$$T_{dew} = \frac{237.3\frac{17.27T_{air}}{237.3+T_{air}} + 237.3\log(U)}{17.27 - \frac{17.27T_{air}}{237.3+T_{air}} - \log(U)} \tag{A2a}$$

$$e_{air} = 4.596\exp(17.27T_{dew}/(237.3+T_{dew})) \tag{A2b}$$

$$R_{AL} = \sigma(T_{air}+273)^4(A_T + 0.031\sqrt{e_{air}})(1-RL) \tag{A2c}$$

where A_T is a constant coefficient (set as 0.6), σ is the Stefan-Boltzmann constant (set as 4.9×10^{-3} J m^{-2}d^{-1}K^{-4}), and RL is the reflection coefficient (set as 0.03).

The water-emitted radiation is also represented by the Stefan-Boltzmann law, according to Equation A3.

$$R_{RA} = \epsilon\sigma(T+273)^4 \tag{A3}$$

where ϵ is the water emissivity (set as 0.97).

Heat loss through evaporation is modeled using Dalton's law and calculated by Equation A4c. The term F_{V_w} defines the transfer of wind velocity, measured at a 7 meters above the surface, to water surface, and is given by Equation A4b. To estimate wind velocity at 7 meters from the input data, which is measured at the 1 meter height, Equation A4a is used.

$$V_{w7} = V_w \frac{\log(1/Z_0)}{\log(7/Z_0)} \tag{A4a}$$

$$F_{V_W} = 19.0 + 0.95 V_{w7}^2 \tag{A4b}$$

$$R_E = F_{V_W} \left(4.596 \exp\left(\frac{17.27T}{237.3 + T} \right) - e_{air} \right) 41{,}800 \tag{A4c}$$

$$\tag{A4d}$$

where Z_0 is the surface roughness in meters (set as 0.001 for smooth water surface).

Similarly, convective heat loss is estimated by Equation A5.

$$R_C = c_1 F (T - T_{air}) 41{,}800 \tag{A5}$$

where c_1 is the Bowen's coefficient in mmHg^{o}C^{-1} (set as 0.47).

APPENDIX B – ADDITIONAL CAPIVARI INPUT DATA

Table B1 – Capivari monthly averaged meteorological and hydrological data

Month	T_{air} (^{o}C)	U (%)	V_w (ms^{-1})	Q_{in} (m^{3}s^{-1})	Q_{out} (m^{3}s^{-1})	T_{Win} (^{o}C)
Jan	20.26	88.5	2.0	28.18	23.50	20.20
Feb	20.62	87.2	1.9	28.69	27.11	20.47
Mar	19.97	87.6	1.8	24.96	24.66	19.98
Apr	17.98	87.6	1.8	18.50	20.48	18.49
May	14.50	87.3	1.8	18.61	19.32	15.88
Jun	14.11	86.0	1.9	18.12	20.46	15.58
Jul	13.40	85.1	2.0	19.12	20.46	15.05
Aug	14.51	81.8	2.1	16.21	18.46	15.88
Sep	14.98	86.1	2.2	20.29	20.10	16.24
Oct	16.81	88.1	2.2	22.04	22.11	17.61
Nov	18.09	86.3	2.2	20.36	20.57	18.57
Dec	19.51	86.6	2.1	21.14	19.01	19.63

Table B2 – Capivari bathymetric data

Elevation (m)	Area (m^2)	Elevation (m)	Area (m^2)
802.00	52,000	835.10	5,940,000
804.00	188,000	836.17	6,390,000
806.30	352,000	837.09	6,810,000
808.45	588,000	837.79	7,150,000
811.17	908,000	838.83	7,690,000
814.54	1,340,000	839.74	8,200,000
817.17	1,710,000	840.39	8,580,000
819.56	2,080,000	841.65	9,360,000
822.15	2,520,000	842.94	10,200,000
824.42	2,950,000	844.27	11,100,000
826.56	3,400,000	845.54	12,000,000
828.39	3,830,000	847.30	13,200,000
830.50	4,390,000	848.50	14,300,000
832.35	4,950,000	850.00	15,200,000
833.73	5,420,000		

APPENDIX C – CPMOPSO EVALUATION

CONCEPT OVERVIEW

Nature inspired metaheuristics are valuable tools to optimize complex problems in which traditional exact methods that guarantee solution optimality are not applicable (ROTHLAUF, 2011). Metaheuristic algorithms also have the advantage of being generically designed to generate approximate solutions for a wide range of problems. Evolutionary and Swarm Intelligence algorithms are among the two most used population-based *metaheuristics* to solve hard optimization problems (BOUSSAïD; LEPAGNOT; SIARRY, 2013).

The Particle Swarm Optimization (PSO) method was developed in the mid nineties by Kennedy e Eberhart (1995) as a simulation algorithm for the movement of bird flocks. Since then the algorithm has been widely and successfully used to optimize a plethora of different problems, ranging from biomedical to electronics and financial applications (POLI, 2007). PSO is mostly used on the optimization of single-objective problems, e. g., AlRashidi e El-Hawary (2009), Boussaïd, Lepagnot e Siarry (2013), Ardizzon, Cavazzini e Pavesi (2015), Jiang et al. (2007), and Jiang et al. (2010). Different modifications have been developed to optimize multiple objectives simultaneously, e. g., Reyes-sierra e Coello (2006), Fieldsend e Singh (2002), Coello, Pulido e Lechuga (2004), Ho et al. (2005), and Alvarez-Benitez, Everson e Fieldsend (2005).

Although these Multi-Objective PSO (MOPSO) techniques effectively solve different mathematical benchmark functions, according to the No-Free-Lunch theorems by Wolpert e Macready (1997), such methods cannot be generalized to be as successful when applied to other problems. Therefore a comprehensive parametric combination of these methods into a single technique may offer a 'better coverage' of such problems, since it enables the use of the best (or the combination of such) implementation to solve a given problem.

Difficulties that arise from extending single-objective to multi-objectives PSO implementations are addressed in this research. In section C the main ideas regarding multi-objective optimization and the trade-off of objectives, formalized as Pareto definitions, are presented and in section C the standard Particle Swarm Optimization technique is outlined. The proposed Combined Pareto Multi-Objective Particle Swarm Optimization (CPMOPSO) method, which combines different state-of-the-art PSO modifications, is presented in section C. The performances of the combinations of these techniques under varying magnitudes are assessed by using two complex mathematical test functions with known analytical solutions in section C. Final comments and conclusions regarding the

proposed PSO extension are drawn in section C.

PARETO CONCEPTS

Typically on multi-objective problems, a single solution that is the best for all objectives does not exist, instead a trade-off in which the solutions that 'perform' better in some of the objectives tend to 'underperform' in the remaining ones. Such trade-off is mathematically defined in the **Pareto dominance** concepts (REYES-SIERRA; COELLO, 2006).

Definition 5 A multi-objective optimization problem can be generally defined as the **minimization** of an **objective function** $f : \mathbb{R}^{ND} \rightarrow \mathbb{R}^{NO}$, where $\mathbb{R}^{ND}$ represents the decision space with ND variables and $\mathbb{R}^{NO}$ the objectives space with NO objectives. A vector $\vec{x} \in \mathbb{R}^{ND}$ is referred to as a **solution**.

Definition 6 Given two vectors $\vec{a}, \vec{b} \in \mathbb{R}^{NO}$, it is defined that $\vec{a} \leq \vec{b}$ if, and only if, $\vec{a}_i \leq \vec{b}_i$ for $i = 1, \ldots, NO$. Also that $\vec{a}$ **dominates** $\vec{b}$ (denoted by $\vec{a} \prec \vec{b}$) if $\vec{a} \leq \vec{b}$ and $\vec{b} \neq \vec{a}$. The domination concept is also extended to the decision space so that $f(\vec{x}) \prec f(\vec{x}\,') \implies \vec{x} \prec \vec{x}\,'$.

Definition 7 A solution $\vec{x} \in \mathcal{P} \subset \mathbb{R}^{ND}$ is **non-dominated** with respect to $\mathcal{P}$, if, and only if, $f(\vec{x}) \leq f(\vec{x}\,')$, for all $\vec{x}\,' \in \mathcal{P}$. A set $\mathcal{P}$ is said to be **non-dominated** if every solution $\vec{x} \in \mathcal{P}$ is non-dominated with respect to $\mathcal{P}$.

Definition 8 A solution $\vec{x}^* \in \mathbb{R}^{ND}$ is **Pareto-optimal** if it is non-dominated with respect to $\mathbb{R}^{ND}$. The **Pareto-optimal Set** $\mathcal{P}^*$ is defined such as:

$$\mathcal{P}^* = \left\{ \vec{x} \in \mathbb{R}^{ND} | \, \vec{x} \text{ is Pareto-optimal} \right\}$$

The **Pareto-front** $\mathcal{F}^*$ is defined by the evaluation of the Pareto-optimal set:

$$\mathcal{F}^* = \left\{ f(\vec{x}) \in \mathbb{R}^{ND} | \, \vec{x} \in \mathcal{P}^* \right\}$$

Note that, by definition, the Pareto-optimal set is a non-dominated set, since it is a subset of the search space and that if $f(\vec{x}\,') \not\prec f(\vec{x})$ for all $\vec{x}\,' \in \mathbb{R}^{ND}$ then the same is valid for all $\vec{x}\,' \in \mathcal{P}^*$.

SINGLE-OBJECTIVE PARTICLE SWARM OPTIMIZATION

The PSO algorithm is tied to swarm intelligence principles such as the ability of individuals to respond to quality changes in the environment in a diverse and stable manner. It simulates the movement of multiple particles, each with its own individual position, through a velocity variable that is calculated based on the best position found so

far by the particle itself (referred to as personal best) and the one found by the whole swarm (referred to as global best or leader).

The main equation used in the standard single-objective PSO implementation is the velocity calculation and position update (KENNEDY; EBERHART, 1995):

$$v_p^{t+1} = \omega v_p^t + c_1 r_1 \left(P_{b,p}^t - x_p^t\right) + c_2 r_2 \left(G_b^t - x_p^t\right) \tag{C1a}$$

$$x_p^{t+1} = x_p^t + v_p^{t+1} \tag{C1b}$$

where v_p^t and x_p^t are the velocity and position of the particle p at iteration t, r_1 and r_2 are pseudorandom uniform numbers $U(0,1)$, ω is the *inertia*, which controls the trade-off between global and local experience, c_1 and c_2 are, respectively, the local and global acceleration parameters, $P_{b,p}^t$ is the personal best position of the p particle and G_b^t is the best position found by the whole swarm so far.

COMBINED PARETO MULTI-OBJECTIVE PARTICLE SWARM OPTIMIZATION

When dealing with multiple objectives, instead of maintaining a single optimal solution, most algorithms rely on a non-dominated set that is updated at every iteration. In the multiple-objective PSO such set is commonly stored in an external archive A, which has three basic operations: insertion of a new solution, leader selection and solution removal (COELLO COELLO; LECHUGA, 2002), (FIELDSEND; SINGH, 2002), and (COELLO; PULIDO; LECHUGA, 2004).

To ensure that the archive remains a non-dominated set, the insertion operation first goes through the entire external archive and, for each stored solution, performs a dominance check that yields one of three cases: 1) the stored solution dominates the new one, halting the insertion procedure; 2) the new solution dominates the stored one and the stored solution is removed; 3) both are non-dominated, nothing happens and the next archived solution is checked. If the checking process cover the whole archive without halting, the new solution is inserted.

Since every solution in the archive is non-dominated, and therefore 'equally good', the process of selecting a stored solution as leader in Equation C1 requires careful consideration. Previous multi-objective problem solving algorithms selected leaders are based on different criteria: the distribution of the archive solutions in the objectives space (FIELDSEND; SINGH, 2002), (COELLO; PULIDO; LECHUGA, 2004), and (COELLO COELLO; LECHUGA, 2002); dominant solutions and the number of dominated swarm members (ALVAREZ-BENITEZ; EVERSON; FIELDSEND, 2005) and number of iterations that the solutions persisted in the archive (HO et al., 2005).

The proposed Combined Pareto Multi-Objective Particle Swarm Optimization (CPMOPSO), whose concept is given in Figure C1, is a combination of these different leader

selection criteria and adapted single objective techniques, e. g., Master-Slave subswarms PSO (JIANG et al., 2010), Adaptive Search Diversification PSO (ARDIZZON; CAVAZZINI; PAVESI, 2015) and particle mutation (COELLO; PULIDO; LECHUGA, 2004).

Figure C1 – Combination of different PSO extensions into a single method

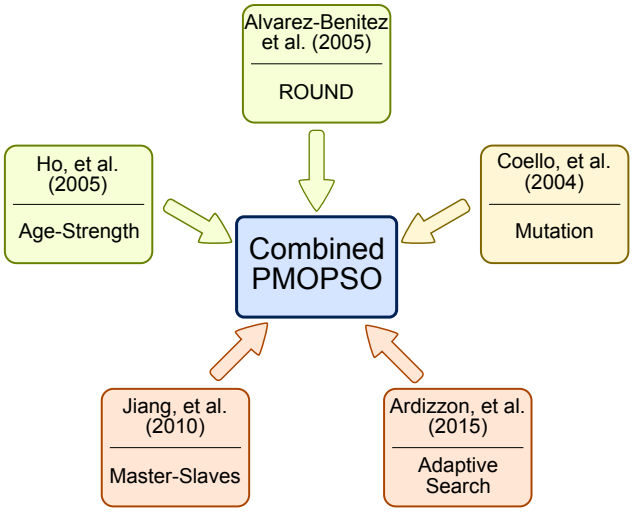

Mutation and search space constraints

Two types of mutation are employed to enhance local search and avoid local minima: the velocity and the position mutation. The velocity mutation, adapted from Alvarez-Benitez, Everson e Fieldsend (2005), is implemented through an additional term e_k in Equation C1a, resulting in:

$$v_p^{t+1} = \omega v_p^t + c_1 r_1 \left(P_{b,p} - x_p^t\right) + c_2 r_2 \left(G_b - x_p^t\right) + e_k \tag{C2}$$

and

$$e_k = \begin{cases} \mathcal{N}\left(\mu = 0, \sigma = \dfrac{x_{max} - x_{min}}{2}\right) & \text{if } r \leq p_m^{vel} \\ 0 & \text{otherwise} \end{cases} \tag{C3}$$

where $\mathcal{N}(\mu, \sigma)$ is the normal distribution with mean μ and standard deviation σ and r is a pseudorandom uniform number $U(0, 1)$ and $p_m^{vel} \in [0, 1]$ is the velocity mutation probability that is used to select whether the mutation will be applied or not.

The position mutation by Coello, Pulido e Lechuga (2004) enhances exploration during early PSO iterations by using a mathematical function that rapidly decreases as more iterations are executed. The probability function used was $(1 - i/NI)^{5/mr}$, where i is the current PSO iteration, NI is the total number of iterations and mr, whose value is 0.5, is the mutation rate parameter which controls how fast the function decreases.

Algorithm Algorithm C1 presents the full mutation process, that works as follows: if the probability function is 'satisfied', a dimension d in the ND-dimensional position vector x_p is randomly selected, afterwards, the mutation lower and upper boundaries are

also calculated based on the probability function and on the lower (LB) and upper (UB) boundaries of the selected dimension, and finally the mutated value for the d-th dimension of the x_p position vector is randomly selected between the mutation's lower and upper boundaries.

Algorithm C1 Mutate

procedure MUTATE($x_p, ND, i, NI, mr, LB, UB$)
  $r \leftarrow \text{RAND}(0, 1)$
  if $r \leq (1 - i/NI)^{5/mr}$ **then**
    $d \leftarrow$RAND_INT$(1, ND)$
    $mrange \leftarrow \left(UB^d - LB^d\right)(1 - i/NI)^{5/mr}$
    $lb \leftarrow \max\left(x_p^d - mrange, LB^d\right)$
    $ub \leftarrow \min\left(x_p^d + mrange, UB^d\right)$
    $x_p^d \leftarrow \text{RAND}(lb, ub)$

To ensure that the updated position remains under the viable domain set by each lower and upper boundaries, the damping wall is used, adapted from Huang e Mohan (2005), according to Algorithm Algorithm C2.

Algorithm C2 Damping Walls

procedure DAMPING WALLS(x_p^d, V_p^d, LB^d, UB^d)
  while $x_p^d + V_p^d < LB^d$ or $x_p^d + V_p^d > UB^d$ **do**
    if $x_p^d + V_p^d < LB^d$ **then**
      $V_p^d \leftarrow \text{RAND}(0, 1)\left(LB^d - x_p^d - V_p^d\right)$
      $x_p^d \leftarrow LB^d$
    if $x_p^d + V_p^d > UB^d$ **then**
      $V_p^d \leftarrow \text{RAND}(0, 1)\left(UB^d - x_p^d - V_p^d\right)$
      $x_p^d \leftarrow UB^d$

Leader selection

As in previous implementations, e. g., COELLO COELLO e Lechuga (2002), Coello, Pulido e Lechuga (2004), and Alvarez-Benitez, Everson e Fieldsend (2005), each swarm member selects its own leader as a member of the external archive, and therefore the leader G_b^t in Equation C2 becomes $G_{b,p}^t$. This process is divided in two steps: the constraining of the set of selectable solutions and probability Roulette-Wheel selection of weighted archive solutions.

Dominator leader

For each particle x_p the subset $S_{x_p} \subseteq A$ is formed by all solutions in the external archive that dominate x_p. If such set is empty, i. e., the particle is itself a member of the

archive, than the whole archive is used, according to:

$$S_{x_p} = \begin{cases} \{a \in A | a \prec x_p\} & \text{if } x_p \notin A \\ A & \text{if } x_p \in A \end{cases} \tag{C4}$$

Each leader $G_{b,p}^t \in S_{x_p}$ is then selected from this constricted subset of the external archive in order to enhance the convergence of the algorithm (ALVAREZ-BENITEZ; EVERSON; FIELDSEND, 2005).

Weighted selection

After the constriction of the archive to the S_{x_p} subset, a discrete probability distribution, in which each archived solution has a different probability of being selected as leader, is calculated based on the number of iterations that the solution a has been in the archive and the amount of swarm particles that it dominates. The age criteria is implemented through the variable age^a which is calculated according to the number of iterations k_a that the archive member a persisted in the archive:

$$age^a = \min\left(1.02^{k_a}, 100\right) \tag{C5}$$

where, in contrast to the original implementation of Ho et al. (2005), the upper boundary of 100 was added to prevent the maintenance of obsolete solutions in the archive.

The domination criteria from Alvarez-Benitez, Everson e Fieldsend (2005), represented by the dom_a variable, is the amount of swarm members dominated by the archive member a, i. e., $dom_a = |\{x_p \in X | a \prec x_p\}|$. The goal of these 2 criteria is to promote the diversity and spread of solutions in the archive. Since each swarm member has a different subset of eligible leaders, to adjust a probability distribution, it is necessary to adimensionalize the criteria regarding each S_{x_p} and invert them to promote members with lower criteria values:

$$p_{x_p}(a) = \begin{cases} 1 & \text{if } a \in S_{x_p} \text{ and } \left|S_{x_p}\right| = 1 \\ \dfrac{w_{dom}\left(1 - \frac{dom_a}{T_{x_p}^{dom}}\right) + w_{age}\left(1 - \frac{age_a}{T_{x_p}^{age}}\right)}{\left|S_{x_p}\right| - 1} & \text{if } a \in S_{x_p} \text{ and } \left|S_{x_p}\right| > 1 \\ 0 & \text{if } a \notin S_{x_p} \end{cases} \tag{C6}$$

where $T_{x_p}^{age} = \sum_{a \in S_{x_p}} age_a$, $T_{x_p}^{dom} = \sum_{a \in S_{x_p}} dom_a$, w_{dom} and w_{age} are the weights to promote solutions in less populated locations and newer solutions, respectively. Both weights need to satisfy $w_{dom} + w_{age} = 1$ so that Equation C6 characterize a discrete probability distribution function, i. e., $\sum_{a \in A} p_{x_p}(a) = 1$ and $p_{x_p}(a) \geq 0$ for all $x_p \in X$ and $a \in A$.

Adaptive parameters

Implementations with parameters that changed its values throughout the PSO simulation have been previously developed, e. g. linear inertia reduction of the inertia weight by Shi e Eberhart (1999). A recent study by Ardizzon, Cavazzini e Pavesi (2015) performed extensive analysis regarding the Adaptive Search Diversification (ASD) single objective PSO technique, which has the goal of enforcing swarm members' cooperation by enabling settler-explorer relationships among particles.

The settler-explorer mechanic is achieved in ASD by dynamically lowering global optimum influence and enhancing the effect of a particle's personal experience as further away it is from the current global best position. This promotes exploration on particles that are farther from the current solution, avoiding premature convergence, and boosts local search around the best solution by particles that are close to it.

However, in order to be used in a multi-objective scope, the ASD technique must be adapted in the sense that, instead of a single global guide, a potentially different leader is selected from a set of non-dominated solutions for each particle in each iteration. In this MO adaptation, instead of using the distance to the global best to set different parameters values in each dimension, a single value is used for each parameter for all dimensions based on the distance from the particle to the current Pareto-front. This distance d_p is calculated as the distance between the particle's position (in the objective space) to the line segment between by the two closest (also in the objective space) archive members.

Similar to Ardizzon, Cavazzini e Pavesi (2015), PSO parameters are then adjusted in such a way that the particle cooperation is enhanced, but the algorithm's convergence is maintained. To achieve that, upper and lower limits, e. g., $c_{1_{max}}$, $c_{2_{min}}$, $c_{2_{max}}$, ω_{min} and ω_{max}, are used to ensure that the parameters remains inside a reasonable domain. A maximum distance $d_{max} = \max(d_1, \ldots, d_{NP})$, is then used to adjust quadratic functions so that the relationships in Figure C2 are achieved.

Figure C2 – Behavior of the Adaptive Search Diversification parameters

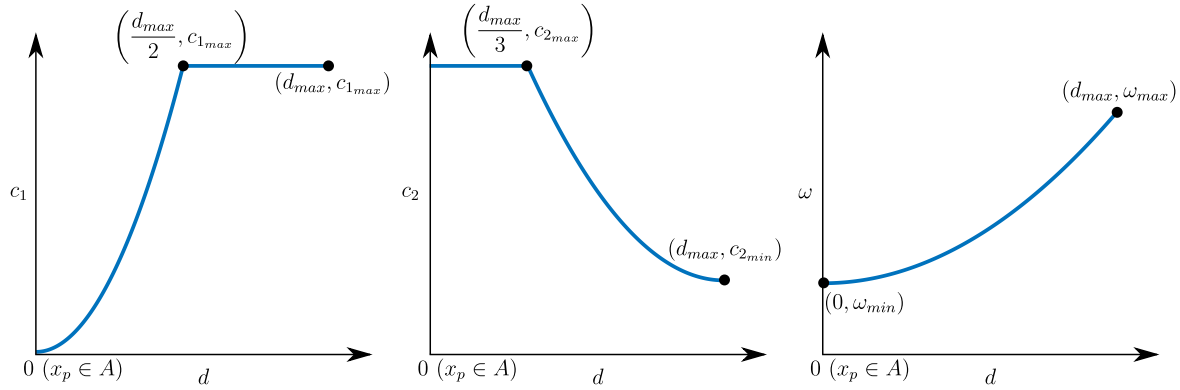

Solving the quadratic equations to find the proper coefficients yields the following

formulas to calculate adaptive PSO parameters:

$$c_1^p = \min\left(\frac{4c_{1_{max}}}{d_{max}^2} d_p^2, c_{1_{max}}\right) \tag{C7a}$$

$$c_2^p = \min\left[\frac{9\left(c_{2_{max}} - c_{2_{min}}\right)}{4d_{max}^2}\left(d_p^2 - 2d_{max}d_p + \frac{5}{9}d_{max}^2\right), 0\right] + c_{2_{max}} \tag{C7b}$$

$$\omega^p = \frac{\omega_{max} - \omega_{min}}{d_{max}^2}\left(d_p^2 - d_{max}^2\right) + \omega_{max} \tag{C7c}$$

Subswarms

The CPMOPSO implementation of subswarms is based on the Master-slave Swarms Shuffling Evolution PSO (MSSE-PSO) (JIANG et al., 2010). However, since MSSE-PSO was developed to solve single objective problems, it needs to be adapted to use external archives instead of swarm optima. This adaptation is done by using a master archive A_{master} that contains the best solutions from the master and slaves subswarms, and several (one for each of the slave subswarms) slave archives A_{ss_i}. The set of slave subswarms is denoted by $SS = \{ss_1, \ldots, ss_{NSS}\}$ where NSS is the number of slave swarms.

Each subswarm is optimized using potentially different parameters and criteria weights, e. g., $c_{1_{max}}$ and w_{dom}. While the particles in the master swarm select its leaders from the master archive, the slaves select from their own individual external archive. Similarly to Jiang et al. (2010), the slave archives are periodically reset and repopulated with partitions from the master archive, as described in Algorithm C3, where the reset function clears the slave archives archive and resets the position and velocity of every every particle to a valid random value. These merges occur in every $\frac{NI}{10}$ iterations.

Algorithm C3 Merge

```
1: procedure MERGE(A_master, SS)
2:     [A^1_master, ..., A^NSS_master] ← partition(A_master)
3:     for each ss_i ∈ SS do
4:         reset(ss_i)
5:         for each x_p ∈ A^i_master do
6:             insert(A_ss_i, x_p)
```

BENCHMARK TESTS

Test problems

Two nonlinear mathematical test functions were used to assess the performance of the different techniques used in the Combined Pareto MOPSO. These tests were developed by Deb et al. (2002) generic functions regarding both decision and objective dimensions, and that were based on the combination of relatively simple hyper surfaces, such as

hyperplanes and hyperspheres, with an additional functional g that has several local minima.

The test functions shown in Table C1 are instances from the generic problems of Deb et al. (2002), with 3 objectives and 15 decision variables. In these instances, two variables x_1 and x_2 were used to characterize the plane (DTLZ1) and the sphere (DTLZ3), while the remaining 13 variables were used in the functional g, which is described in the footnote of Table C1.

Table C1 – Multi-objective test problems

Problem	Objectives*	Boundaries
DTLZ1	$f_1(x) = 0.5x_1x_2(1+g(x))$ $f_2(x) = 0.5x_1(1-x_2)(1+g(x))$ $f_3(x) = 0.5(1-x_1)(1+g(x))$	$x \in [0,1]^{15}$
DTLZ3	$f_1(x) = \cos(x_1\pi/2)\cos(x_2\pi/2)(1+g(x))$ $f_2(x) = \cos(x_1\pi/2)\sin(x_2\pi/2)(1+g(x))$ $f_3(x) = \sin(x_1\pi/2)(1+g(x))$	$x \in [0,1]^{15}$

$^*g(x) = 100\left\{|\vec{x}| - 2 + \sum_{k=3}^{15}\left[(x_k - 0.5)^2 - cos(20\pi(x_k - 0.5))\right]\right\}$

The global minimum of the g functional is $g(x_3 = 0.5, x_4 = 0.5, \ldots, x_{15} = 0.5) = 0$, while the minimum for the (f_1, f_2, f_3) objectives are: the plane defined by the $(0.5, 0, 0)$, $(0, 0.5, 0)$ and $(0, 0, 0.5)$ points for the DTLZ1 function and the $(+, +, +)$ octave of the origin centered sphere with unitary radius for the DTLZ3 problem.

Two metrics were used to analyze the performance of the implemented optimization algorithms: the Generational Distance (GD) which measures the closeness of a given set of points to the problem's true Pareto-front, and the Spacing (SP) to measure the spread of the solutions in the output Pareto-front:

$$GD = \frac{\sqrt{\sum_{a\in A} d_a^2}}{n} \tag{C8a}$$

$$SP = \sqrt{\frac{\sum_{a\in A}\left(\bar{d}_{neigh} - d_{neigh,a}\right)^2}{|A| - 1}} \tag{C8b}$$

where d_a is the distance between solution a and the Pareto-front, $d_{neigh,a}$ is the distance between the solution a and its closest neighbor solution and $\bar{d}_{neigh}$ is the average of all $d_{neigh,a}$.

The calculation of the distances between the solutions and the analytical Pareto-front are done differently in these two test problems: for DTLZ1 d_a is calculated as the distance between the solution and its projection on the Pareto plane, i. e., $d_a = \frac{f_1^a + f_2^a + f_3^a}{\sqrt{3}}$, and for DTLZ3 it is calculated based on the point to origin distance ($d_a = \sqrt{{f_1^a}^2 + {f_2^a}^2 + {f_3^a}^2} - 1$).

Numerical experiments

To mitigate the inherent influence of randomness in the performance of this *metaheuristic* algorithm, 20 simulations with different seeds were executed for each analysis. Two stopping criteria were used for the particle swarm algorithm: the maximum number of iterations $NI = 3000$ and the maximum external archive set $|A| = 10,000$. The optimization was halted upon achieving either of the two criteria.

The impact of constraining the eligible leaders set from the whole archive A to the set of solutions S_{x_p} is displayed on Table C2. In these simulations the swarm was composed by $NP = 100$ particles with local and global acceleration coefficients of $c_1 = 0.5$ and $c_2 = 1.5$, respectively, and inertia values of $\omega = 0.2$. The performance metrics for the simulations with Adaptive Search Diversification (ASD) parameters, whose values were limited by $c_{1_{max}} = 1.5$, $c_{2_{min}} = 0.5$, $c_{2_{max}=2.0}$, $\omega_{min} = 0.2$ and $\omega_{max} = 0.5$, are also shown in Table C2.

Table C2 – Performance metrics for different eligible leaders set and parametrizations. The best values across implementations are highlighted in bold

		$G^t_{b,p} \in A$ Fixed Params.		$G^t_{b,p} \in S_{x_p}$ Fixed Params.		$G^t_{b,p} \in S_{x_p}$ ASD Params.	
		DTLZ1	DTLZ3	DTLZ1	DTLZ3	DTLZ1	DTLZ3
GD	Best	13.027	54.581	**0.007**	**9.6E-5**	0.011	2.5E-4
	Avg.	14.548	62.026	**0.057**	0.086	0.062	**0.038**
	Worst	16.993	78.319	**0.136**	0.504	0.137	**0.143**
	Std.	1.050	5.473	0.033	0.108	0.035	0.040
SP	Best	15.263	39.065	**4.3E-4**	**1.6E-4**	6.7E-4	2.2E-4
	Avg.	20.807	54.754	**0.006**	0.013	0.020	**0.005**
	Worst	30.439	73.050	**0.022**	0.092	0.274	**0.016**
	Std.	3.904	9.206	0.005	0.023	0.060	0.005
t_{comp}	Avg.	**2.656**	**2.611**	6.444	4.479	5.087	4.810
$\|A\|$	Avg.	264	189	755	839	342	630

The data on Table C2 show that the constrained selection from the S_{x_p} set improved both the quality (GD) and the diversity (SP) by at least 5 orders of magnitude for both test problems while increasing the computational cost by only a factor of three. Although ASD got slightly outperformed when solving the DTLZ1 problem, it significantly outperformed the fixed parameters implementations on both average and worst case for the DTLZ3 problem. Therefore, together with the ASD parameters, the $G^t_{b,p} \in S_{x_p}$ selection was used in further analysis.

Different combinations of (w_{dom}, w_{age}) were executed to assess if the algorithm performs better by favoring newer solution over solutions in less populated locations, or vice versa, and its resulting performances are shown in Figure C3.

Figure C3 – Impact of varying the weight of leader selection criteria on CPMOPSO performance. The random $G^t_{b,p} \in S_{x_p}$ selection (third column of Table C2), is plotted as 'no criteria'.

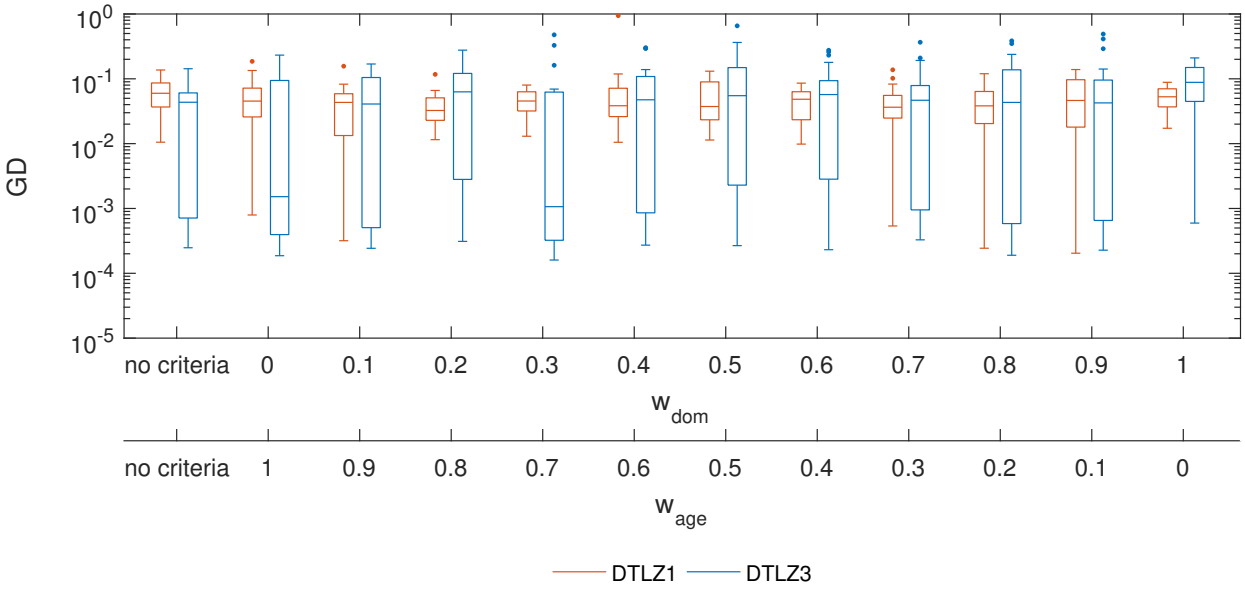

Despite the apparent differences, there is no significant impact of employing different criteria combinations on the performance of the algorithm (Kruskal-Wallis; $p = 0.8080$ for DTLZ1 and $p = 0.2327$ for DTLZ3). Although some of the combinations, such as $w_{dom} = 0$ and $w_{age} = 1$, presented better GD values when optimizing the DTLZ3 function, such differences may be due to the inherent randomness of the applied PSO technique. The similarity between the performances of the no criteria and exclusive dominator criteria ($w_{dom} = 1$) implementations that is displayed in Figure C3 was previously identified by Alvarez-Benitez, Everson e Fieldsend (2005).

To analyze the impact of using multiple subswarms, 200 simulations were executed with 0 to 9 slave swarms (Figure C4). The use of multiple subswarms increases the computational cost of the simulations since the number of particles and number of stored solutions increases linearly with the number of slave swarms. In every simulations the master swarm used $w_{dom} = 0.1$ and $w_{age} = 0.9$ as criteria weight to promote newly inserted solutions, while slave subswarms used $w_{dom} = 0.8$ and $w_{age} = 0.2$ to promote exploration of less populated regions.

The exponential decrease of the worst, best and median cases of the GD measure, highlights the effectiveness of using multiple slave subswarms. Although such decrease is more evident in the optimizations of the DTLZ3 problem it is also present, however not as regular, in the metrics for the DTLZ1 optimization. The GD measure is significantly lower for simulations with more than 5 slave subswarms when compared with simulations that use less slaves (Kruskal-Wallis; $p = 1.6310^{-6}$ for DTLZ1 and $p = 1.0510^{-23}$ for DTLZ3).

Figure C4 – Impact of the number of slave subswarms on CPMOPSO performance

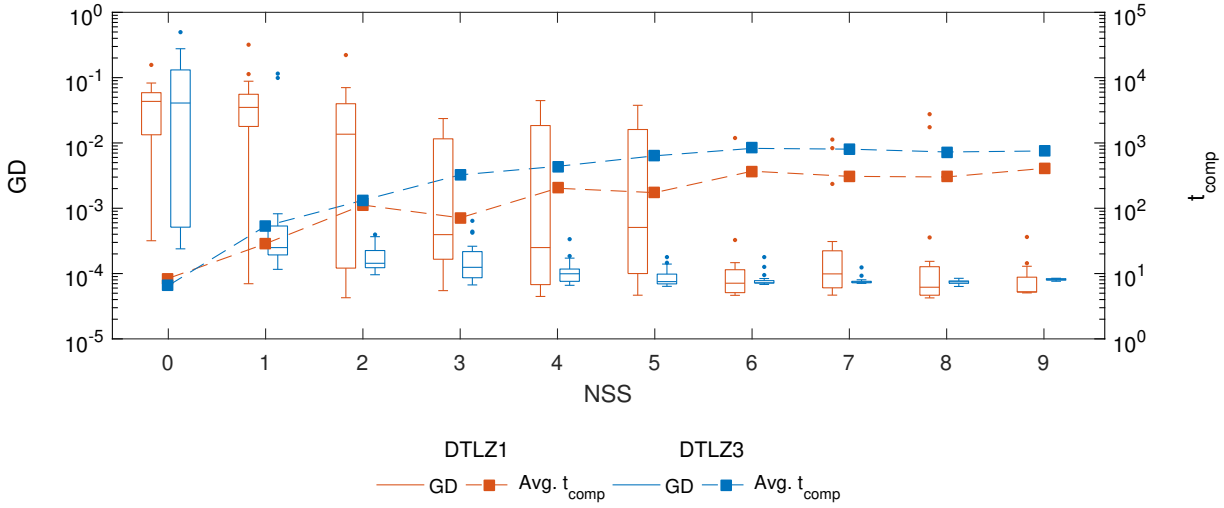

Even though the amount of function evaluations required by each simulation is proportional to the number of slave subswarms, all simulations that used more than 5 slave subswarms did not differ regarding the average computational cost. This occurs due to the fact that the computational time required to evaluate these test functions is not relevant when compared to the cost of ordering and updating the master external archive.

The impact of combining different techniques is depicted in Figure C5, in which the simulations that were plotted were the ones with GD values closer to the median of its class.

Figure C5 – Output (red dot) and analytical (black surface) Pareto-fronts for different technique combinations

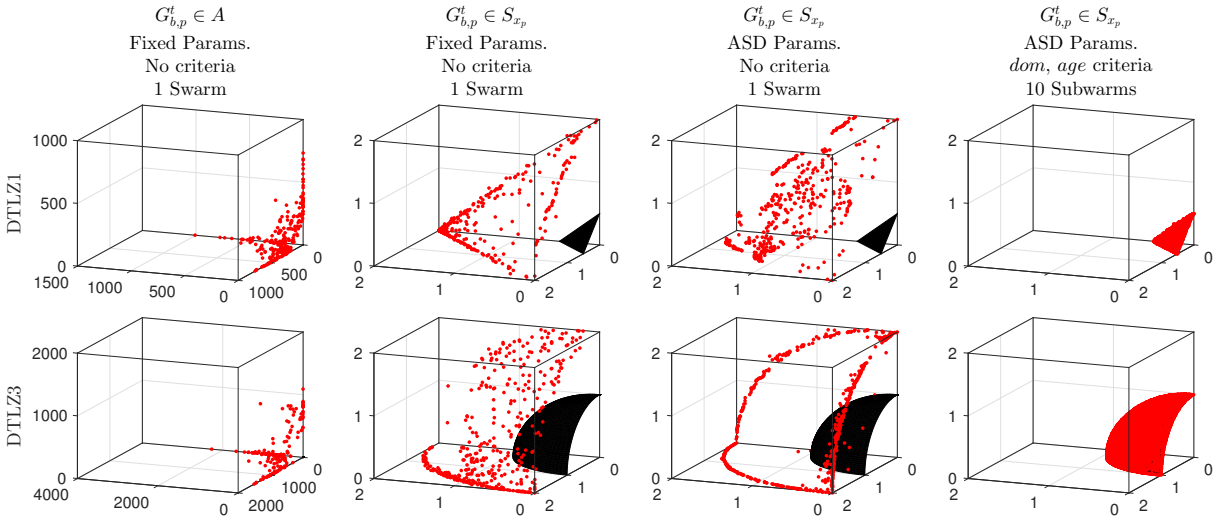

The enhanced performance of the eligible leaders set constraining, that is also evidenced by Table C2, is clearly visible in Figure C5 by the reduction of about three order of magnitudes in the scale of the plot. Although, according to Table C2, the use

of ASD parameters yielded better performances for the DTLZ3, Figure C5 shows that the fixed parameters approach presented better Pareto front coverage. The exponential improvement of the GD measure that is shown in Figure C4 is also evidenced by the fact that the simulation using 10 subswarms (1 master and 9 slaves) outputted Pareto-fronts is right on top of the analytical solutions for both DTLZ1 and DTLZ3 problem.

CONSIDERATIONS

Several researchers have focused on adapting the standard single-objective particle swarm optimization into a tool to solve multi-objective problems, and many different approaches were developed. The proposed CPMOPSO combines all these PSO implementations into a parameterized method which enables optimizations to be executed by either the methods themselves or a mixture of them. This enables the strength of these different techniques to complement each other in order to achieve better Pareto-front optimizations.

As was also discovered by Alvarez-Benitez, Everson e Fieldsend (2005), the constraining of the leader selection set of a particle to only solutions that dominates it, greatly increased the quality of the final optimization result, while the use of adaptive parameter values and criteria based on how many iterations the solution persisted in the archive generally enhanced the spread of the external archive members.

Finally, the addition of the adapted master-slave subswarms dynamic managed to decrease the variability of the performances of simulations under different random generator seeds, while exponentially increasing the quality of these outputs. For the DTLZ3 test problem, the output Pareto front of all the 20 simulations matched almost exactly the surface of the analytical solution, while mostly the same occurred for the DTLZ1 optimizations.

Although the computational cost increases with both the number of slave subswarms and the size of the external archive, the CPMOPSO technique also enables parallel computing and efficient data structures, e. g., the ones developed by Fieldsend e Singh (2002) and Coello, Pulido e Lechuga (2004), to be used to reduce the runtime of the algorithm.

According to the No-Free-Lunch theorem by Wolpert e Macready (1997), the good performance of the CPMOPSO algorithm when solving these two mathematical test functions cannot be generalized to other untested problems. Therefore further tests regarding more complex test functions with potentially more objectives and decision variables are required to better infer the method's stability and quality of output.